Contrails

Cleared: March 6th, 1972
Clearing Authority: Air Force Materials Laboratory

FOREWORD

This report was prepared by Nuclear Metals, Inc., West Concord, Massachusetts, under Contract AF33(616)-7382. The contract was initiated under Project No. 7351, "Metallic Materials," Task No. 735101, "Refractory Metals." It was accomplished under the technical direction of Mr. Thomas D. Cooper of the Metals and Ceramics Branch, Air Force Materials Laboratory, Research and Technology Division, Wright-Patterson Air Force Base, Ohio.

Mr. Victor Nerses of the Nuclear Metals, Inc. Research Department was the engineer in charge under the over-all supervision of Mr. J. L. Klein, Vice President. Dr. E. J. Rapperport, formerly Group Leader of the Fundamental Metallurgy Group, Research Department (now with Ledgemont Laboratory, Lexington, Massachusetts) was the engineer in charge during the first half of this program. The authors wish to acknowledge the assistance of: Advanced Metals Research Corporation, Somerville, Massachusetts, which performed (under the supervision of Dr. S. Moll) the electron microprobe analyses cited in this work; Wright-Patterson Air Force Base, Dayton, Ohio, which performed (under the supervision of Mr. C. Hartley and Mr. K. Hubbard) the computer analyses of the diffusion composition-penetration profiles to yield diffusion coefficients; Mr. E. Field, Mr. A. Bompane, and Mr. P. Femino, Project Technicians, for preparation and treatment of the standards and samples used in this project. This report has been given the Nuclear Metals, Inc. internal number NMI-9422.

This project has been accomplished as a part of the Air Force Metallic Materials Program. The program encompasses the following areas:

1. Refractory metals
2. Diffusion
3. Refractory metals phase diagrams

Suggestions concerning the need for additional research investigations in the field of diffusion in refractory metals or related subjects will be appreciated.

Approved for Public Release

Contrails

Approved for Public Release

Contrails

ABSTRACT

Interdiffusion coefficients for the systems W-Ru, W-Ir, W-Rh, W-Pt, Cb-Cr and Mo-$MoSi_2$ have been calculated in the temperature range from 900°C to 2100°C. Tables of interdiffusion coefficients for constituent compositions ranging from 99 a/o to 1 a/o are presented.

This technical documentary report has been reviewed and is approved.

T. Perlmutter
Chief, Physical Metallurgy Branch
Metals and Ceramics Division
AF Materials Laboratory

Approved for Public Release

Contrails

TABLE OF CONTENTS

Approved for Public Release

Contrails

TABLE OF CONTENTS (continued)

Approved for Public Release

Contrails

TABLE OF CONTENTS (continued)

Approved for Public Release

Contrails

TABLE OF CONTENTS (continued)

Approved for Public Release

Contrails

ILLUSTRATIONS

Approved for Public Release

Contrails

ILLUSTRATIONS (continued)

Approved for Public Release

Contrails

ILLUSTRATIONS (continued)

Approved for Public Release

Contrails

ILLUSTRATIONS (continued)

Approved for Public Release

Contrails

ILLUSTRATIONS (continued)

Approved for Public Release

Contrails

TABLES

Approved for Public Release

Contrails

TABLES (continued)

Approved for Public Release

Contrails

I. INTRODUCTION

In the past few years the importance of diffusion in refractory metals has become increasingly emphasized because of the use of these metals for high temperature applications such as aerospace vehicles and jet engines. For practical as well as for fundamental reasons, the rates of diffusion in alloys of these metals are of considerable consequence. Most reactions which occur in the solid state are dependent on the diffusion of atoms through the lattice structure and along grain boundaries. Thus, diffusion is frequently rate-controlling in processes such as grain growth, homogenization, oxidation, age hardening, sintering, creep, and elastic relaxation.

Although there is information in the literature (a recent review of diffusion in refractory metals has been made by Peterson)[1] pertaining to diffusion in refractory metals, very little of this information can be considered reliable, for a variety of reasons. Refractory metals have very high melting points, and at reasonably attainable temperatures the diffusion coefficients and width of the diffusion zone are relatively small. Reliable determination of concentration profiles is rather difficult under these circumstances. Another difficulty encountered with refractory metals (for example, tungsten alloys with the platinum group metals in particular) is that their alloys are difficult to analyze chemically with any degree of precision. Thus, concentration gradients determined by direct chemical analysis are often inaccurate, and the resulting diffusion coefficients have large uncertainties. In addition to these inherent problems in experimental techniques, reported values of diffusion data are often suspect because of impure starting materials, inaccurate temperature measurements, and inadequate heat treating equipment.

The introduction of relatively new experimental techniques for diffusion studies has alleviated some of these problems. In particular, the utilization of the electron microprobe analyzer allows direct determination

---

Manuscript released by authors February 1964 for publication as an ML Technical Documentary Report.

Approved for Public Release

Contrails

of concentration gradients in zones which had previously been considered far too small for accurate analysis. With present techniques the microprobe permits direct composition determination of refractory alloys at individual points as close together as one micron. Not only does this instrument provide the determination of composition at extremely small intervals, but in conjunction with standards and refined X-ray analysis it circumvents the entire problem of composition determination by wet chemical techniques.

In addition to the utilization of the electron microprobe for the determination of the composition-penetration profiles, in the present program use was made of a digital computer for the Boltzmann-Matano analysis of the composition-penetration profile found. The results of this study are presented in the following sections of this report.

II. SUMMARY

A. Diffusion in Refractory Metals

The results obtained in the present work from the interdiffusion of platinum, iridium, rhodium and ruthenium with tungsten, from the interdiffusion of chromium and columbium, and of molybdenum disilicide and molybdenum are tabulated in Table 1.

In this work, Advanced Metals Research Corporation, Somerville, Massachusetts, was a subcontractor to Nuclear Metals, Inc., West Concord, Massachusetts, and performed the electron microbeam probe analyses.

An IBM 7090 digital computer at Wright-Patterson Air Force Base was used to obtain the Boltzmann-Matano solution of Fick's first law.

B. Experimental Techniques

1. Materials

The purity of all the elements used for the diffusion runs was at least 99.9 percent. This purity was enhanced by arc-melting (whenever used), and was considered adequate for this program.

Approved for Public Release

TABLE 1

SUMMARY OF DIFFUSION RESULTS

System	Temp. (°C)	Time (hrs.)	Grade of Couple*	Interdiffusion Coefficients ($cm^2/hr.$)					Comments
				5 a/o Ru α	39 a/o σ	70 a/o β	90 a/o β		
W-Ru	1300 ± 20	1750	B +	4.3×10^{-11}	- - -	2.7×10^{-9}	2.9×10^{-9}		0.003 in. zone
	1645 ± 15	300	B +	4.1×10^{-10}	- - -	3.5×10^{-8}	1.3×10^{-8}		0.003 in. zone
	1785 ± 15	168	B +	2.6×10^{-9}	1.7×10^{-7}	3.9×10^{-7}	2.8×10^{-8}		
	1955 ± 5	117	B +	9.4×10^{-9}	3.4×10^{-7}	2.2×10^{-7}	9.9×10^{-8}		
	2025 ± 10	63	A	2.4×10^{-8}	7.9×10^{-7}	3.5×10^{-7}	1.6×10^{-7}		0.006 in. zone
				93,500	61,000	49,500	57,200		Q values, cal./mole
				20	0.044	0.063	0.037		D_o values ($cm^2/hr.$)
				3 a/o Ir α	24 a/o σ	50 a/o ε	60 a/o ε	90 a/o β_{Ir}	
W-Ir	1300 ± 20	1750	C +	4.5×10^{-11}	- - -	8.2×10^{-10}	- - -	2.6×10^{-11}	0.001 in. zone
	1385 ± 25	417	C	2.1×10^{-10}	- - -	2.4×10^{-9}	2.8×10^{-9}	3.9×10^{-10}	0.002 in. zone porous and cracked.
	1645 ± 15	300	C -	2.9×10^{-10}	- - -	3.2×10^{-8}	1.7×10^{-8}	2.4×10^{-9}	Porous at interface.
	1800 ± 25	200	C -	9.1×10^{-10}	- - -	2.1×10^{-8}	2.3×10^{-8}	1.7×10^{-9}	Porous and cracked.
	1955 ± 5	117	B +	2.9×10^{-9}	1.1×10^{-7}	3.7×10^{-8}	4.9×10^{-8}	3.2×10^{-8}	Somewhat porous at 95 a/o Ir.
	2025 ± 10	63	B +	1.1×10^{-8}	1.8×10^{-7}	9.2×10^{-8}	8.2×10^{-8}	4.0×10^{-8}	Excellent couple
	2110 ± 13	52	B	3.8×10^{-8}	2.6×10^{-7}	2.2×10^{-7}	2.3×10^{-7}	2.2×10^{-7}	0.004 in. zone. Zone breadth not uniform.
				170,000	60,800	120,400	120,400	145,400	Q values, cal./mole
				1.41×10^{8}	0.0085	5.37×10^{4}	5.37×10^{4}	3.98×10^{6}	Calculated D_o values ($cm^2/hr.$)

* Grades indicate quality of diffusion zones.

(Table continued on next page.)

Approved for Public Release

Confidential

TABLE 1 (continued)

System	Temp. (°C)	Time (hr)	Grade of Couple*	Interdiffusion Coefficients (cm^2/hr.)							Comments
				3 a/o Rh α	60 a/o ε	70 a/o ε	90 a/o β				
W-Rh	1300 ± 20	1750	B-	8.1×10^{-11}	9×10^{-9}	1.2×10^{-8}	1.8×10^{-8}				
	1385 ± 25	417	C	4.6×10^{-10}	5×10^{-8}	6.8×10^{-8}	2.6×10^{-8}				Interface is porous and cracked.
	1645 ± 15	300	B	5.2×10^{-10}	8.9×10^{-8}	1.0×10^{-7}	1.2×10^{-7}				
	1800 ± 25	200	B	5.4×10^{-9}	2.3×10^{-7}	3.5×10^{-7}	3.9×10^{-7}				**
	1800 ± 5	67	C	$5. \times 10^{-9}$	2.9×10^{-7}	4.4×10^{-7}	5.0×10^{-7}				**
				58,000	41,700	43,400	41,600				Q values, cal/mole.
				0.00457	0.00525	0.0112	0.00912				D_o values (cm^2/hr.).
				2 a/o Pt (β)	50 a/o γ	55 a/o γ	65 a/o ε	77 a/o α	80 a/o α	85 a/o α	
W-Pt	1300 ± 20	1750	A	3.6×10^{-10}	$.8 \times 10^{-9}$	3.1×10^{-9}	-----	1.9×10^{-8}	2.3×10^{-8}	3.3×10^{-8}	.004 in. zone.
	1473 ± 12	432	A	-----	7.9×10^{-8}	8.6×10^{-8}	1.1×10^{-8}	1.7×10^{-7}	1.8×10^{-6}	2.0×10^{-6}	.003 in. zone.
	1645 ± 15	300		3.5×10^{-9}	6.8×10^{-8}	4.6×10^{-8}	4.0×10^{-7}	4.7×10^{-6}	1.4×10^{-6}	1.6×10^{-6}	.0025 in. zone.
	1700 ± 11	96	A	-----	7.6×10^{-8}	8.2×10^{-7}	1.0×10^{-7}	1.0×10^{-6}	1.5×10^{-6}	3.2×10^{-6}	.002 in. zone.
	1743 ± 10	24	A	1.9×10^{-8}	1.7×10^{-7}	2.0×10^{-7}	2.8×10^{-7}	$5. \times 10^{-6}$	3.4×10^{-6}	-----	.0015 in. zone.
				139,000	83,600	82,100	92,000	78,000	75,400	74,200	Q values, cal/mole.
				11×10^5	17	12	158	63	43	46	D_o values (cm^2/hr.).

* Grades indicate quality of diffusion zones.

** Entry in 3 a/o column actually is for 2 a/o.

(Table continued on next page.)

Approved for Public Release

TABLE 1 (continued)

System	Temp. (°C)	Time (hrs.)	Grade of Couple*	Interdiffusion Coefficients (cm^2/hr.)					Comments
				2[a]/o Cb(γ)	34[a]/o $CbCr_2$	38[a]/o $CbCr_2$	90[a]/o α	95[a]/o α	
Cr/Cb	1101 ± 20	432	A	4.7×10^{-10}	- - -	1.0×10^{-9}	6.1×10^{-10}	8.6×10^{-10}	.001 in. zone
	1251 ± 10	342	A	5.0×10^{-9}	6.5×10^{-8}	1.0×10^{-8}	4.3×10^{-9}	5.4×10^{-9}	.0015 in. zone
	1400 ± 9	168	C	1.5×10^{-7}	- - - -	5.0×10^{-7}	6.5×10^{-8}	7.2×10^{-8}	Crack at interface, .002 in. zone
	1502 ± 10	95	D	1.8×10^{-6}	1.1×10^{-6}	1.7×10^{-6}	5.8×10^{-7}	3.5×10^{-7}	Crack at interface, .0025 in. zone
	1575 ± 10	24	C	5.4×10^{-6}	9.0×10^{-6}	8.6×10^{-6}	8.6×10^{-7}	5.4×10^{-7}	Crack at interface, .003 in. zone
	1624 ± 8	9	C	1.1×10^{-5}	1.7×10^{-5}	7.2×10^{-6}	1.7×10^{-6}	9.4×10^{-7}	Crack at interface, .0055 in. zone
				97,900	94,000	94,800	92,000	86,000	Q values, cal/mole
				123,000	93,000	85,100	9,550	1,100	D_o values (cm^2/hr.)
				31[a]/o Mo ($MoSi_2$)		60[a]/o Mo_3Si_2	Mo_3Si	98[a]/o α	
Mo/$MoSi_2$	904 ± 6	700	B	- - - -		3.2×10^{-10}		- - - -	.003 in. zone
	1098 ± 6	500	A	- - - -		5.8×10^{-9}		1.7×10^{-9}	.002 in. zone
	1365 ± 10	44	B	6.8×10^{-9}		4.0×10^{-7}	Phase	7.6×10^{-9}	.005 in. zone
	1626 ± 4	2.5	B	5.0×10^{-7}		2.4×10^{-5}	sup-	3.1×10^{-7}	.006 in. zone
	1715 ± 7	1	A	6.5×10^{-7}		- - - -	pressed	2.6×10^{-7}	.006 in. zone
				88,500		74,300		78,000	Q values, cal/mole
				347		302		16.2	D_o values (cm^2/hr.)

* Grades indicate quality of diffusion zones.

Approved for Public Release

Contrails

2. Preparation of Materials for Diffusion Couples

Materials received as powder (tungsten, iridium, ruthenium and rhodium) were compacted into pellets and nonconsumably arc-melted on water-cooled copper hearths, using an inert atmosphere and a tungsten electrode.

3. Composition Determination of Standard Alloys

The compositions of the tungsten-iridium, tungsten-rhodium, and tungsten-ruthenium standard alloys were established by the use of weight-balances at various stages of alloy preparation. The compositions of the tungsten-platinum, molybdenum-silicon, and chromium-columbium standard alloys were determined by direct chemical analysis.

4. Temperature Measurement

Optical pyrometry was the principal temperature measurement technique. The pyrometer used was calibrated at the National Bureau of Standards.

5. Composition-Penetration Profile Determination

The technique for composition analysis used in determining the composition-penetration profile was X-ray fluorescence, utilizing the electron microprobe analyzer.

6. Boltzmann-Matano Analysis

An IBM 7090 digital computer was used as the main method for the Boltzmann-Matano analysis of the composition-penetration profile. Some of the Boltzmann-Matano analyses were done graphically.

Approved for Public Release

Contrails

III. DIFFUSION IN THE SYSTEM TUNGSTEN-RUTHENIUM

A. Diffusion Couple Preparation and Treatment

1. Material

The ruthenium and the tungsten utilized for both the diffusion couples and the standard alloys were obtained as powders of purity greater than 99.9 percent. The tungsten was obtained from the General Electric Corporation, and the ruthenium from the Baker Corporation. Typical analyses for these powders are given in Table 2. It is probable, however, that the purity was increased during the arc-melting consolidation above the figures given in Table 2, as may be seen in the before and after analyses in Table 3.

2. Arc-Melting

The powders were compacted in a hardened steel die and were than repeatedly arc-melted. In order to compact the tungsten powder, it was necessary to mix two particle sizes; the ruthenium compacted very easily under pressures of approximately 30,000 psi.

Arc-melting was conducted in a multiple depression water-cooled copper hearth utilizing a nonconsumable tungsten electrode. The system was capable of a vacuum of 5×10^{-6} mm Hg with a leak rate of approximately 20 micron-liters per hour. The ionizing gas utilized in the arc-melter was a mixture of argon and helium, which was purified by passing through tantalum chips at 600°C and zirconium chips at 800°C.

In addition to arc-melting the stock for use in the diffusion couples, it was necessary to arc-melt standard alloys at compositions across the phase diagram. These standards were used in the electron microprobe analysis of the composition gradients, and their melting and handling were of particular importance in obtaining accurate concentration profiles.

Approved for Public Release

Contrails

TABLE 2

TYPICAL CHEMICAL ANALYSIS OF TUNGSTEN AND RUTHENIUM POWDERS USED

Impurity Element	Content in parts per million by weight	
	Tungsten G.E. Co.	Ruthenium Baker Co.*
Al	10	10
Ca	10	--
Si	20	10
Fe	10	100
Cr	10	--
Ni	10	--
Cu	30	10
W	30	--
Mn	10	--
Mg	10	1
Sn	10	--

* Manufacturer states this element is 99.9% pure. This analysis is made from comparison with spectrographic results from Johnson-Matthey Co. material.

Approved for Public Release

Contrails

TABLE 3

SPECTROGRAPHIC ANALYSIS OF RUTHENIUM AND TUNGSTEN
BEFORE AND AFTER ARC MELTING

Impurity*	Ruthenium		Tungsten	
	Before	After	Before	After
Ag	nd	nd	nd	nd
Al	10-100	1-10	1-10	nd
Cu	10-100	1-10	1-10	nd
Fe	--	--	10-100	nd
Mg	1-10	<1	10-100	nd
Mn	nd	nd	1-10	nd
Mo	nd	nd	1-10	nd
Ni	nd	nd	10-100	nd
Pt	--	--	--	--
Ru	--	--	--	--
Si	10-100	1-10	10-100	1-10

* Impurity content in parts per million by weight. The values were obtained by visual comparison with spectrographic plates from Johnson-Matthey Co. high purity materials.

Approved for Public Release

Contrails

Since reliable wet chemical analysis was not available in the system tungsten-ruthenium, it was necessary to establish rigorous procedures to maintain checks on the standard alloy compositions by careful weight balances throughout processing. Table 4 lists the tungsten-ruthenium standards used with the maximum uncertainties of their compositions. The deviations were obtained by attributing the entire loss of weight first to ruthenium and then to tungsten. This assumption is undoubtedly too conservative, and the true compositions are probably within 0.5 atom percent of the nominal compositions.(2)

3. Bonding of Couples

Subsequent to arc-melting of small (30-40 gm) melts of the pure tungsten and pure ruthenium, the buttons were machine ground to flat and parallel faced discs of approximately 1/8 inch thickness. These discs were then hand-polished on metallographic abrasive paper through 4/0 grit prior to thermal bonding. In some instances, the ground and polished discs were large enough in diameter to be sectioned into several pieces for use in separate diffusion couples.

The machined and polished discs were then assembled in three-layered sandwiches with the ruthenium disc between two pieces of tungsten. This entire sandwich was placed inside a jig for the bonding anneal. The jig had oxidized stainless steel plates touching the tungsten to avoid bonding between the jig and the diffusion couples. Molybdenum bolts connecting the plates were used in the jig in order to insure continuous compression during the bonding treatment, since the expansion coefficient of the jig was less than that of the three-layered diffusion couple.

Bonding of the tungsten-ruthenium-tungsten sandwich was effected by a bonding anneal of 900°C for 16 hours in a vacuum of less than 5×10^{-5} mm Hg. Examination of couples bonded in

Approved for Public Release

Contrails

TABLE 4

COMPOSITION LIMITS FOR MICROPROBE
ANALYSIS OF STANDARD ALLOYS

Nominal Composition Atom Pct. Ru	Minimum Ruthenium Content, Atom Pct.	Maximum Ruthenium Content, Atom Pct.
0 (pure W)	-	-
10.00	6.42	10.22
30.00	29.22	30.19
50.00	48.40	50.87
70.00	68.47	71.94
90.00	89.49	92.75
100 (pure Ru)	–	–

Approved for Public Release

Contrails

this fashion in a system having considerably higher diffusion coefficients than the tungsten-ruthenium system (the columbium-chromium system) revealed that a diffusion zone of less than two microns in breadth is created under the diffusion conditions of bonding.

4. Annealing

After bonding, the three-layered diffusion sandwiches were ready for diffusion annealing. The annealing treatments were conducted in two furnaces. For temperatures above 1600°C, a tantalum tube resistance furnace was used, which was capable of a vacuum of approximately 5×10^{-6} mm Hg and which had a leak rate of 20 micron-liters per hour. The second furnace was utilized for temperatures below 1600°C (except as noted), and had a molybdenum resistance winding on an Al_2O_3 core. This furnace was also a vacuum furnace with a capability of 5×10^{-6} mm Hg. In the molybdenum wound furnace, the temperature was measured with a Pt/Pt-10% Rh thermocouple connected to recorders so that variations of temperature might be noted.

Measurements of temperature in the tantalum tube furnace were made with an optical pyrometer calibrated by the National Bureau of Standards, and the constancy of temperature was monitored with a radiation pyrometer connected to a recorder. Considerable care was exercised in attaining near black-body radiation for pyrometer temperature measurements. In addition, the sight glass to the furnace was carefully calibrated for its transmission correction curve and was shielded from incident metal vapor from within the furnace except for the few seconds required to take temperature measurements.[2] From time to time throughout the program, the temperature measuring techniques were checked by determining the melting point of pure platinum. In no case did the experimentally determined melting point of platinum deviate by more than 3°C from

Approved for Public Release

Contrails

the accepted value of 1769°C.[3] Extensive experience and checks with the high temperature furnace and with the optical pyrometer have led to a confidence level of ± 10°C at all temperatures encountered in this study.

5. Sectioning

After annealing at the desired temperatures and times, the three-layered sandwiches were removed from the furnace, mounted in Bakelite, and sectioned on planes perpendicular to the layer interfaces. In making these sections, care was taken to penetrate approximately 1/16th of an inch into the couple so that spurious surface effects would be eliminated. The sectioning was done by hand on metallographic abrasive papers, followed by hand polishing on metallographic wheels through 1/4 micron diamond paste. In general, no etching was done on the specimens in order to avoid preferential dissolution and deposition on a microscale on the diffusion couple. Such effects would confuse subsequent microprobe analysis.

B. Determination of Composition Profiles

1. General

In the work described in this paper, the composition profiles were determined by the use of an electron microprobe analyzer on sections perpendicular to the diffusion interfaces.

This instrument is capable of focusing a beam of electrons on a spot smaller than one micron in diameter. The electrons excite X-rays, characteristic of the elements irradiated, which can be analyzed to yield quantitative chemical analyses of the spot irradiated.[4] The microprobe used was equipped with an optical microscope and the electron beam was focused upon desired points across the diffusion interface. The wave lengths emitted by the elements in the specimen were diffracted, and thus separated, by an analyzing crystal, with their intensities recorded by properly located

Approved for Public Release

Contrails

radiation counters. By comparing the intensity of an element's characteristic radiation from the sample (normalized to that of the pure element) with that of carefully made standards, quantitative analyses were obtained for the irradiated spots. In some cases it is possible to compute directly the composition from normalized intensity without the use of standards;[4] however, in this work standards of known composition were utilized.

2. Correlation of Characteristic X-Ray Intensity with Composition

a. Standards

The composition standard alloys made for this system were manufactured with particular care. Accurately weighed stock of premelted material was combined and arc-melted repeatedly. Weight losses were obtained on the melted stock and only those alloys which had exhibited very small weight losses in processing were retained as standards (see Table 4).

The alloys of Table 4 were utilized as standards by simultaneously determining (on two spectrographs) the intensity of tungsten L_{α_1} and ruthenium L_{α_1} characteristic radiation from suitably prepared specimens. These intensity values, normalized to those of the pure elements, were plotted against composition. The plot obtained (Figure 1) was used as a master plot to obtain the composition-distance profiles in the diffusion couples. In obtaining data points in two-phased alloys, the beam was coarsened to as much as a 100 micron diameter to obtain composition averaging. Each point of Figure 1 is an average result of from ten to twenty separate determinations. This procedure provided good counting statistics and also demonstrated the high degree of homogeneity within the alloys.

Approved for Public Release

Contrails

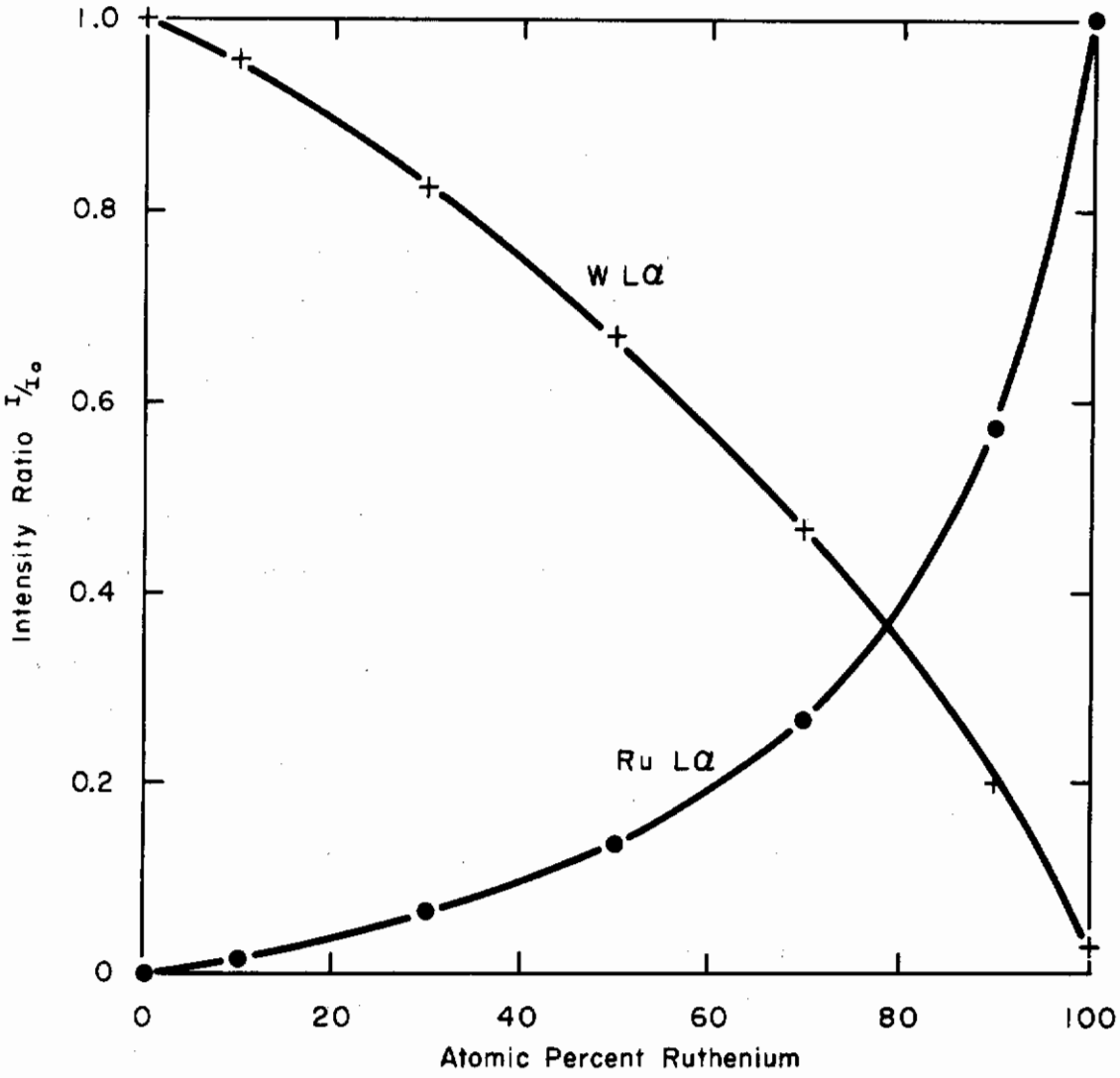

Figure 1. Plot of Normalized Characteristic L_{α_1} Radiation for Tungsten and Ruthenium vs Composition of Tungsten-Ruthenium Binary Standard Alloys

Approved for Public Release

Contrails

In the determination of the intensity ratios given in Figure 1 the background count was not subtracted. This procedure was followed because it would have been extremely awkward to shift the position of the analyzing crystal off the radiation peak in order to determine the background for each of the points at which the composition was determined. The use of a master-curve with background included thus avoided background corrections for all subsequent readings.

All microprobe data was taken with 30 KV accelerating potential, using a bent mica analyzing crystal, a helium X-ray path, an argon flow proportional counter, and a take-off angle of about 15.5°.

3. Traversing of Couples

The data points of the composition profile were determined by translating the sample step-wise through the axis of the electron beam so that the beam made a 45° angle of traverse with respect to the diffusion interface. This was done primarily to allow the X-ray radiation which was utilized in composition measurement to traverse material lying only in a given plane parallel to the diffusion interface.* Hence, only material of the same composition as that of the irradiated spot was traversed by the X-rays used in composition analysis. Fluorescent contributions from adjacent areas was minimized by utilizing the longer wavelength L spectra. The composition-distance profile was made by a series of fixed steps, whose values were obtained by reading a micrometer on the stage. These steps varied from 0.001 inch (25 microns) to 0.0001 inch (2.5 microns), depending on the width of the zone and the necessity for fine resolution. The impinging electrons cause a "contamination spot" to be left on the surface of the specimen so that it was possible to check the accuracy of the micrometer motion optically

---

* This geometry is optimum for the particular microprobe used in this program.

Approved for Public Release

Contrails

by examination of the specimen in a measuring microscope. Optical measurement showed the distance error to be negligible.

4. Composition-Penetration Profiles

Five temperatures were used for diffusion treatments in this work. The times and temperatures of these treatments are given in Table 5. The composition-penetration profiles found on the five annealed specimens are given in Figures 2, 3, 4, 5 and 6. These figures contain the data points taken with respect to only one of the constituents. In nearly all cases the sum of the compositions of tungsten and ruthenium taken independently at a single point add to percentages between 99 and 101. Thus, only one set of data points are given. Examination of the couples at high magnifications yielded independent measurements of the position of phase boundaries. These measurements were easily correlated with the contamination spots of the electron microprobe to yield precise information on phase boundary positions, and hence, composition values.[5] The values obtained in this fashion are given at the phase boundary locations in Figures 2 through 6, and were found to check closely with those obtained by other extrapolation techniques on the same data as well as independent phase boundary measurements.[2] Figure 7 illustrates the correlation that may be made between the tungsten-ruthenium phase diagram 1955°C isotherm and the composition-penetration curve of the diffusion couple annealed at that same temperature.

C. Interdiffusion Coefficient Determinations

1. General

In analyzing for the interdiffusion coefficient in multiphase diffusion couples, it is acceptable to use the Boltzmann-Matano analysis only if diffusion is the rate limiting process (and not such processes as the nucleation of new phases etc.).[6,7] In applying the Boltzmann-Matano solution, one may analyze the entire profile ignoring the phase boundaries in order to establish the Matano interface and then perform the usual graphical operations in the

Approved for Public Release

Contrails

TABLE 5

TIMES AND TEMPERATURES OF ANNEALING TREATMENTS GIVEN TO COUPLES OF TUNGSTEN AND RUTHENIUM

Nominal Temperature (°C)	Temperature Deviation (°C)	Time of Anneal (hours)
1300	± 20	1750
1645	± 15	300
1785	± 15	168
1955	± 5	117
2025	± 10	63

Approved for Public Release

Contrails

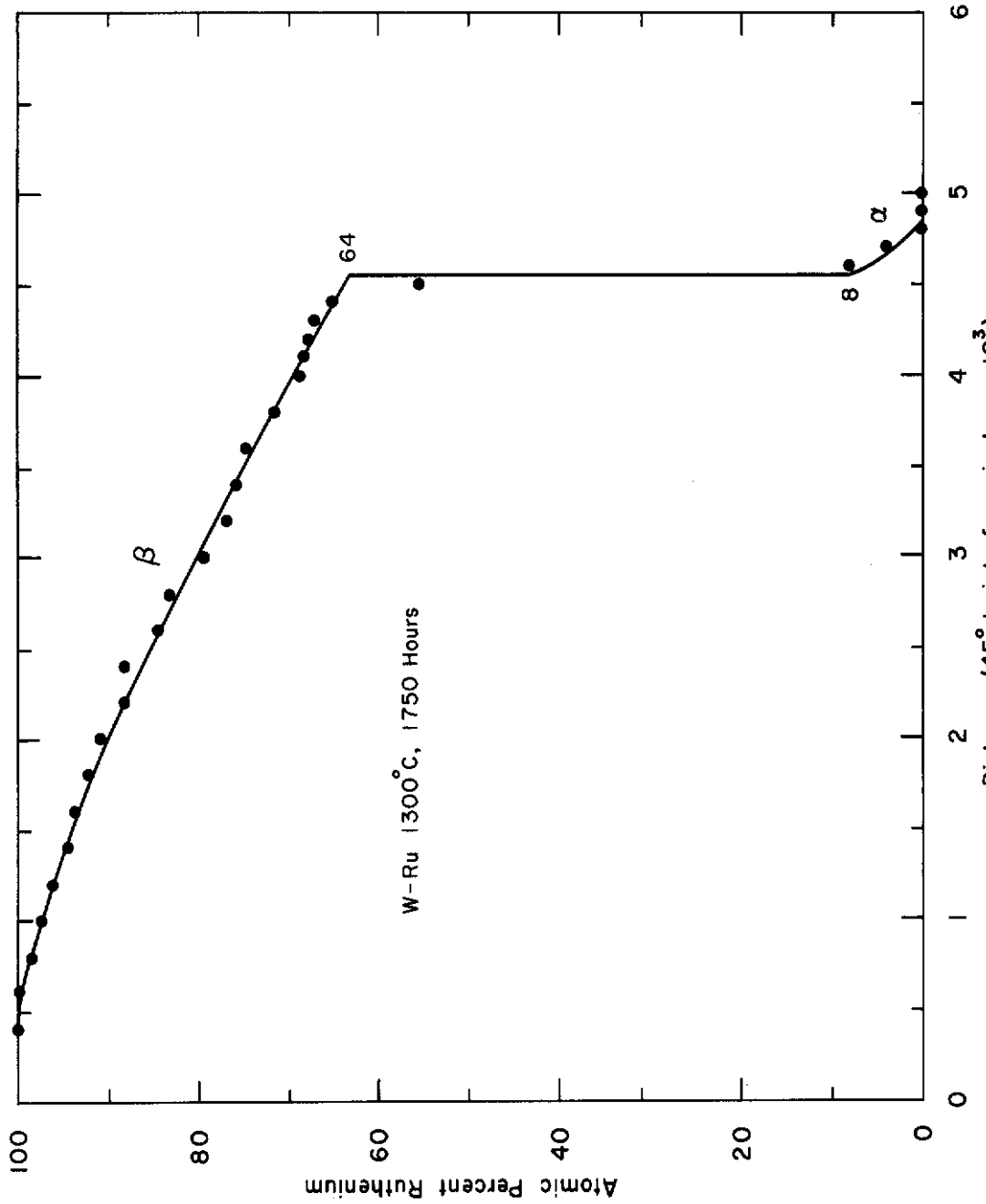

Figure 2. Composition vs Penetration Profile, W-Ru System, 1300°C

Approved for Public Release

Contrails

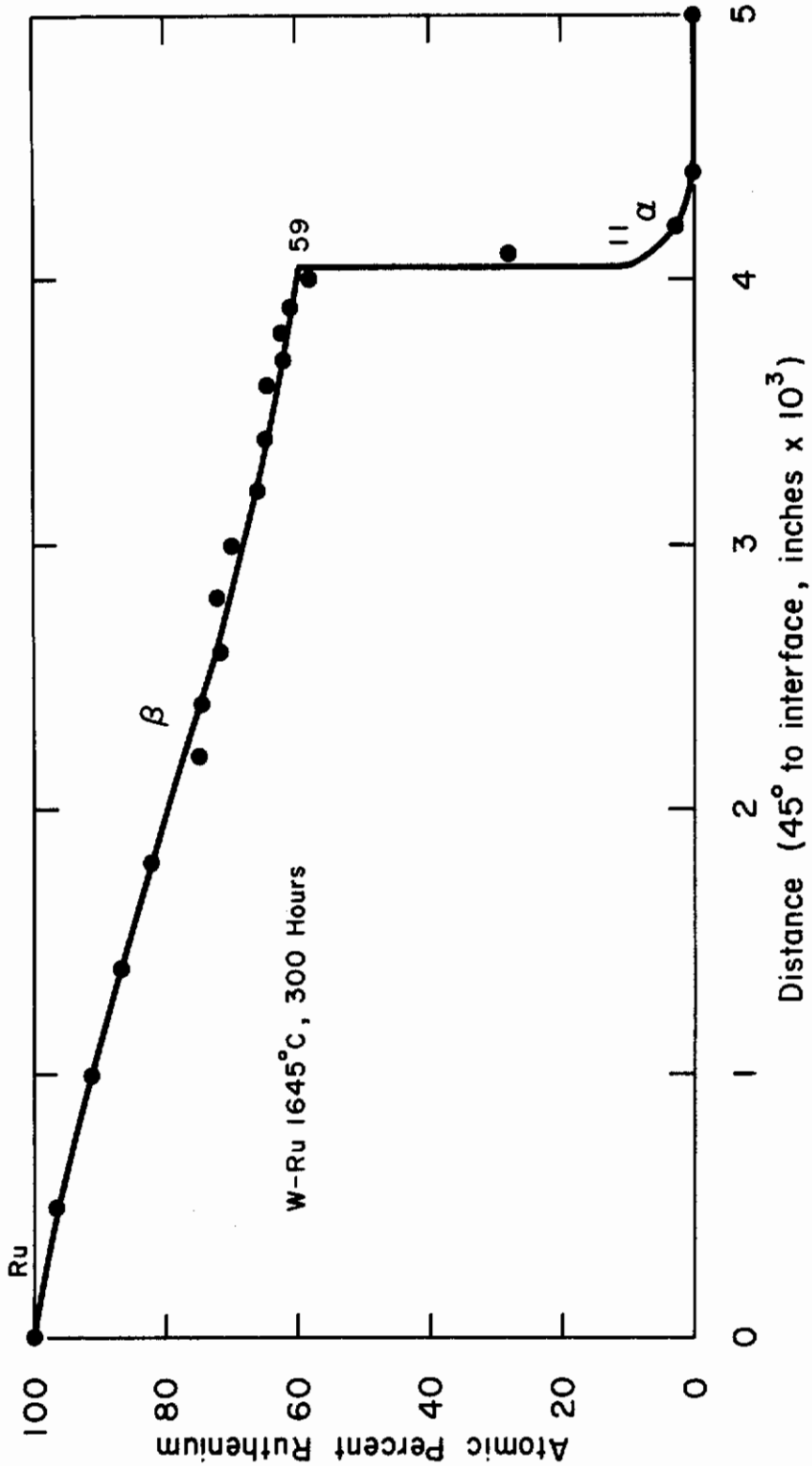

Figure 3. Composition vs Penetration Profile, W-Ru System, 1645°C.

Approved for Public Release

Contrails

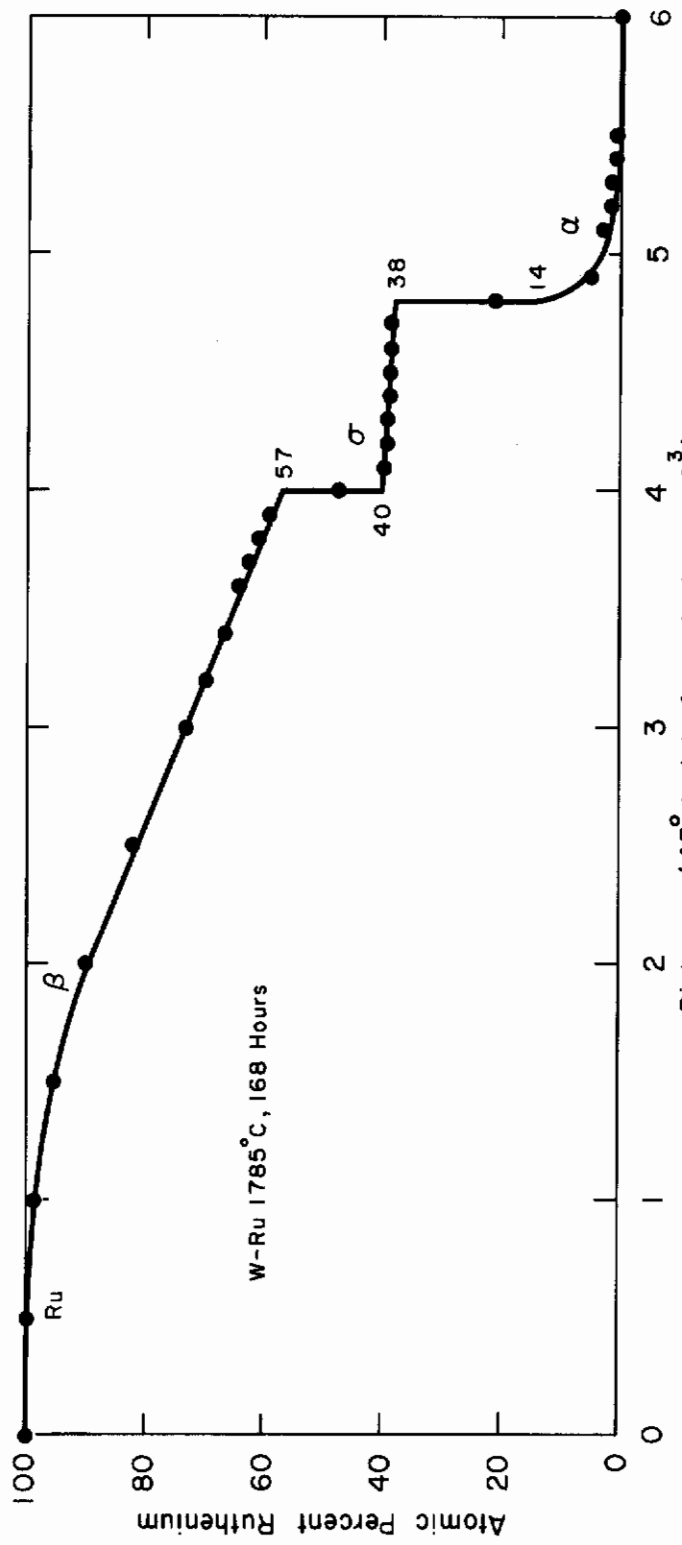

Figure 4. Composition vs. Penetration Profile, W-Ru System, 1785°C.

Approved for Public Release

Contrails

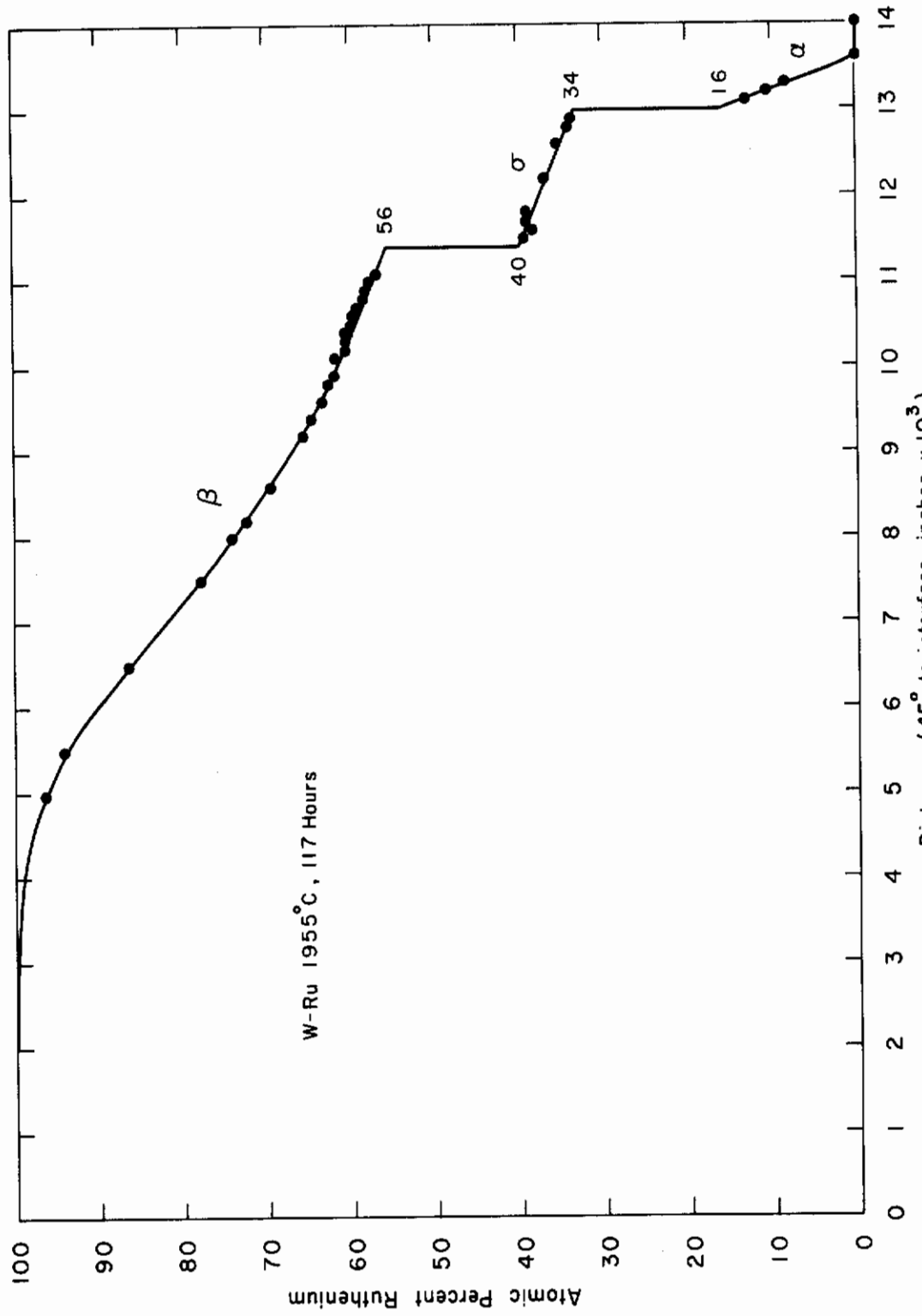

Figure 5. Composition vs Penetration Profile, W-Ru System, 1955°C.

Approved for Public Release

Contrails

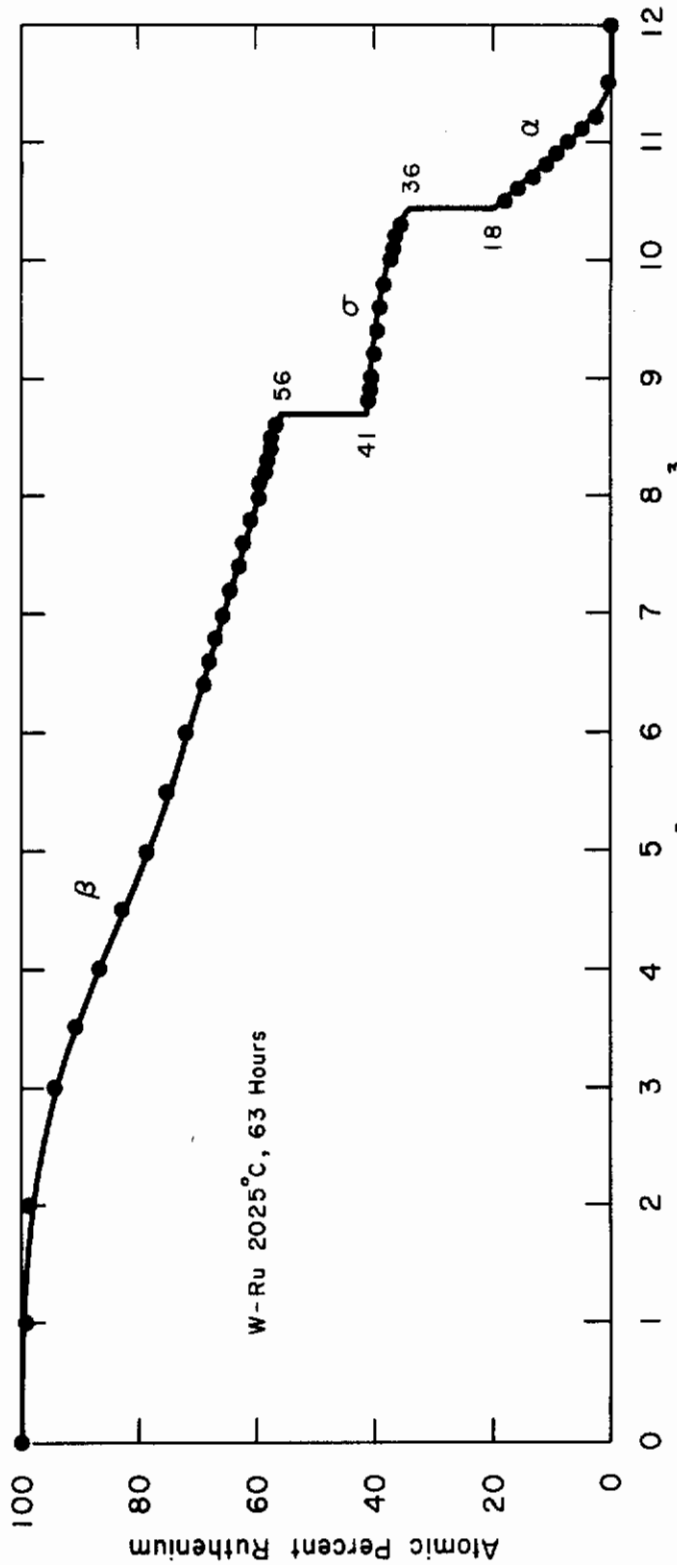

Figure 6. Composition vs Penetration Profile, W-Ru System, 2025°C.

Approved for Public Release

Contrails

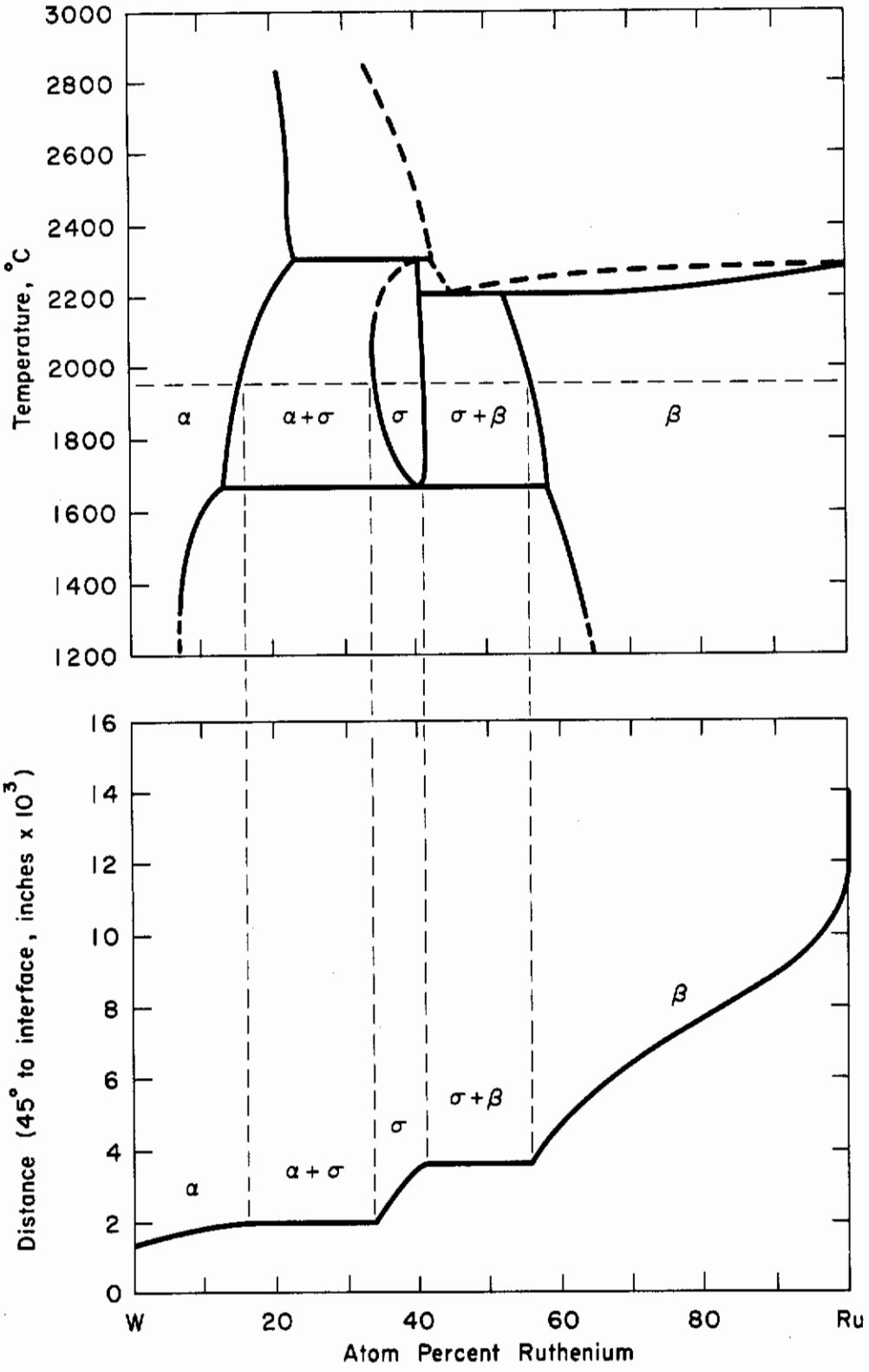

Figure 7. Illustration of the Correlation Between the W-Ru Phase Diagram and the Composition vs Distance Curve of the Diffusion Couple Annealed at 1955°C.

Approved for Public Release

Contrails

normal fashion.

One may establish that diffusion is the rate limiting process by noting the variation of the intermediate phase thickness with time (it should be parabolic) or by ascertaining that the phase in question has at its boundaries the equilibrium concentrations for the phase boundaries of the phase in question.

It was this second concept which was utilized primarily in this work. The phase boundary values obtained from the discontinuities of the concentration vs distance plots of **Figures 2 - 6** were found to agree quite well with those obtained by normal metallographic and X-ray techniques, as well as with those obtained from microprobe analysis of equilibrated two-phase alloys.[2]

Although it is not necessary that all phases present in the equilibrium diagram appear in the diffusion zone between two elements,[8] this circumstance fortunately occurred in this case. Thus, diffusion data for all stable phases in this system were available from couples of the pure elements.

2. Boltzmann-Matano Solution for Interdiffusion Coefficient

Among the most satisfactory methods for obtaining interdiffusion coefficient values from composition-distance profiles is the Boltzmann-Matano analysis. This solution of Fick's first law results in the expression

$$\tilde{D} = -\frac{1}{2t}\frac{dx}{dc}\int_{c_i}^{c} x\,dc \qquad \text{Eq(1)}$$

where: $\tilde{D}$ = the interdiffusion coefficient in $cm^2/sec.$,

t = the time in seconds,

x = the distance in cm perpendicular to the diffusion interface,

c = the concentration in amount per unit volume at the point of interest,

c_i = the concentration in amount per unit volume at the reference concentration.

Approved for Public Release

Contrails

The techniques generally utilized in applying this solution to the composition-distance profiles experimentally determined involve graphical operations to obtain the components of the interdiffusion coefficient expression above; i.e., the slope of the composition-distance curve at the composition of interest, and the area expressed by the integral.[9]

This graphical procedure was followed in the case of the five couples analyzed in this work, but only as a check upon the primary analysis technique. For the principal determination of the interdiffusion coefficients, the Boltzmann-Matano solution of Fick's first law was numerically determined with an IBM 7090 digital computer in the following fashion:

(1) The raw data were plotted manually on probability paper to determine if an error function relationship was obtained between composition and distance. (In all cases in this work, the data in a given phase field fell onto no more than two straight line segments on such a plot.)

(2) The raw data were placed into the computer for a least square analysis to obtain the straight line segments of the inverse error function plots.

(3) The computer regenerated the composition versus distance data at regular intervals, found the Matano interface by numerical integration, found the slope of the concentration-penetration curve at each interval, and integrated the curve to each interval point to obtain the integral factor in the Boltzmann-Matano solution.

(4) The values of the various factors comprising the interdiffusion coefficient were then multiplied, and a printed record of the interdiffusion coefficient versus concentration in one atom percent steps in each phase was obtained.

Approved for Public Release

Contrails

A detailed accounting of this procedure is given in Appendix I by C. S. Hartley, who in collaboration with K. Hubbard devised this scheme.

D. Results and Discussion

1. Interdiffusion Coefficient as a Function of Composition

The data points of Figures 2 through 6 were processed in a computer to yield the interdiffusion coefficient as a function of composition in each of the three phases of this system. Interdiffusion coefficients vs composition are tabulated in Table 6 for the profiles of Figures 2, 3, 4, 5, and 6. The computer results of the interdiffusion coefficients for a single phase field exhibit discontinuities. The exact reasons for these discontinuities are not known but believed to be associated with the arbitrarily imposed boundary conditions for the computer programming.

2. Variation of Interdiffusion Coefficients with Temperature

It has been common practice[6,7] to represent the variation of the interdiffusion coefficient with temperature by an equation of the form:

$$\widetilde{D} = D_o e^{-Q/RT} \qquad \text{Eq(2)}$$

where

$\widetilde{D}$ = interdiffusion coefficient (cm^2/sec.)

D_o = frequency factor (cm^2/sec.)

Q = activation energy for diffusion (cal./mole)

R = gas constant (cal/mole - ^oK)

T = temperature (^oK)

It has also been common practice to represent the temperature dependence of the intrinsic and self-diffusion coefficients by the same form exponential expression. These relationships are mutually exclusive, strictly speaking, because in combination they require a

Approved for Public Release

Contrails

TABLE 6

INTERDIFFUSION COEFFICIENTS OF THE W-Ru SYSTEM
FOR DIFFERENT COMPOSITIONS AT SEVERAL TEMPERATURES

Annealing Temperature (^{o}C)	Annealing Time (hrs.)	Phase	Composition (a/o Ru)	Interdiffusion Coefficient, $\tilde{D}$ ($cm^2/hr.$)
2025	63	β Ru	99	1.00×10^{-7}
			98	1.10×10^{-7}
			97	1.18×10^{-7}
			96	1.25×10^{-7}
			95	1.32×10^{-7}
			94	1.38×10^{-7}
			93	1.44×10^{-7}
			92	1.50×10^{-7}
			91	1.56×10^{-7}
			90	1.61×10^{-7}
			89	1.67×10^{-7}
			88	1.73×10^{-7}
			87	1.79×10^{-7}
			86	1.85×10^{-7}
			85	1.92×10^{-7}
			84	1.98×10^{-7}
			83	2.05×10^{-7}
			82	2.12×10^{-7}
			81	2.20×10^{-7}
			80	2.27×10^{-7}
			79	2.36×10^{-7}
			78	2.44×10^{-7}
			77	2.53×10^{-7}
			76	2.63×10^{-7}
			75	2.74×10^{-7}
			74	2.86×10^{-7}
			73	2.98×10^{-7}
			72	3.12×10^{-7}
			71	3.28×10^{-7}
			70	3.46×10^{-7}
			69	3.66×10^{-7}
			68	3.89×10^{-7}
			67	4.17×10^{-7}
			66	4.51×10^{-7}
			65	4.94×10^{-7}
			64	5.52×10^{-7}
			63	6.34×10^{-7}
			62	7.68×10^{-7}

(Table continued on next page.)

Approved for Public Release

Contrails

TABLE 6 (continued)

Annealing Temperature (°C)	Annealing Time (hrs.)	Phase	Composition (a/o Ru)	Interdiffusion Coefficient, $\tilde{D}$ ($cm^2/hr.$)
2025	63	β Ru	61	1.05×10^{-6}
			60	3.07×10^{-6}
		σ + β Ru	59-42	2Ø
		σ	41	7.97×10^{-7}
			40	7.93×10^{-7}
			39	7.87×10^{-7}
			38	7.80×10^{-7}
			37	7.70×10^{-7}
		αW + σ	36-22	2Ø
		αW	21	5.08×10^{-8}
			20	4.84×10^{-8}
			19	4.63×10^{-8}
			18	4.43×10^{-8}
			17	4.23×10^{-8}
			16	4.05×10^{-8}
			15	3.88×10^{-8}
			14	3.71×10^{-8}
			13	3.55×10^{-8}
			12	3.40×10^{-8}
			11	3.24×10^{-8}
			10	3.10×10^{-8}
			9	2.95×10^{-8}
			8	2.81×10^{-8}
			7	2.66×10^{-8}
			6	2.52×10^{-8}
			5	2.37×10^{-8}
			4	2.22×10^{-8}
			3	2.05×10^{-8}
			2	1.86×10^{-8}
			1	1.62×10^{-8}
1955	117	β Ru	99	5.39×10^{-8}
			98	6.13×10^{-8}
			97	6.71×10^{-8}
			96	7.23×10^{-8}
			95	7.70×10^{-8}
			94	8.16×10^{-8}
			93	8.60×10^{-8}
			92	9.03×10^{-8}
			91	9.46×10^{-8}
			90	9.88×10^{-8}

(Table continued on next page.)

Approved for Public Release

Contrails

TABLE 6 (continued)

Annealing Temperature (°C)	Annealing Time (hrs.)	Phase	Composition (a/o Ru)	Interdiffusion Coefficient, $\tilde{D}$ ($cm^2/hr.$)
1955	117	β Ru	89	1.03×10^{-7}
			88	1.08×10^{-7}
			87	1.12×10^{-7}
			86	1.16×10^{-7}
			85	1.21×10^{-7}
			84	1.26×10^{-7}
			83	1.31×10^{-7}
			82	1.36×10^{-7}
			81	1.42×10^{-7}
			80	1.47×10^{-7}
			79	1.53×10^{-7}
			78	1.59×10^{-7}
			77	1.66×10^{-7}
			76	1.72×10^{-7}
			75	1.80×10^{-7}
			74	1.87×10^{-7}
			73	1.96×10^{-7}
			72	2.04×10^{-7}
			71	2.14×10^{-7}
			70	2.24×10^{-7}
			69	2.35×10^{-7}
			68	2.47×10^{-7}
			67	2.60×10^{-7}
			66	2.75×10^{-7}
			65	2.91×10^{-7}
			64	3.09×10^{-7}
			63	3.29×10^{-7}
			62	3.52×10^{-7}
			61	3.78×10^{-7}
			60	4.07×10^{-7}
			59	4.40×10^{-7}
			58	4.78×10^{-7}
			57	5.18×10^{-7}
		σ + β Ru	56-41	2Ø
		σ	40	3.28×10^{-7}
			39	3.39×10^{-7}
			38	3.37×10^{-7}
			37	3.34×10^{-7}
			36	3.31×10^{-7}
			35	3.27×10^{-7}
			34	3.23×10^{-7}

(Table continued on next page.)

Approved for Public Release

Contrails

TABLE 6 (continued)

Annealing Temperature (°C)	Annealing Time (hrs.)	Phase	Composition (a/o Ru)	Interdiffusion Coefficient, $\tilde{D}$ (cm^2/hr.)
1955	117	αW + σ	33-18	2Ø
		αW	17	1.25×10^{-8}
			16	1.23×10^{-8}
			15	1.20×10^{-8}
			14	1.18×10^{-8}
			13	1.16×10^{-8}
			12	1.31×10^{-8}
			11	1.11×10^{-8}
			10	1.08×10^{-8}
			9	1.06×10^{-8}
			8	1.03×10^{-8}
			7	1.00×10^{-8}
			6	9.72×10^{-9}
			5	9.41×10^{-9}
			4	9.07×10^{-9}
			3	8.68×10^{-9}
			2	8.22×10^{-9}
			1	7.57×10^{-9}
1785	168	β Ru	99	1.58×10^{-8}
			98	1.60×10^{-8}
			97	1.61×10^{-8}
			96	1.61×10^{-8}
			95	1.62×10^{-8}
			94	1.62×10^{-8}
			93	1.62×10^{-8}
			92	1.62×10^{-8}
			91	1.63×10^{-8}
			90	1.63×10^{-8}
			89	1.63×10^{-8}
			88	1.63×10^{-8}
			87	1.63×10^{-8}
			86	1.64×10^{-8}
			85	1.64×10^{-8}
			84	1.64×10^{-8}
			83	1.64×10^{-8}
			82	1.64×10^{-8}
			81	1.64×10^{-8}
			80	1.64×10^{-8}
			79	1.65×10^{-8}
			78	1.65×10^{-8}
			77	1.65×10^{-8}
			76	3.07×10^{-8}

(Table continued on next page.)

Approved for Public Release

Contrails

TABLE 6 (continued)

Annealing Temperature (°C)	Annealing Time (hrs.)	Phase	Composition (a/o Ru)	Interdiffusion Coefficient, $\tilde{D}$ (cm^2/hr.)
1785	168	β Ru	75	3.07×10^{-8}
			74	3.07×10^{-8}
			73	3.07×10^{-8}
			72	3.06×10^{-8}
			71	3.05×10^{-8}
			70	3.04×10^{-8}
			69	3.03×10^{-8}
			68	3.02×10^{-8}
			67	3.01×10^{-8}
			66	2.99×10^{-8}
			65	2.98×10^{-8}
			64	2.96×10^{-8}
			63	2.94×10^{-8}
			62	2.92×10^{-8}
			61	2.89×10^{-8}
			60	2.87×10^{-8}
			59	2.84×10^{-8}
			58	2.82×10^{-8}
		σ + β Ru	57-40	2Ø
		σ	39	2.19×10^{-7}
			38	3.40×10^{-8}
		αW + σ	37-7	2Ø
		αW	6	5.01×10^{-9}
			5	5.02×10^{-9}
			4	5.02×10^{-9}
			3	5.03×10^{-9}
			2	5.04×10^{-9}
			1	5.05×10^{-9}
1645	300	β Ru	99	1.20×10^{-8}
			98	1.20×10^{-8}
			97	1.21×10^{-8}
			96	1.21×10^{-8}
			95	1.21×10^{-8}
			94	1.21×10^{-8}
			93	1.22×10^{-8}
			92	1.22×10^{-8}
			91	1.22×10^{-8}
			90	1.22×10^{-8}
			89	1.22×10^{-8}
			88	1.22×10^{-8}
			87	1.23×10^{-8}
			86	1.23×10^{-8}

(Table continued on next page.)

Approved for Public Release

Contrails

TABLE 6 (continued)

Annealing Temperature (^{o}C)	Annealing Time (hrs.)	Phase	Composition (^{a}/o Ru)	Interdiffusion Coefficient, $\tilde{D}$ (cm^2/hr.)
1645	300	β Ru	85	1.23×10^{-8}
			84	1.23×10^{-8}
			83	1.23×10^{-8}
			82	1.23×10^{-8}
			81	1.24×10^{-8}
			80	1.24×10^{-8}
			79	1.24×10^{-8}
			78	1.24×10^{-8}
			77	3.60×10^{-8}
			76	3.61×10^{-8}
			75	3.60×10^{-8}
			74	3.59×10^{-8}
			73	3.57×10^{-8}
			72	3.55×10^{-8}
			71	3.53×10^{-8}
			70	3.50×10^{-8}
			69	3.46×10^{-8}
			68	3.42×10^{-8}
			67	3.38×10^{-8}
			66	3.34×10^{-8}
			65	3.28×10^{-8}
			64	3.23×10^{-8}
			63	3.18×10^{-8}
			62	3.11×10^{-8}
			61	3.05×10^{-8}
		αW + β Ru	60-12	2Ø
		αW	11	4.96×10^{-10}
			10	4.87×10^{-10}
			9	4.78×10^{-10}
			8	4.69×10^{-10}
			7	4.59×10^{-10}
			6	4.49×10^{-10}
			5	4.38×10^{-10}
			4	4.26×10^{-10}
			3	4.12×10^{-10}
			2	3.96×10^{-10}
			1	3.74×10^{-10}
1300	1750	β Ru	99	---------
			98	1.50×10^{-9}
			97	1.72×10^{-9}
			96	1.92×10^{-9}
			95	2.10×10^{-9}

(Table continued on next page.)

Approved for Public Release

Contrails

TABLE 6 (continued)

Annealing Temperature (°C)	Annealing Time (hrs.)	Phase	Composition (a/o Ru)	Interdiffusion Coefficient, $\tilde{D}$ ($cm^2/hr.$)
1300	1750	β Ru	94	2.27×10^{-9}
			93	2.44×10^{-9}
			92	2.60×10^{-9}
			91	2.76×10^{-9}
			90	2.91×10^{-9}
			89	3.06×10^{-9}
			88	3.19×10^{-9}
			87	3.32×10^{-9}
			86	3.43×10^{-9}
			85	3.52×10^{-9}
			84	3.59×10^{-9}
			83	3.64×10^{-9}
			82	3.66×10^{-9}
			81	3.66×10^{-9}
			80	3.64×10^{-9}
			79	3.60×10^{-9}
			78	3.53×10^{-9}
			77	3.45×10^{-9}
			76	3.36×10^{-9}
			75	3.26×10^{-9}
			74	3.15×10^{-9}
			73	3.04×10^{-9}
			72	2.92×10^{-9}
			71	2.79×10^{-9}
			70	2.68×10^{-9}
			69	2.56×10^{-9}
			68	2.45×10^{-9}
			67	2.35×10^{-9}
			66	2.24×10^{-9}
			65	2.13×10^{-9}
			64	2.04×10^{-9}
		αW + β Ru	63-10	2Ø
		αW	9	4.65×10^{-11}
			8	4.56×10^{-11}
			7	4.46×10^{-11}
			6	4.36×10^{-11}
			5	4.25×10^{-11}
			4	4.14×10^{-11}
			3	3.96×10^{-11}
			2	3.80×10^{-11}
			1	3.66×10^{-11}

Approved for Public Release

Contrails

single exponential, variable in the temperature, to equal the sum of two other exponentials, also variable in temperature. Excepting the trivial case where all three activation energies are equal, this is not a realizable condition, as may be seen from a power expansion of the exponential relationships substituted into the Darken[9] equation

$$D = n_A D_B + n_B D_A \qquad \text{Eq(3)}$$

where: n_A and n_B are the mole fractions of elements A and B, and D_A and D_B are the intrinsic diffusion coefficients of A and B.

Although thorium oxide chips were placed at the interfaces of some of the diffusion couples in an effort to determine the interface motion, these procedures were fruitless. No trace of the original interface nor of the added thorium oxide was obtained. Therefore, the values for the intrinsic diffusion coefficients were unavailable.

Plots of the logarithm of the interdiffusion coefficient versus reciprocal temperature were made for various compositions across the phase diagram. These are presented for a composition in each phase field in Figures 8 and 9.

It is to be noted that the data of Figures 8 and 9 do not all fall on straight lines. This has been observed in other work and has been the subject of critical discussion.[10] In general, this condition may arise because the exponential relationship of D and 1/T is not correct; because the activation energy of the process is not constant with temperature; or because the data is faulty. In the plots of Figures 8 and 9, little weight was given to questionable data so that more realistic curves might be obtained.

A summary of the interdiffusion coefficient values for selected compositions in each phase field is given in Table 7. The activation energies, Q, and the frequency factors, D_o, that are listed in this table were obtained from the slopes of plots such as are given in Figures 8 and 9. The slopes of these curves were taken at the high temperature regions in all cases, as the diffusion zones were broader and considered somewhat more reliable. From the way the curves are formed, it should be noted that such a procedure gives a maximum value of both Q and D_o for the temperature interval studied.

Approved for Public Release

Contrails

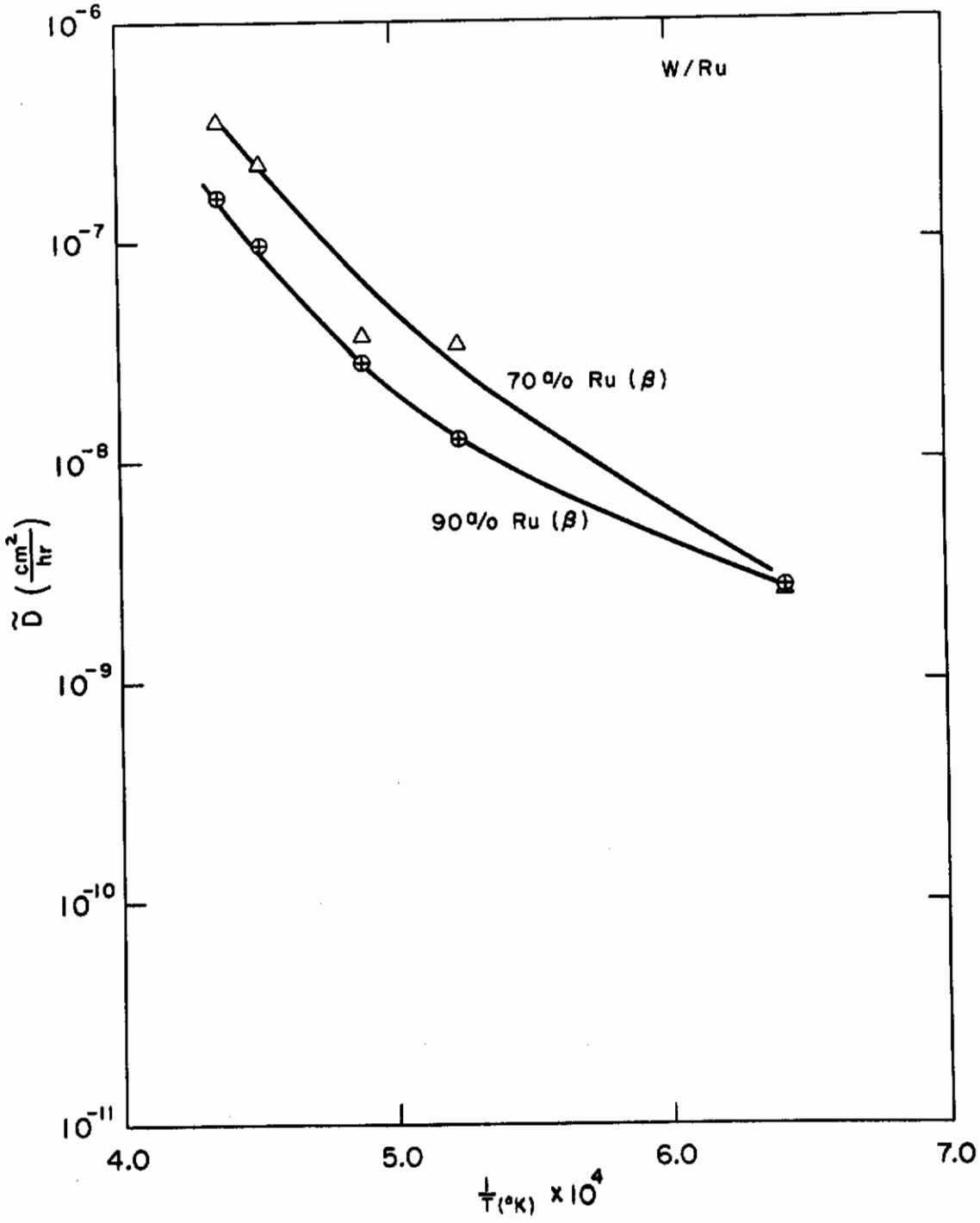

Figure 8. Plot of Logarithm of the Interdiffusion Coefficient vs Reciprocal Temperature for Couples in the W-Ru System.

Approved for Public Release

Contrails

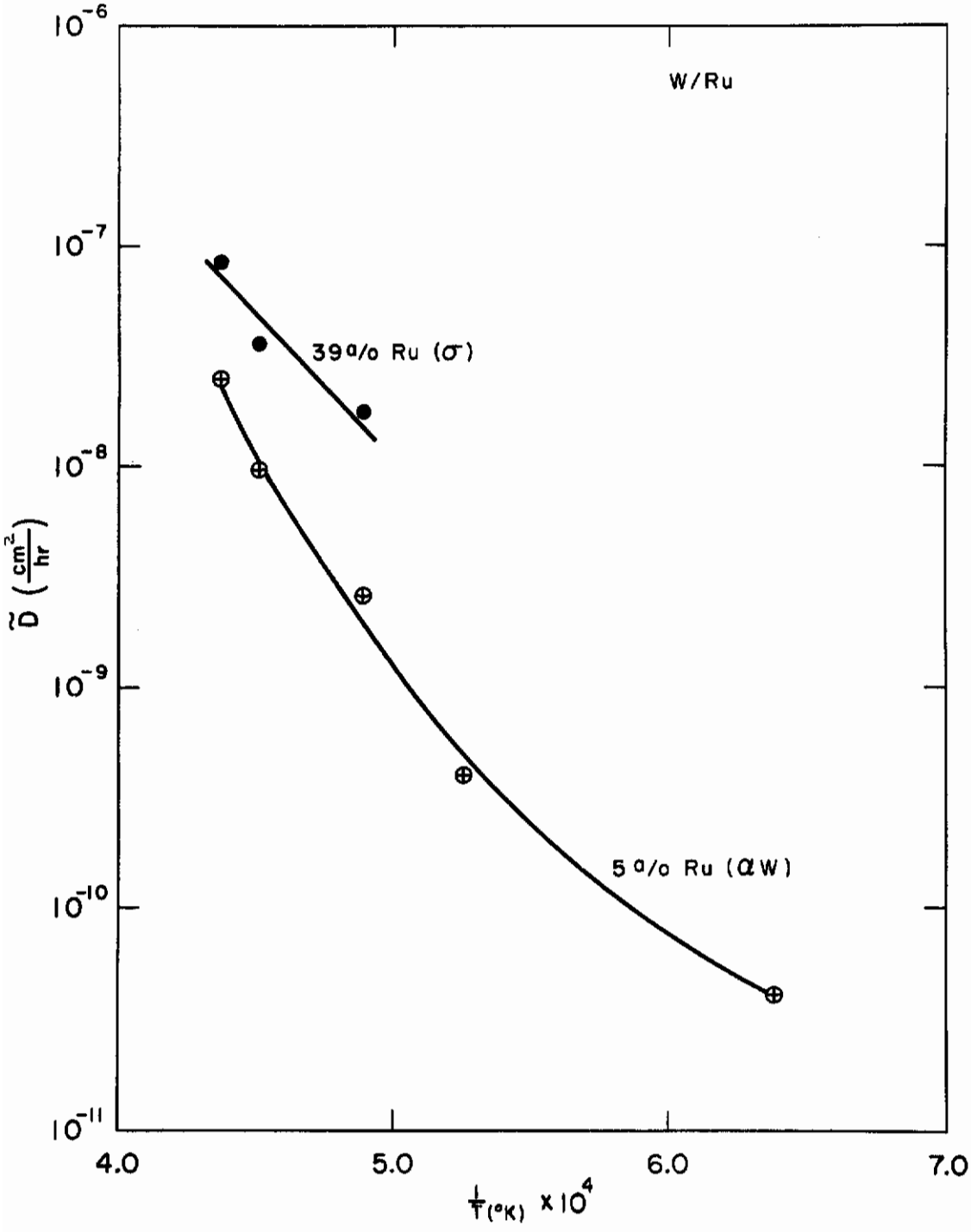

Figure 9. Plot of the Logarithm of the Interdiffusion Coefficient vs Reciprocal Temperature for Couples in the W-Ru System.

Approved for Public Release

TABLE 7

TABULATION OF W-Ru DIFFUSION RESULTS

Temp. (°C)	Time (hrs.)	Grade of Couple*	Interdiffusion Coefficients (cm^2/hr.)				Comments
			5[a]/o Ru α	39[a]/o α	70[a]/o β	90[a]/o β	
1300	1750	B +	4.3×10^{-11}	- -	2.7×10^{-9}	2.9×10^{-9}	0.003 in. zone
1645	300	B +	4.1×10^{-10}	- -	3.5×10^{-8}	1.3×10^{-8}	0.003 in. zone
1785	168	B +	2.6×10^{-9}	1.7×10^{-7}	3.9×10^{-7}	2.8×10^{-8}	
1955	117	B +	9.4×10^{-9}	3.4×10^{-7}	2.2×10^{-7}	9.9×10^{-8}	
2025	63	A	2.4×10^{-8}	7.9×10^{-7}	3.5×10^{-7}	1.6×10^{-7}	0.006 in. zone
			93,500	61,000	49,500	57,200	Q values, cal_s/mole
			20	0.044	0.063	0.037	D_o values (cm^2/hr.)

* Grades indicate quality of diffusion zones.

Approved for Public Release

Confidential

Contrails

IV. DIFFUSION IN THE SYSTEM TUNGSTEN-IRIDIUM

A. Diffusion Couple Preparation and Treatment

1. Material

The iridium used in both the standards and the diffusion couples was obtained as powder of purity greater than 99.9 percent from Bishop and Co. The tungsten used is that described in Section III.A.1. A typical analysis of the iridium used is given in Table 8.

2. Arc-Melting

Arc-melting was performed under conditions virtually identical to those described in Section III.A.2 for the tungsten-ruthenium system. As with the tungsten-ruthenium system, weight balances were taken with the tungsten-iridium system to establish maximum composition deviations for the standards. The standards in this system were arc-melted of premelted pellets to minimize weight losses. This procedure differed from the melting of mixed powders in the W-Ru system.

The inherent disadvantage in this technique is the difficulty of producing an alloy with exactly the desired composition. On the other hand, although it is easier to weigh exactly a predetermined amount of powder, the rather large losses which attend the melting of powder compacts make it somewhat inferior to the technique of continuing premelted pellets. Table 9 shows W-Ir standard results.

3. Bonding of Couples

The couples of the W-Ir system were bonded into three layered sandwiches as described in the section on the W-Ru system III.A.3.

4. Annealing

The comments of Section III.A.4 on the W-Ru system apply here also.

Approved for Public Release

Contrails

TABLE 8

TYPICAL ANALYSIS OF IRIDIUM USED

Impurity Element	Contents Expressed in ppm
Al	3
Cu	3
Fe	50
Pb	--
Mg	10
Mn	--
Si	30
Ag	1
Sn	--
Pt	50
Pd	1
Rh	200
Ru	--

TABLE 9

COMPOSITIONS AND TOLERANCES OF W-Ir COMPOSITION STANDARDS

Minimum ^{a}/o Ir	Maximum ^{a}/o Ir	Nominal ^{a}/o Ir	Tolerance ^{a}/o Ir
5.04	5.23	5.14	± 0.10
25.29	25.30	25.29	± 0.01
40.56	40.64	40.60	± 0.04
54.61	54.78	54.70	± 0.09
69.12	69.49	69.30	± 0.19
93.95	94.01	93.98	± 0.03

Approved for Public Release

Contrails

5. Sectioning

The couples of the W-Ir system were sectioned as described in the section on the W-Ru system (III.A.5).

B. Determination of Composition Profiles

In almot all details the determination of the W-Ir composition profiles parallel the determination of those in the W-Ru system described in Sections III.B.1 and III.B.2.

A plot of the normalized X-ray intensities of the W-Ir standards versus composition is given in Figure 10. The composition-penetration profiles determined for the seven annealed specimens are given in Figures 11, 12, 13, 14, 15, 16, and 17. The times and temperatures of these seven annealing treatments are given in Table 10.

C. Interdiffusion Coefficient Determinations

Comparison of the phase boundary values given in Figures 11 through 17 with the W-Ir phase diagram (see Appendix II) shows the presence of all equilibrium phases with equilibrium boundary values. These composition correlations indicate that the reactions were diffusion controlled in this system also.

The computer methods for solving the Boltzmann-Matano expression for the interdiffusion coefficient as described in Section III.C.2 for the W-Ru system were also employed on the profiles of the W-Ir couples.

D. Results and Discussion

The profile data of Figures 11 through 17 were processed by a computer to yield the interdiffusion coefficients as functions of composition in each of the four phases of this system. Interdiffusion coefficient versus composition are tabulated in Table 11 for the profiles of Figures 11 through 17. Discontinuities of the interdiffusion coefficients within a single phase region have been discussed in Section III.D.1 of the W-Ru system.

Plots of the logarithm of the interdiffusion coefficient versus reciprocal temperature were made for various compositions in the single phase fields across the diagram. These are presented in Figures 18 and 19.

Approved for Public Release

Contrails

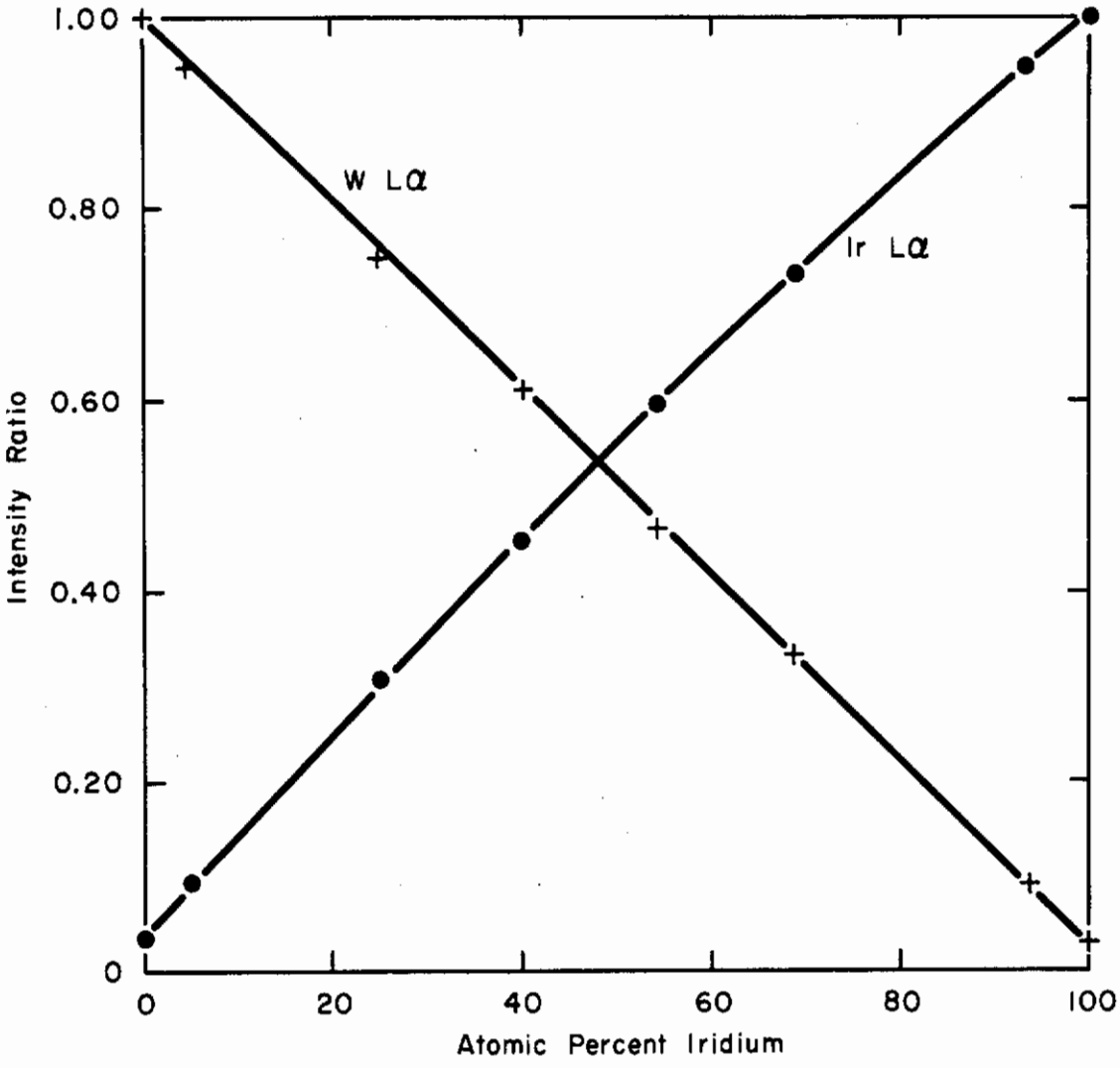

Figure 10. Plot of Normalized Intensity of Characteristic Radiation of Ir and W vs Composition. The Lα lines of both elements were used.

Approved for Public Release

Contrails

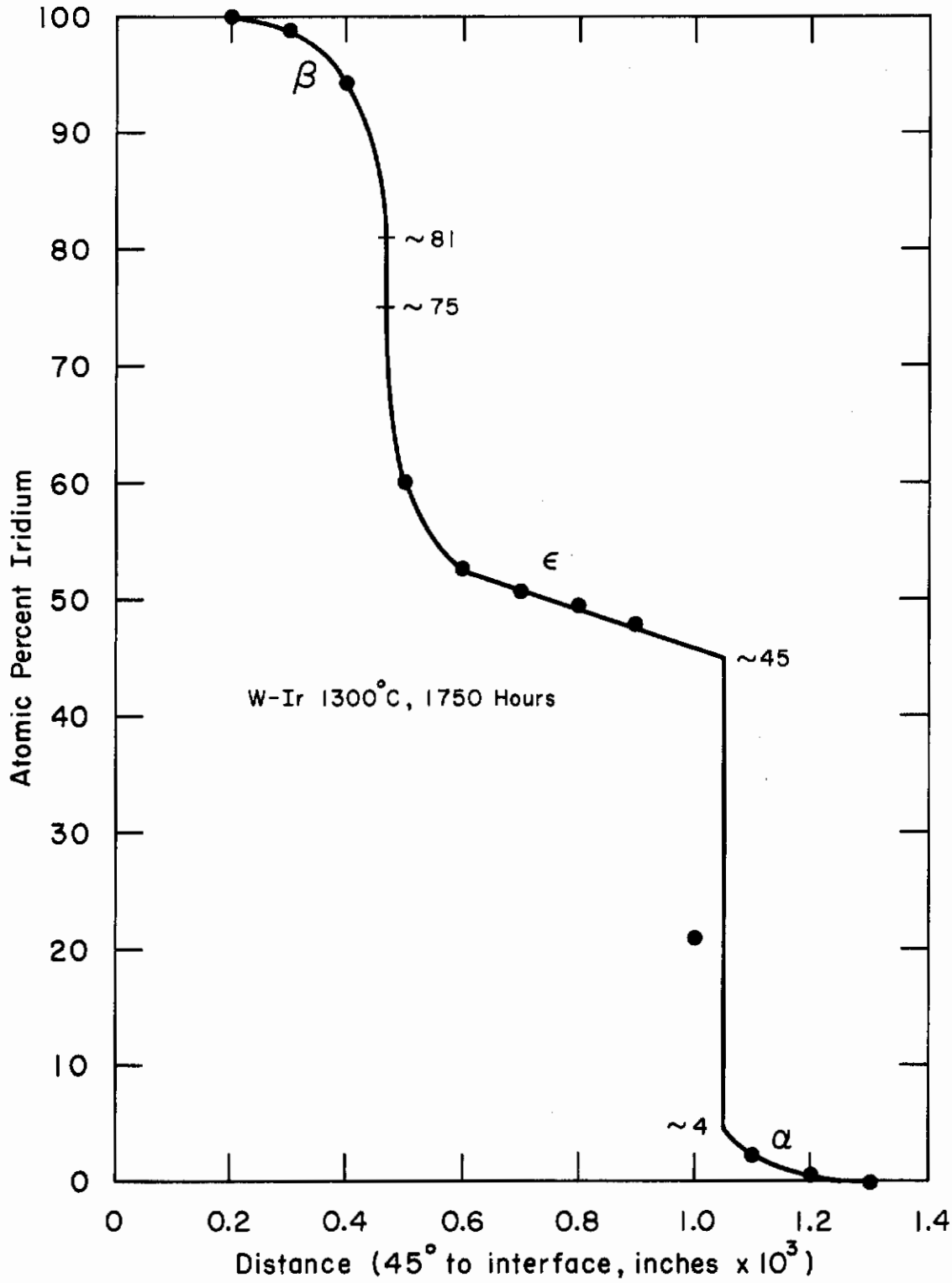

Figure 11. Composition vs Penetration Profile, W-Ir System, 1300°C.

Approved for Public Release

Contrails

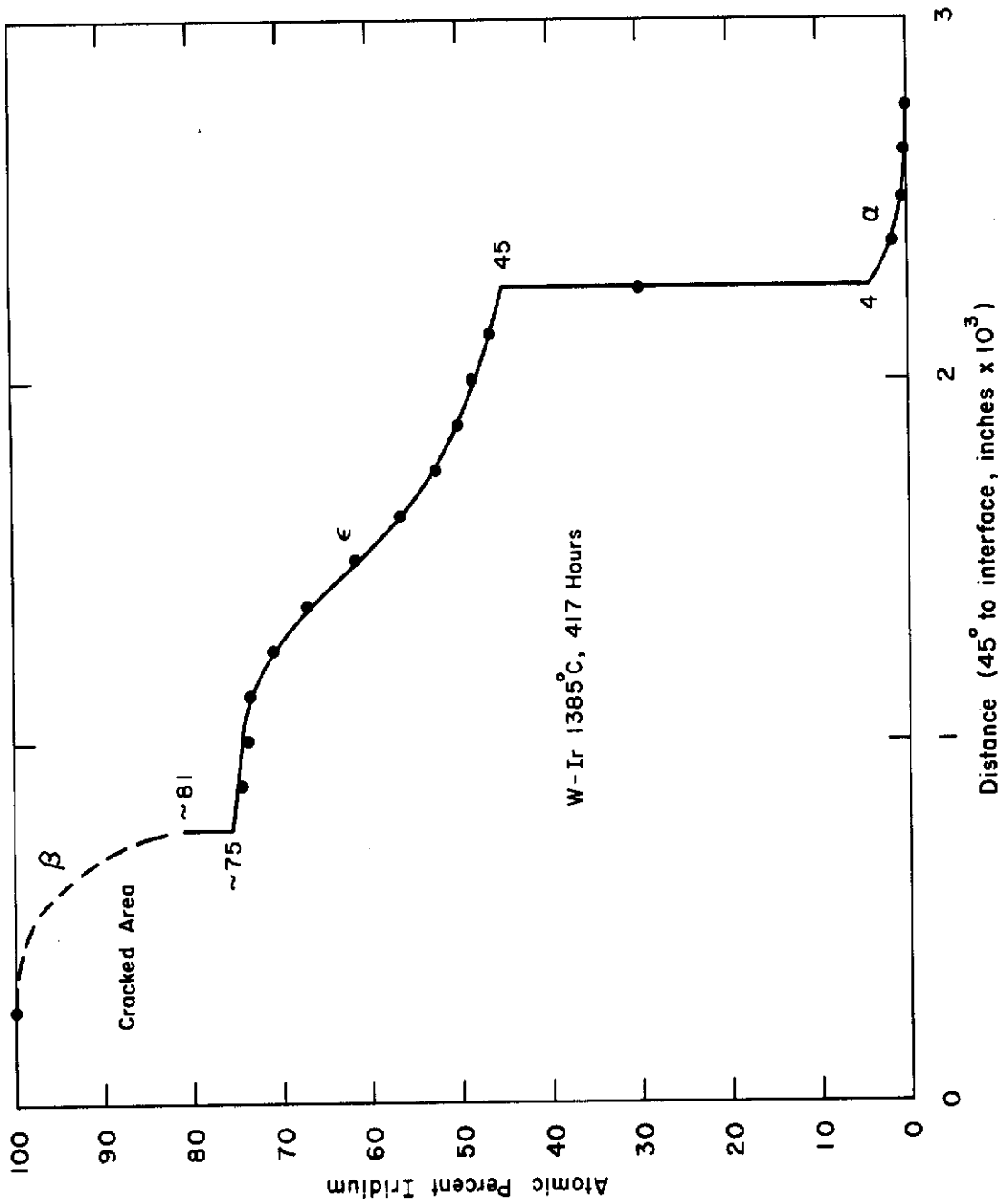

Figure 12. Composition vs. Penetration Profile, W-Ir System, 1385°C.

Approved for Public Release

Contrails

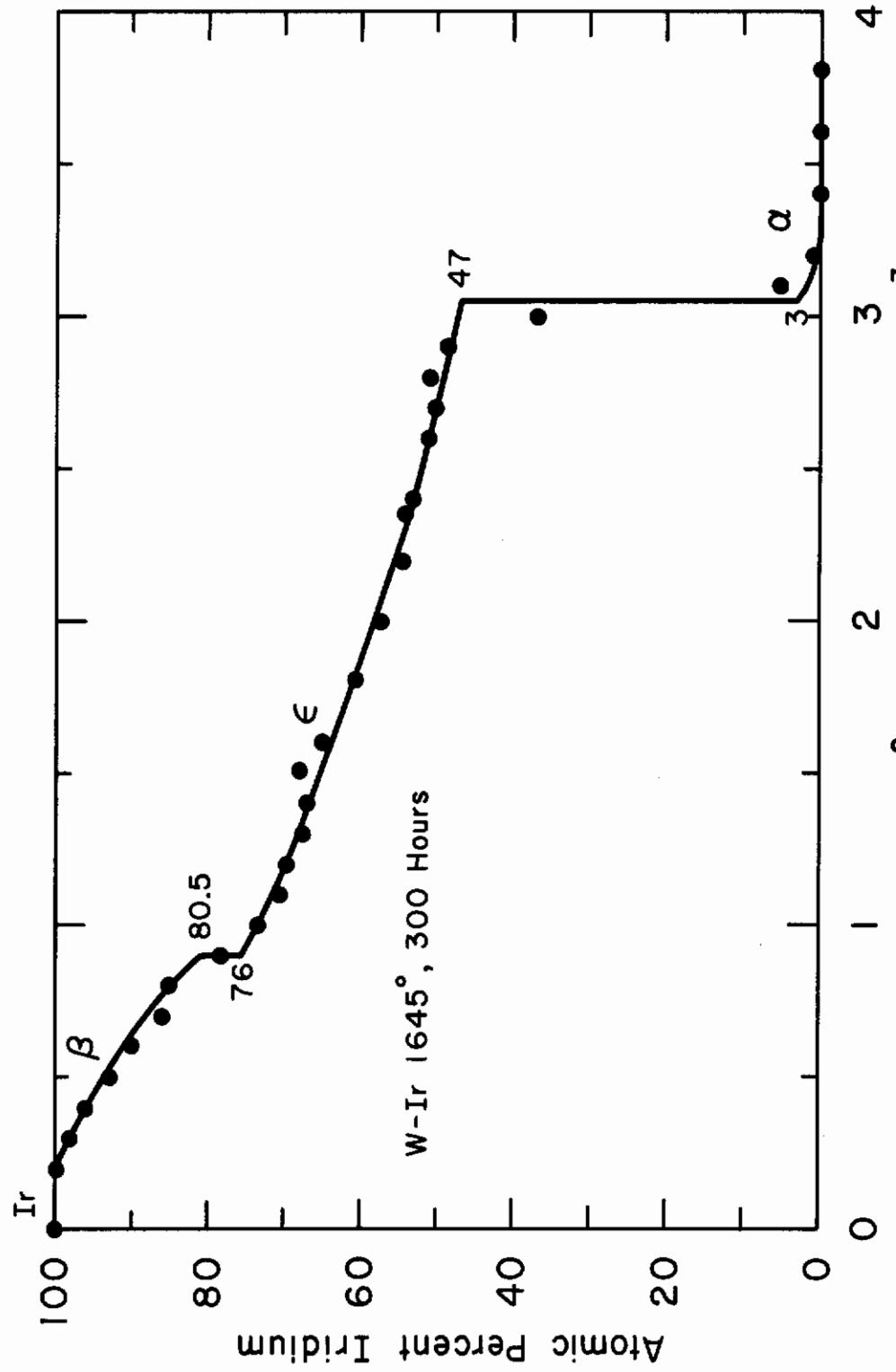

Figure 13. Composition vs Penetration Profiles, W-Ir System, 1645°C.

Approved for Public Release

Contrails

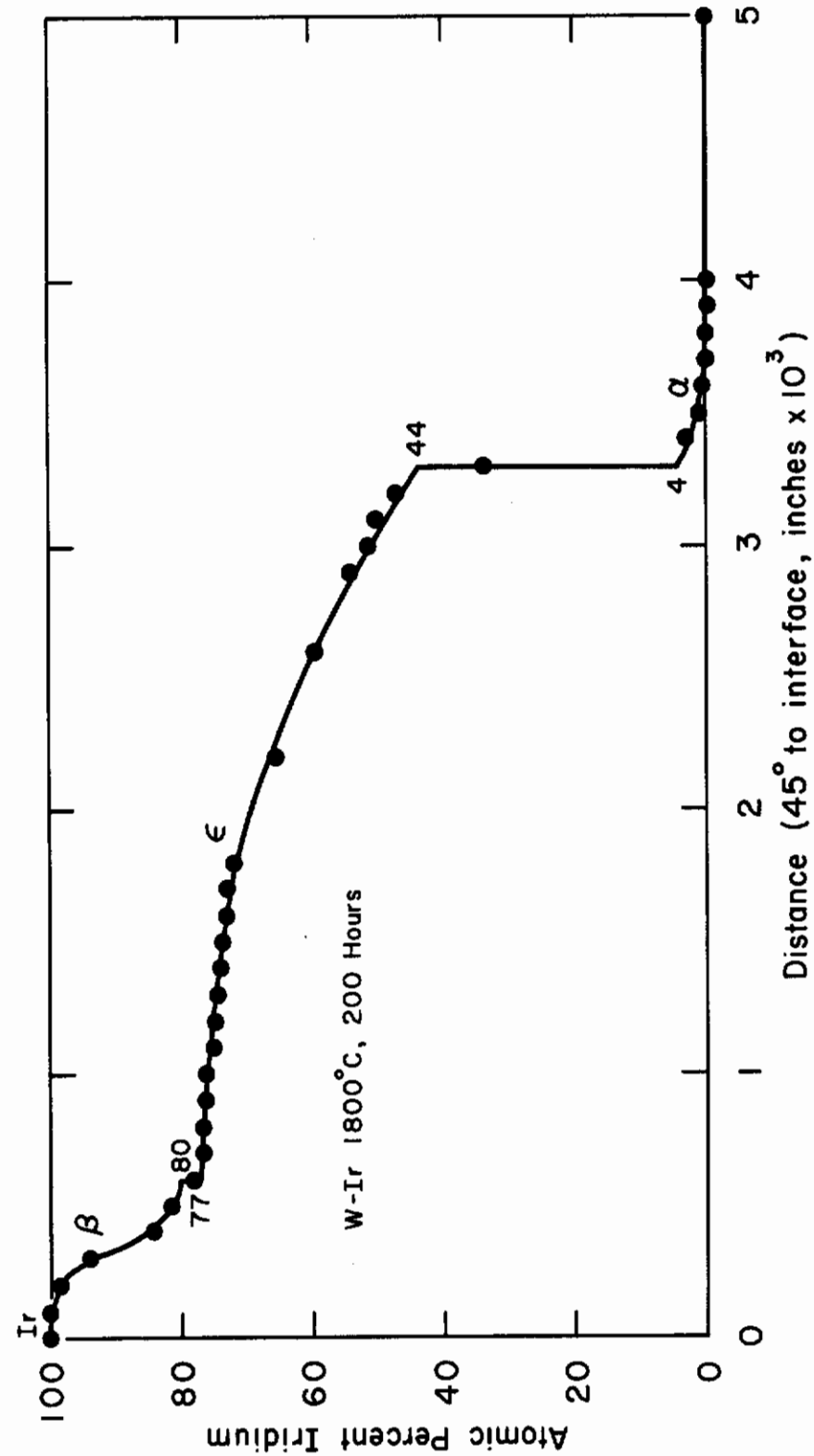

Figure 14. Composition vs. Penetration Profile, W-Ir System, 1800°C.

Approved for Public Release

Contrails.

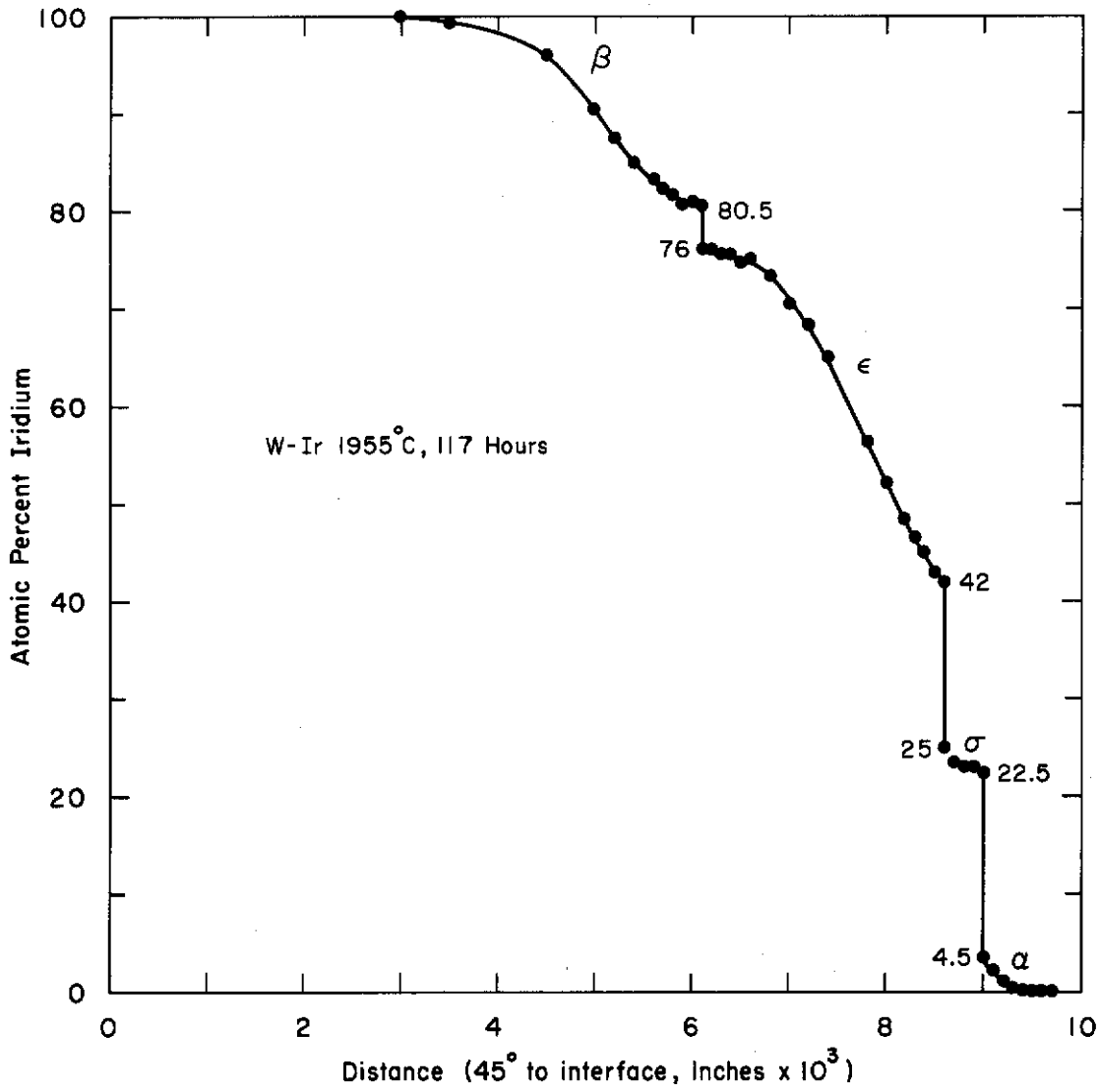

Figure 15. Composition vs Penetration Profile, W-Ir System, 1955 $^{\circ}$ C.

Approved for Public Release

Contrails

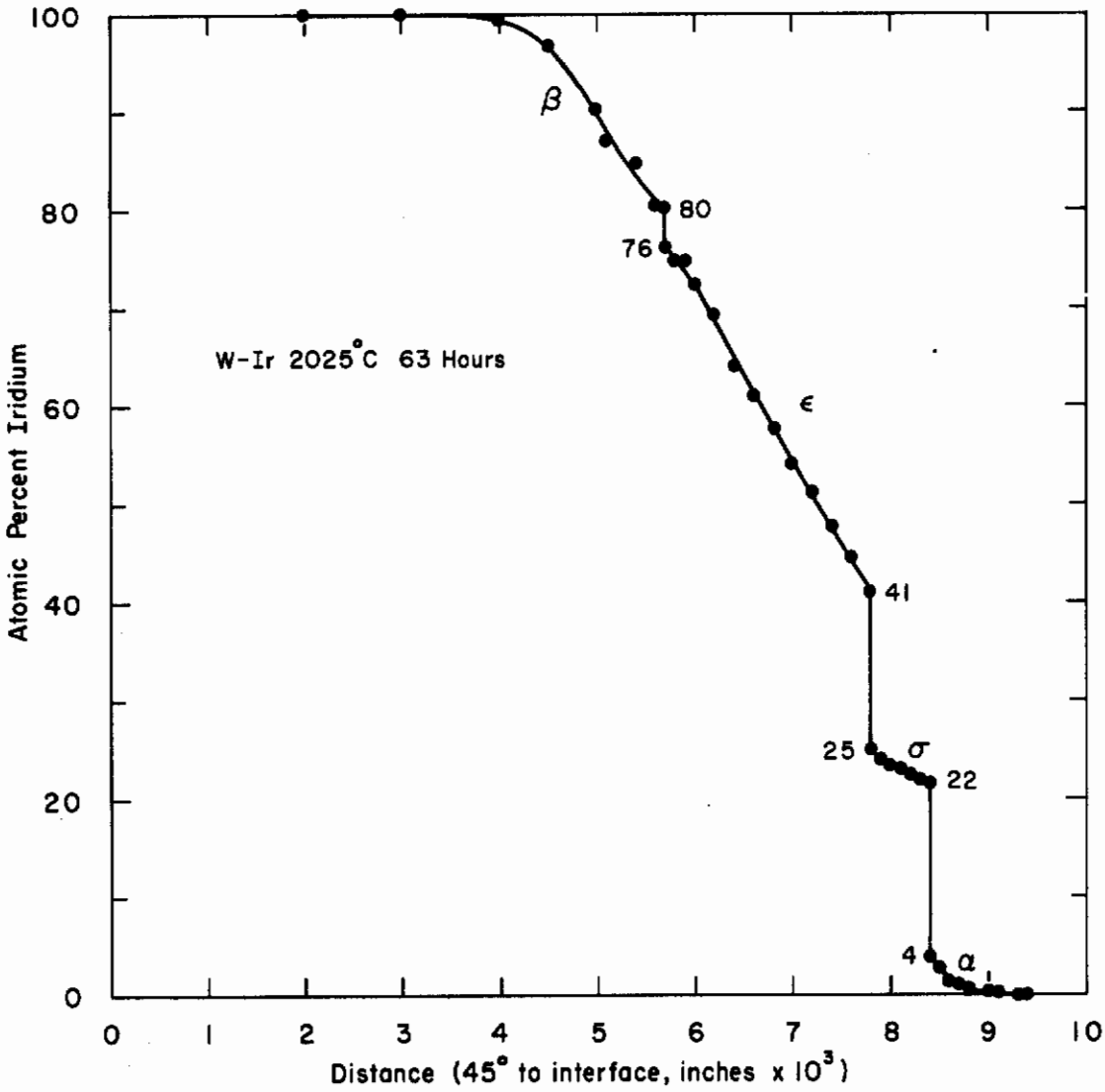

Figure 16. Composition vs Penetration Profiles, W-Ir System, 2025° C.

Approved for Public Release

Contrails

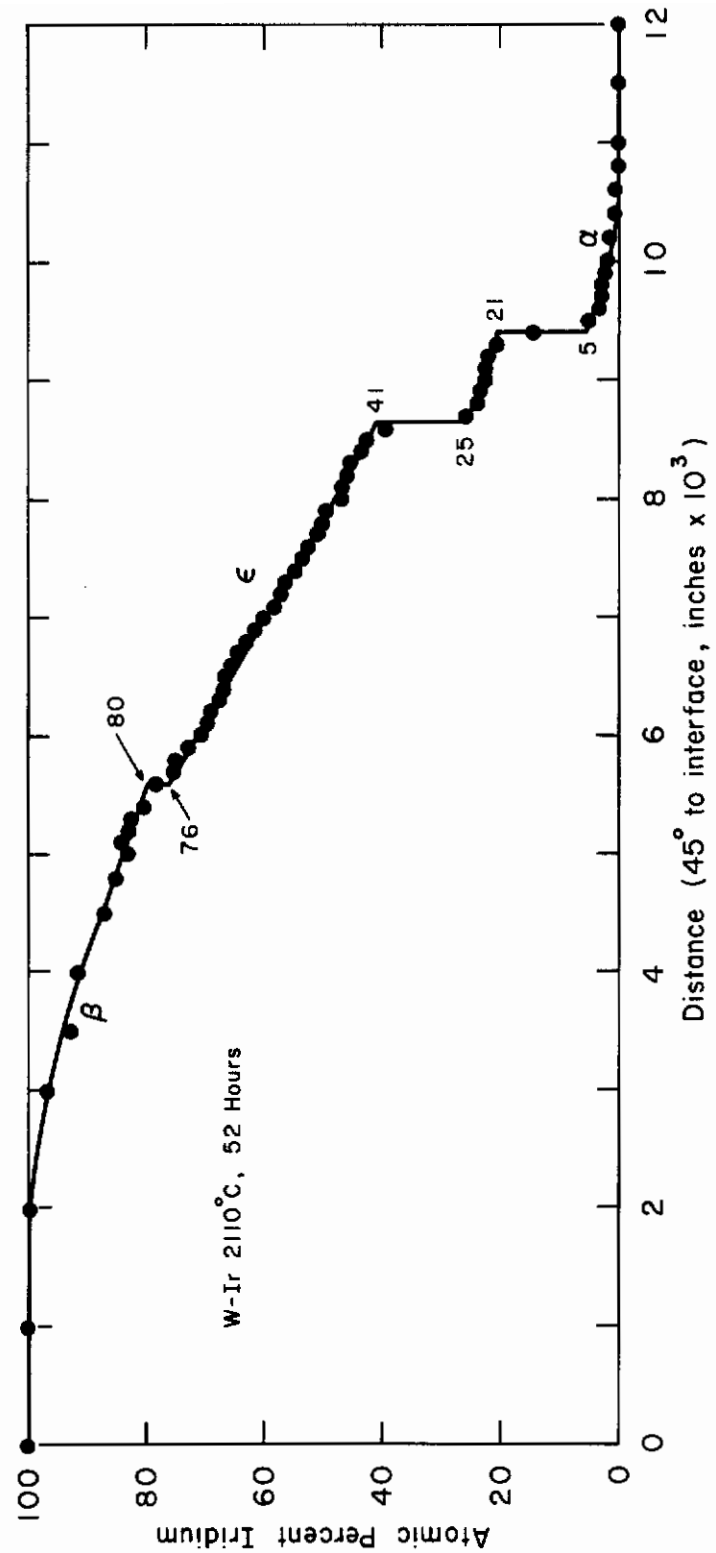

Figure 17. Composition vs Penetration Profiles, W-Ir System, 2110°C.

Approved for Public Release

Contrails

TABLE 10

TIMES AND TEMPERATURES OF ANNEALING TREATMENTS GIVEN TO COUPLES OF TUNGSTEN AND IRIDIUM

Nominal Temperature (°C)	Temperature Deviation (°C)	Time of Anneal (hours)
1300	± 20	1750
1385	± 25	417
1645	± 15	300
1800	± 25	200
1955	± 5	117
2025	± 10	63
2110	± 13	52

Approved for Public Release

Contrails

TABLE 11

INTERDIFFUSION COEFFICIENTS OF THE W-Ir SYSTEM FOR DIFFERENT COMPOSITIONS AT SEVERAL TEMPERATURES

Annealing Temperature (^{o}C)	Annealing Time (hrs.)	Phase	Composition (^{a}/o Ir)	Interdiffusion Coefficient, $\tilde{D}$ (cm^2/hr.)
2110	52	β Ir	99	2.19×10^{-7}
			98	2.23×10^{-7}
			97	2.24×10^{-7}
			96	2.24×10^{-7}
			95	2.24×10^{-7}
			94	2.23×10^{-7}
			93	2.23×10^{-7}
			92	2.22×10^{-7}
			91	2.22×10^{-7}
			90	2.21×10^{-7}
			89	2.21×10^{-7}
			88	2.20×10^{-7}
			87	2.20×10^{-7}
			86	2.19×10^{-7}
			85	2.18×10^{-7}
			84	2.18×10^{-7}
			83	2.17×10^{-7}
			82	2.17×10^{-7}
			81	2.16×10^{-7}
			80	2.16×10^{-7}
			79	2.15×10^{-7}
			78	2.14×10^{-7}
		ε + β Ir	77-76	2Ø
		ε	75	2.42×10^{-7}
			74	2.42×10^{-7}
			73	2.41×10^{-7}
			72	2.41×10^{-7}
			71	2.40×10^{-7}
			70	2.40×10^{-7}
			69	2.40×10^{-7}
			68	2.39×10^{-7}
			67	2.38×10^{-7}
			66	2.37×10^{-7}
			65	2.37×10^{-7}
			64	2.36×10^{-7}
			63	2.35×10^{-7}
			62	2.34×10^{-7}
			61	2.33×10^{-7}

(Table continued on next page.)

Approved for Public Release

Contrails

TABLE 11 (continued)

Annealing Temperature (°C)	Annealing Time (hrs.)	Phase	Composition (a/o Ir)	Interdiffusion Coefficient, $\tilde{D}$ (cm^2/hr.)
2110	52	β Ir	60	2.32×10^{-7}
			59	2.31×10^{-7}
			58	2.30×10^{-7}
			57	2.29×10^{-7}
			56	2.28×10^{-7}
			55	2.26×10^{-7}
			54	2.25×10^{-7}
			53	2.24×10^{-7}
			52	2.22×10^{-7}
			51	2.21×10^{-7}
			50	2.19×10^{-7}
			49	2.18×10^{-7}
			48	2.16×10^{-7}
			47	2.14×10^{-7}
			46	2.13×10^{-7}
			45	2.11×10^{-7}
			44	2.09×10^{-7}
			43	2.07×10^{-7}
			42	2.05×10^{-7}
			41	2.03×10^{-7}
			40	2.00×10^{-7}
		σ + ε	39-25	2Ø
		σ	24	2.56×10^{-7}
			23	2.54×10^{-7}
			22	2.51×10^{-7}
			21	2.48×10^{-7}
		αW + σ	20-8	2Ø
		αW	7	3.95×10^{-8}
			6	3.91×10^{-8}
			5	3.86×10^{-8}
			4	3.81×10^{-8}
			3	3.74×10^{-8}
			2	3.67×10^{-8}
			1	3.57×10^{-8}
2025	63	β Ir	99	2.45×10^{-8}
			98	2.72×10^{-8}
			97	2.93×10^{-8}
			96	3.11×10^{-8}
			95	3.27×10^{-8}
			94	3.42×10^{-8}
			93	3.57×10^{-8}

(Table continued on next page.)

Approved for Public Release

Contrails

TABLE 11 (continued)

Annealing Temperature (°C)	Annealing Time (hrs.)	Phase	Composition (a/o Ir)	Interdiffusion Coefficient, $\tilde{D}$ (cm^2/hr.)
2025	63	β Ir	92	3.72×10^{-8}
			91	3.86×10^{-8}
			90	4.00×10^{-8}
			89	4.15×10^{-8}
			88	4.29×10^{-8}
			87	4.44×10^{-8}
			86	4.59×10^{-8}
			85	4.75×10^{-8}
			84	4.91×10^{-8}
			83	5.08×10^{-8}
			82	5.25×10^{-8}
			81	5.44×10^{-8}
			80	5.63×10^{-8}
			79	6.18×10^{-8}
		ε + β Ir	78-76	2Ø
		ε	75	6.83×10^{-8}
			74	6.93×10^{-8}
			73	7.02×10^{-8}
			72	7.12×10^{-8}
			71	7.21×10^{-8}
			70	7.31×10^{-8}
			69	7.40×10^{-8}
			68	7.49×10^{-8}
			67	7.58×10^{-8}
			66	7.68×10^{-8}
			65	7.77×10^{-8}
			64	7.86×10^{-8}
			63	7.95×10^{-8}
			62	8.64×10^{-8}
			61	8.14×10^{-8}
			60	8.23×10^{-8}
			59	8.32×10^{-8}
			58	8.41×10^{-8}
			57	8.50×10^{-8}
			56	8.60×10^{-8}
			55	8.69×10^{-8}
			54	8.79×10^{-8}
			53	8.88×10^{-8}
			52	8.98×10^{-8}
			51	9.08×10^{-8}
			50	9.18×10^{-8}
			49	9.27×10^{-8}
			48	9.37×10^{-8}

(Table continued on next page.)

Approved for Public Release

Contrails

TABLE 11 (continued)

Annealing Temperature (°C)	Annealing Time (hrs.)	Phase	Composition (^{a}/o Ir)	Interdiffusion Coefficient, $\tilde{D}$ (cm^2/hr.)
2025	63	β Ir	47	9.47×10^{-8}
			46	9.58×10^{-8}
			45	9.68×10^{-8}
			44	9.79×10^{-8}
			43	9.90×10^{-8}
		σ + ε	42-25	2Ø
		σ	24	1.81×10^{-7}
			23	1.79×10^{-7}
			22	1.77×10^{-7}
		αW + σ	21-4	2Ø
		αW	3	1.11×10^{-8}
			2	1.10×10^{-8}
			1	1.07×10^{-8}
1955	117	β Ir	99	-----
			98	1.64×10^{-8}
			97	1.84×10^{-8}
			96	2.03×10^{-8}
			95	2.20×10^{-8}
			94	2.39×10^{-8}
			93	2.57×10^{-8}
			92	2.77×10^{-8}
			91	2.98×10^{-8}
			90	3.22×10^{-8}
			89	3.48×10^{-8}
			88	3.78×10^{-8}
			87	4.13×10^{-8}
			86	4.56×10^{-8}
			85	5.10×10^{-8}
			84	5.82×10^{-8}
			83	6.87×10^{-8}
			82	8.67×10^{-8}
			81	1.31×10^{-7}
		ε + β Ir	80-77	2Ø
		ε	76	1.33×10^{-7}
			75	1.14×10^{-7}
			74	1.01×10^{-7}
			73	9.22×10^{-7}
			72	8.50×10^{-7}
			71	7.93×10^{-7}
			70	7.45×10^{-7}
			69	7.04×10^{-7}

(Table continued on next page.)

Approved for Public Release

Contrails

TABLE 11 (continued)

Annealing Temperature (°C)	Annealing Time (hrs.)	Phase	Composition (a/o Ir)	Interdiffusion Coefficient, $\tilde{D}$ (cm^2/hr.)
1955	117	ε	68	6.69×10^{-7}
			67	6.38×10^{-7}
			66	6.10×10^{-7}
			65	5.85×10^{-7}
			64	5.63×10^{-7}
			63	5.42×10^{-7}
			62	5.22×10^{-7}
			61	5.05×10^{-7}
			60	4.88×10^{-7}
			59	4.73×10^{-7}
			58	4.59×10^{-7}
			57	4.46×10^{-7}
			56	4.33×10^{-7}
			55	4.21×10^{-7}
			54	4.09×10^{-7}
			53	3.98×10^{-7}
			52	3.88×10^{-7}
			51	3.78×10^{-7}
			50	3.68×10^{-7}
			49	3.59×10^{-7}
			48	3.50×10^{-7}
			47	3.41×10^{-7}
			46	3.32×10^{-7}
			45	3.24×10^{-7}
			44	3.16×10^{-7}
			43	3.08×10^{-7}
			42	3.01×10^{-7}
			41	2.93×10^{-7}
			40	2.81×10^{-7}
		σ + ε	39-25	2Ø
		σ	24	1.06×10^{-7}
			23	1.04×10^{-7}
		αW + σ	22-4	2Ø
		αW	3	2.85×10^{-9}
			2	2.70×10^{-9}
			1	2.48×10^{-9}
1800	200	β Ir	99	1.21×10^{-9}
			98	1.31×10^{-9}
			97	1.38×10^{-9}
			96	1.44×10^{-9}
			95	1.49×10^{-9}
			94	1.54×10^{-9}

(Table continued on next page.)

Approved for Public Release

Contrails

TABLE 11 (continued)

Annealing Temperature (°C)	Annealing Time (hrs.)	Phase	Composition (a/o Ir)	Interdiffusion Coefficient, $\tilde{D}$ ($cm^2/hr.$)
1800	200	β Ir	93	1.59×10^{-9}
			92	1.63×10^{-9}
			91	1.67×10^{-9}
			90	1.71×10^{-9}
			89	1.75×10^{-9}
			88	1.79×10^{-9}
			87	1.82×10^{-9}
			86	1.86×10^{-9}
			85	1.90×10^{-9}
			84	1.15×10^{-8}
			83	1.14×10^{-8}
			82	1.16×10^{-8}
			81	1.17×10^{-8}
		ε + β Ir	80-78	2Ø
		ε	77	8.77×10^{-8}
			76	8.85×10^{-8}
			75	8.89×10^{-8}
			74	8.91×10^{-8}
			73	8.90×10^{-8}
			72	8.85×10^{-8}
			71	2.58×10^{-8}
			70	2.56×10^{-8}
			69	2.54×10^{-8}
			68	2.52×10^{-8}
			67	2.50×10^{-8}
			66	2.49×10^{-8}
			65	2.46×10^{-8}
			64	2.44×10^{-8}
			63	2.41×10^{-8}
			62	2.39×10^{-8}
			61	2.37×10^{-8}
			60	2.34×10^{-8}
			59	2.32×10^{-8}
			58	2.30×10^{-8}
			57	2.27×10^{-8}
			56	2.24×10^{-8}
			55	2.22×10^{-8}
			54	2.19×10^{-8}
			53	2.16×10^{-8}
			52	2.14×10^{-8}
			51	2.11×10^{-8}
			50	2.08×10^{-8}
			49	2.05×10^{-8}

(Table continued on next page.)

Approved for Public Release

Contrails

TABLE 11 (continued)

Annealing Temperature (°C)	Annealing Time (hrs.)	Phase	Composition (a/o Ir)	Interdiffusion Coefficient, $\tilde{D}$ ($cm^2/hr.$)
1800	200	ε	48	2.02×10^{-8}
			47	1.98×10^{-8}
			46	1.95×10^{-8}
		αW + ε	45-4	2Ø
		αW	3	9.14×10^{-10}
			2	8.84×10^{-10}
			1	8.40×10^{-10}
1645	300	β Ir	99	1.90×10^{-9}
			98	2.02×10^{-9}
			97	2.09×10^{-9}
			96	2.15×10^{-9}
			95	2.20×10^{-9}
			94	2.24×10^{-9}
			93	2.29×10^{-9}
			92	2.32×10^{-9}
			91	2.36×10^{-9}
			90	2.40×10^{-9}
			89	2.44×10^{-9}
			88	2.47×10^{-9}
			87	2.50×10^{-9}
			86	2.54×10^{-9}
			85	2.57×10^{-9}
			84	2.60×10^{-9}
			83	2.64×10^{-9}
			82	2.67×10^{-9}
		ε + β Ir	81-76	2Ø
		ε	75	2.22×10^{-8}
			74	1.64×10^{-8}
			73	1.66×10^{-8}
			72	1.67×10^{-8}
			71	1.68×10^{-8}
			70	1.70×10^{-8}
			69	1.71×10^{-8}
			68	1.72×10^{-8}
			67	1.72×10^{-8}
			66	1.73×10^{-8}
			65	1.73×10^{-8}
			64	1.74×10^{-8}
			63	1.74×10^{-8}
			62	1.74×10^{-8}
			61	1.74×10^{-8}
			60	1.73×10^{-8}

(Table continued on next page.)

Approved for Public Release

Contrails

TABLE 11 (continued)

Annealing Temperature (°C)	Annealing Time (hrs.)	Phase	Composition (a/o Ir)	Interdiffusion Coefficient, $\tilde{D}$ (cm^2/hr.)
1645	300	ε	59	1.73×10^{-8}
			58	1.73×10^{-8}
			57	1.72×10^{-8}
			56	1.72×10^{-8}
			55	1.71×10^{-8}
			54	1.70×10^{-8}
			53	3.34×10^{-8}
			52	3.31×10^{-8}
			51	3.28×10^{-8}
			50	3.24×10^{-8}
			49	3.20×10^{-8}
			48	3.15×10^{-8}
		αW + ε	47-4	2Ø
		αW	3	2.95×10^{-10}
			2	2.81×10^{-10}
			1	2.62×10^{-10}
1385	417	β Ir	99	3.11×10^{-10}
			98	3.27×10^{-10}
			97	3.38×10^{-10}
			96	3.47×10^{-10}
			95	3.56×10^{-10}
			94	3.64×10^{-10}
			93	3.71×10^{-10}
			92	3.78×10^{-10}
			91	3.84×10^{-10}
			90	3.91×10^{-10}
			89	3.97×10^{-10}
			88	4.03×10^{-10}
			87	4.10×10^{-10}
			86	4.16×10^{-10}
			85	4.22×10^{-10}
			84	5.18×10^{-10}
			83	5.41×10^{-10}
			82	5.61×10^{-10}
		ε + β Ir	81-78	2Ø
		ε	77	3.50×10^{-9}
			76	3.44×10^{-9}
			75	3.38×10^{-9}
			74	3.33×10^{-9}
			73	3.28×10^{-9}
			72	3.23×10^{-9}
			71	3.18×10^{-9}

(Table continued on next page.)

Approved for Public Release

Contrails

TABLE 11 (continued)

Annealing Temperature (°C)	Annealing Time (hrs.)	Phase	Composition (a/o Ir)	Interdiffusion Coefficient, $\tilde{D}$ (cm^2/hr.)
1385	417	ε	70	3.14×10^{-9}
			69	3.10×10^{-9}
			68	3.06×10^{-9}
			67	3.02×10^{-9}
			66	2.98×10^{-9}
			65	2.94×10^{-9}
			64	2.90×10^{-9}
			63	2.86×10^{-9}
			62	2.83×10^{-9}
			61	2.79×10^{-9}
			60	2.76×10^{-9}
			59	2.72×10^{-9}
			58	2.68×10^{-9}
			57	2.65×10^{-9}
			56	2.61×10^{-9}
			55	2.58×10^{-9}
			54	2.54×10^{-9}
			53	2.51×10^{-9}
			52	2.47×10^{-9}
			51	2.44×10^{-9}
			50	2.40×10^{-9}
			49	2.36×10^{-9}
			48	2.33×10^{-9}
			47	2.29×10^{-9}
			46	2.25×10^{-9}
			45	2.21×10^{-9}
			44	2.18×10^{-9}
			43	2.13×10^{-9}
			42	2.09×10^{-9}
			41	2.02×10^{-9}
		αW + ε	40-5	2Ø
		αW	4	2.11×10^{-10}
			3	2.08×10^{-10}
			2	2.05×10^{-10}
			1	2.00×10^{-10}
1300	1750	β Ir	99	2.34×10^{-11}
			98	2.39×10^{-11}
			97	2.44×10^{-11}
			96	2.47×10^{-11}
			95	2.50×10^{-11}
			94	2.52×10^{-11}
			93	2.55×10^{-11}

(Table continued on next page.)

Approved for Public Release

Contrails

TABLE 11 (continued)

Annealing Temperature (°C)	Annealing Time (hrs.)	Phase	Composition (a/o Ir)	Interdiffusion Coefficient, $\tilde{D}$ ($cm^2/hr.$)
1300	1750	β Ir	92	2.57×10^{-11}
			91	2.60×10^{-11}
			90	2.62×10^{-11}
			89	2.65×10^{-11}
			88	2.67×10^{-11}
			87	2.70×10^{-11}
			86	2.72×10^{-11}
			85	2.74×10^{-11}
		ε + β Ir	84-54	2Ø
		ε	53	8.11×10^{-10}
			52	8.20×10^{-10}
			51	8.24×10^{-10}
			50	8.24×10^{-10}
			49	8.21×10^{-10}
			48	8.14×10^{-10}
			47	8.04×10^{-10}
		αW + ε	46-5	2Ø
		αW	4	4.42×10^{-11}
			3	4.52×10^{-11}
			2	4.64×10^{-11}
			1	4.79×10^{-11}

Approved for Public Release

Contrails

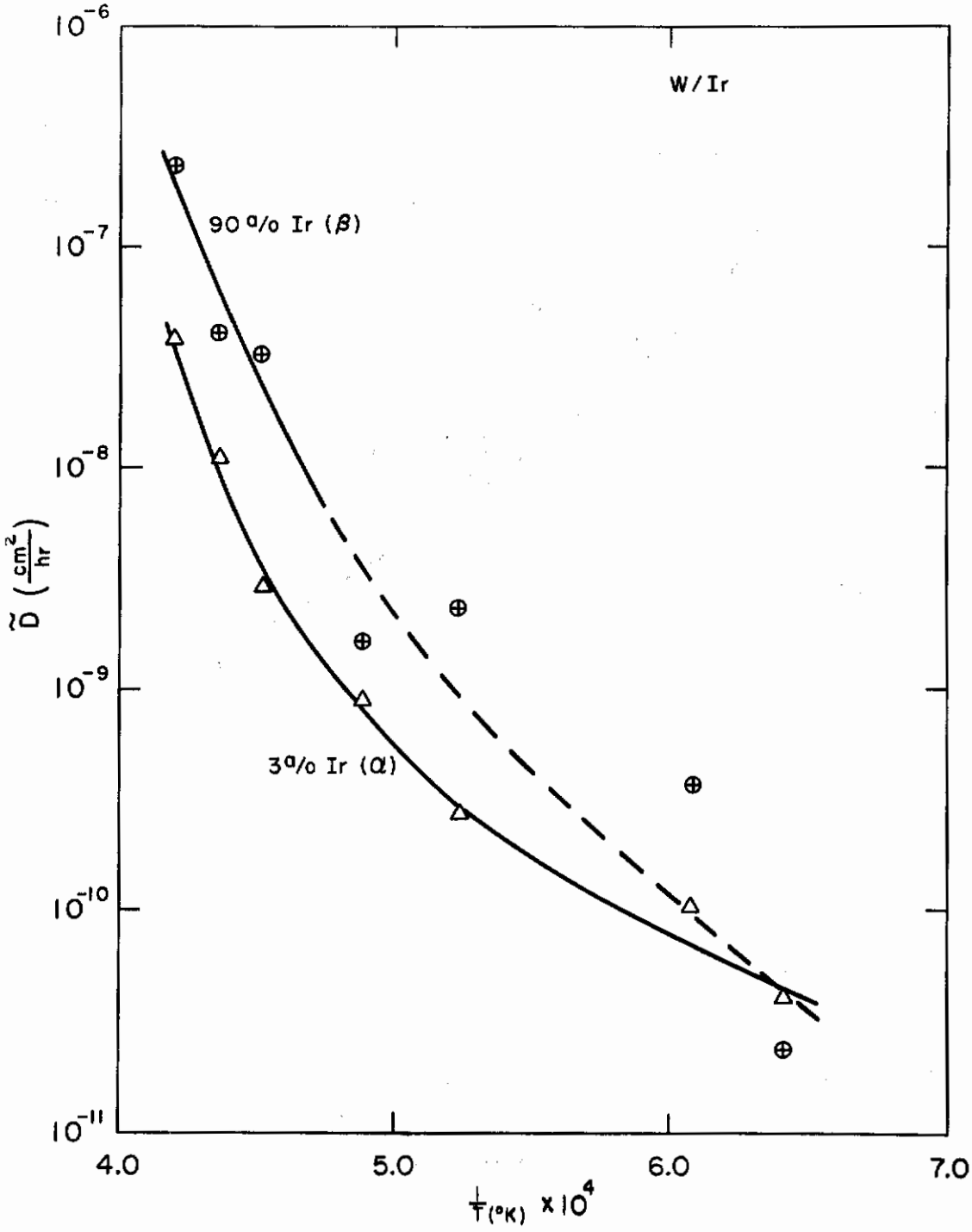

Figure 18. Plot of the Logarithm of Interdiffusion Coefficient vs Reciprocal Temperature for Solid Solution in α and β phases of W-Ir.

Approved for Public Release

Contrails

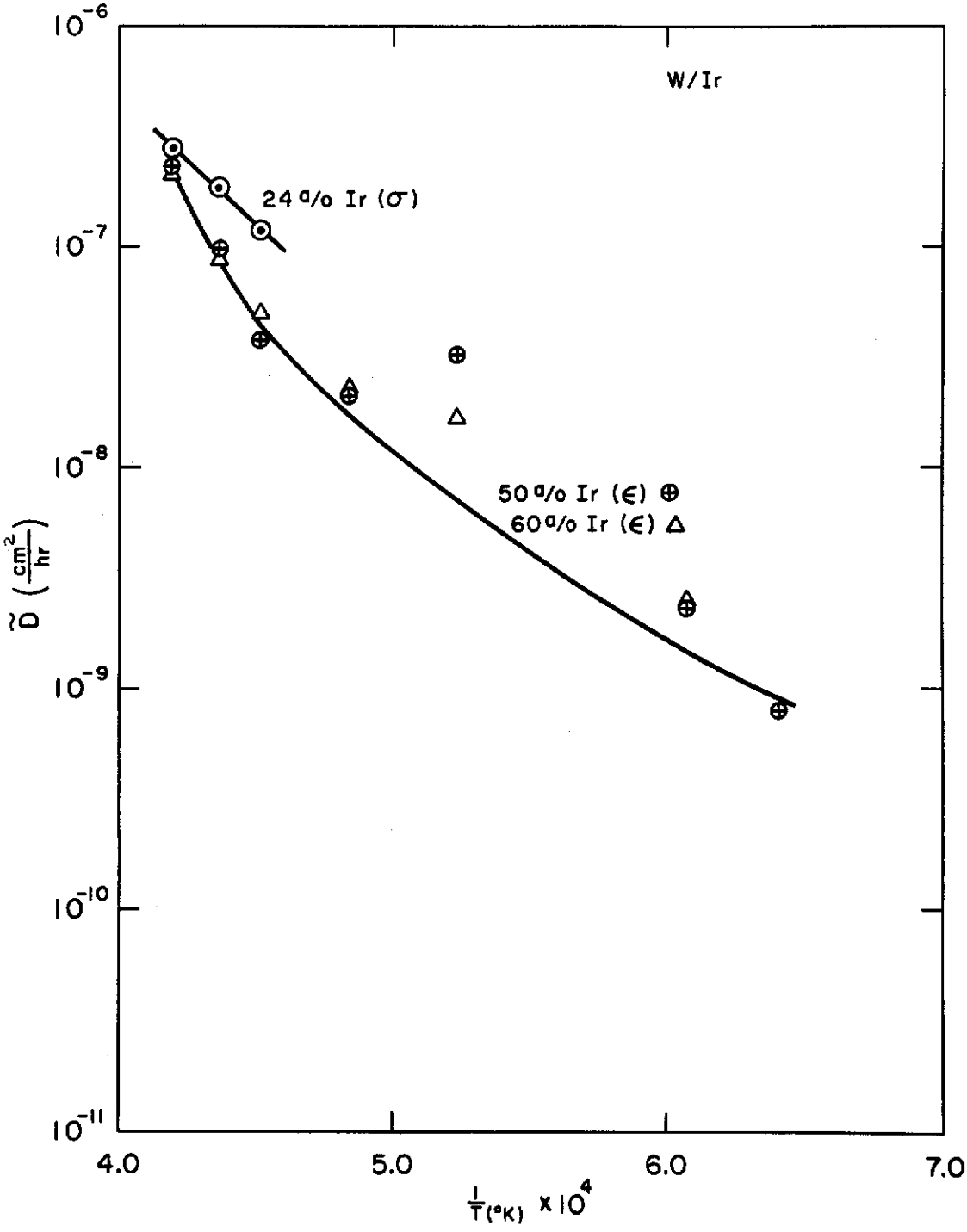

Figure 19. Plot of the Logarithm of Interdiffusion Coefficient vs Reciprocal Temperature for Intermediate Phases α and ε, W-Ir System.

Approved for Public Release

Contrails

A summary of the interdiffusion coefficient values for selected compositions in each phase field is given in Table 12 for the seven temperatures studied. The activation energies and frequency factors were obtained from the highest temperature couples, as in the W-Ru case.

Approved for Public Release

TABLE 12

TABULATION OF W-Ir DIFFUSION RESULTS

Temperature (°C)	Time (hrs.)	Grade of Couple*	Interdiffusion Coefficients ($cm^2/hr.$)					Comments
			3 a/o Ir α	24 a/o σ	50 a/o ϵ	60 a/o ϵ	90 a/o β_{Ir}	
1300	1750	C +	4.5×10^{-11}	--	8.2×10^{-10}	--	2.6×10^{-11}	0.001 in. zone
1385	417	C -	2.1×10^{-10}	--	2.4×10^{-9}	2.8×10^{-9}	3.9×10^{-10}	0.002 in. zone, porous and cracked
1645	300	C -	2.9×10^{-10}	--	3.2×10^{-8}	1.7×10^{-8}	2.4×10^{-9}	Porous at interface
1800	200	C -	9.1×10^{-10}	--	2.1×10^{-8}	2.3×10^{-8}	1.7×10^{-9}	Porous and cracked
1955	117	B +	2.9×10^{-9}	1.1×10^{-7}	3.7×10^{-8}	4.9×10^{-8}	3.2×10^{-8}	Somewhat porous at 95 a/o Ir
2025	63	B +	1.1×10^{-8}	1.8×10^{-7}	9.2×10^{-8}	8.2×10^{-8}	4.0×10^{-8}	Excellent couple 0.004 in. zone
2110	52	B	3.8×10^{-8}	2.6×10^{-7}	2.2×10^{-7}	2.3×10^{-7}	2.2×10^{-7}	Zone breadth not uniform
			170,000	60,800	120,400	120,400	145,400	Q Values, cal/mole
			1.41×10^{8}	0.0085	5.37×10^{4}	5.37×10^{4}	3.98×10^{6}	Calculated D_o values ($cm^2/hr.$)

* Grades indicate quality of diffusion zones.

Approved for Public Release

Contrails

V. DIFFUSION IN THE SYSTEM TUNGSTEN-RHODIUM

A. Diffusion Couple Preparation and Treatment

1. Material

The rhodium used in both the standards and the diffusion couples was obtained as powder of purity greater than 99.9 percent from Bishop and Co. The tungsten used is that described in Section III.A.1. Typical analysis of the rhodium used is given in Table 13.

2. Arc-Melting

Arc-melting was performed under conditions virtually identical to those described in Section III.A.2 on the ruthenium-tungsten system. As with the iridium system, weight balances were taken with the tungsten-rhodium system to establish maximum composition deviations for the standards. The results are given in Table 14. The standards of this system, as for the W-Ir system, were made of premelted stock. The small deviations of composition of Table 14 illustrate the control that can thus be attained.

3. Bonding of Couples

The Couples of the W-Rh system were bonded into three-layered sandwiches as described in the section on the W-Ru system (III.A.3).

4. Annealing

The comments of Section III.A.4 on the W-Ru system apply here also.

5. Sectioning

The couples of the W-Rh system were sectioned as described in the section on the W-Ru system (III.A.5).

B. Determination of Composition Profiles

In almost all details the determination of the W-Rh composition profiles parallel the determination of those in the W-Ru system described in Section III.B.

Approved for Public Release

Contrails

TABLE 13

TYPICAL ANALYSIS OF Rh USED

Impurity Element	Contents Expressed in PPM
Al	5
Cu	5
Fe	60
Pb	20
Mg	1
Mn	1
Si	80
Ag	10
Sn	30
Pt	20
Pd	30
Ir	300
Ru	200

TABLE 14

COMPOSITIONS AND TOLERANCES OF W-Rh
COMPOSITION STANDARDS

Minimum ^{a}/o Rh	Maximum ^{a}/o Rh	Nominal ^{a}/o Rh	Tolerance ^{a}/o Rh
3.89	4.15	4.02	$\pm$ 0.13
24.17	24.56	24.37	$\pm$ 0.20
55.30	55.43	55.37	$\pm$ 0.07
69.76	69.87	69.82	$\pm$ 0.06
79.77	79.83	79.80	$\pm$ 0.03
94.76	94.81	94.78	$\pm$ 0.03

Approved for Public Release

Contrails

A plot of the W-Rh standards with their normalized intensities versus composition is given in Figure 20. The times and temperatures of these annealing treatments are given in Table 15. The composition-penetration profiles found on the five annealed specimens are given in Figures 21, 23, 24, 26, and 27. Figures 22 and 25 are plots over narrow composition ranges to show details at two specific compositions.

C. Interdiffusion Coefficient Determinations

Comparison of the phase boundary values given in Figures 21 through 27 with the phase diagram (see Appendix II) shows the presence of all equilibrium phases with equilibrium boundary values. These composition correlations indicate that the reactions were diffusion controlled in this system also.

The computer methods for solving the Boltzmann-Matano expression for the interdiffusion coefficient as described in Section III.C.2 for the W-Ru system were also employed on the profiles of the W-Rh couples.

D. Results and Discussion

The profile data of Figures 21 through 27 were processed by a computer to yield the interdiffusion coefficients as functions of composition in each of the four phases of this system. Interdiffusion coefficient versus composition are tabulated in Table 16 for the profiles of Figures 21 through 27. Discontinuities of the interdiffusion coefficients within a single phase region have been discussed in Section III.D.1 of the W-Ru system.

Plots of the logarithm of the interdiffusion coefficient versus reciprocal temperature were made for various compositions in the single phase fields across the diagram. These are presented in Figures 28 and 29.

A summary of the interdiffusion coefficient values for selected compositions in each phase field is given in Table 17 for the temperatures studied. The activation energies and frequency factors were obtained from the highest temperature couples, as in the W-Ru case.

Approved for Public Release

Contrails

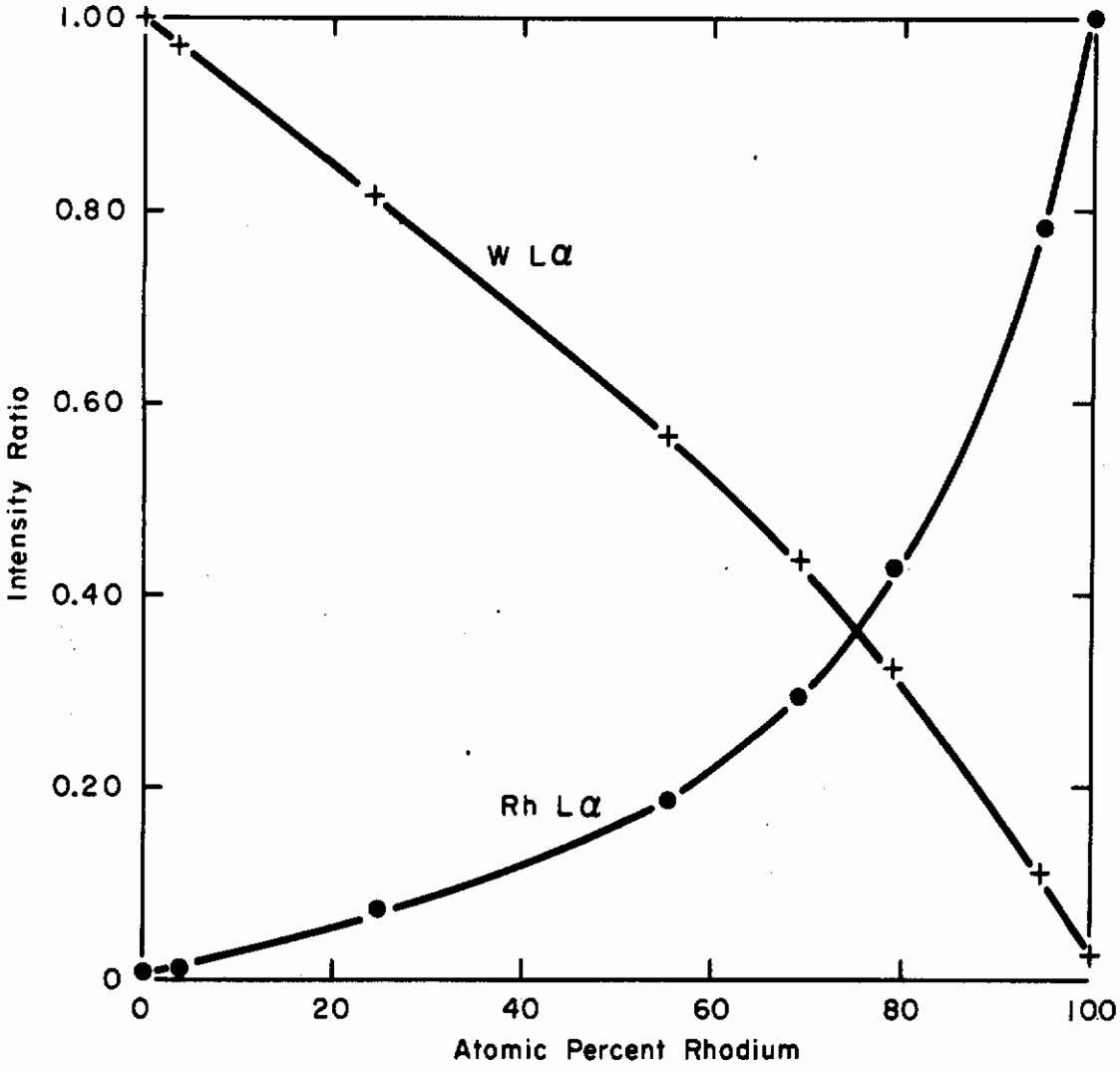

Figure 20. Plot of Normalized Intensity of Characteristic Radiation of Rh and W vs Composition. The Lα X-ray lines of both elements were used.

Approved for Public Release

Contrails

TABLE 15

TIMES AND TEMPERATURES OF ANNEALING TREATMENTS
OF TUNGSTEN-RHODIUM COUPLE

Nominal Temperature (°C)	Temperature Deviation (°C)	Time of Anneal (hours)
1300	± 20	1750
1385	± 25	417
1645	± 15	300
1800	± 25	200
1800	± 5	67

Approved for Public Release

Contrails

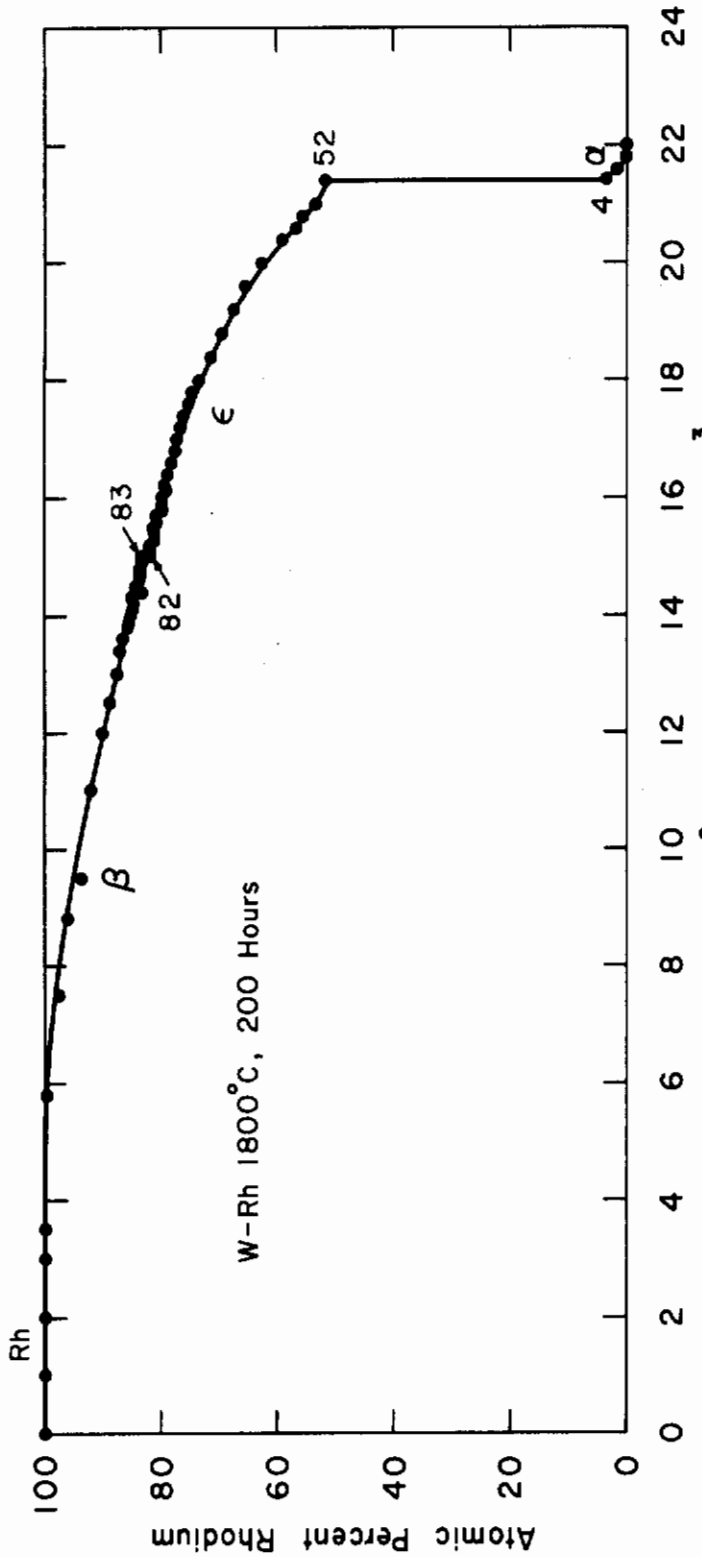

Figure 21. Composition vs Penetration Profile, W-Rh System, 1800°C, 200 hours.

Approved for Public Release

Contrails

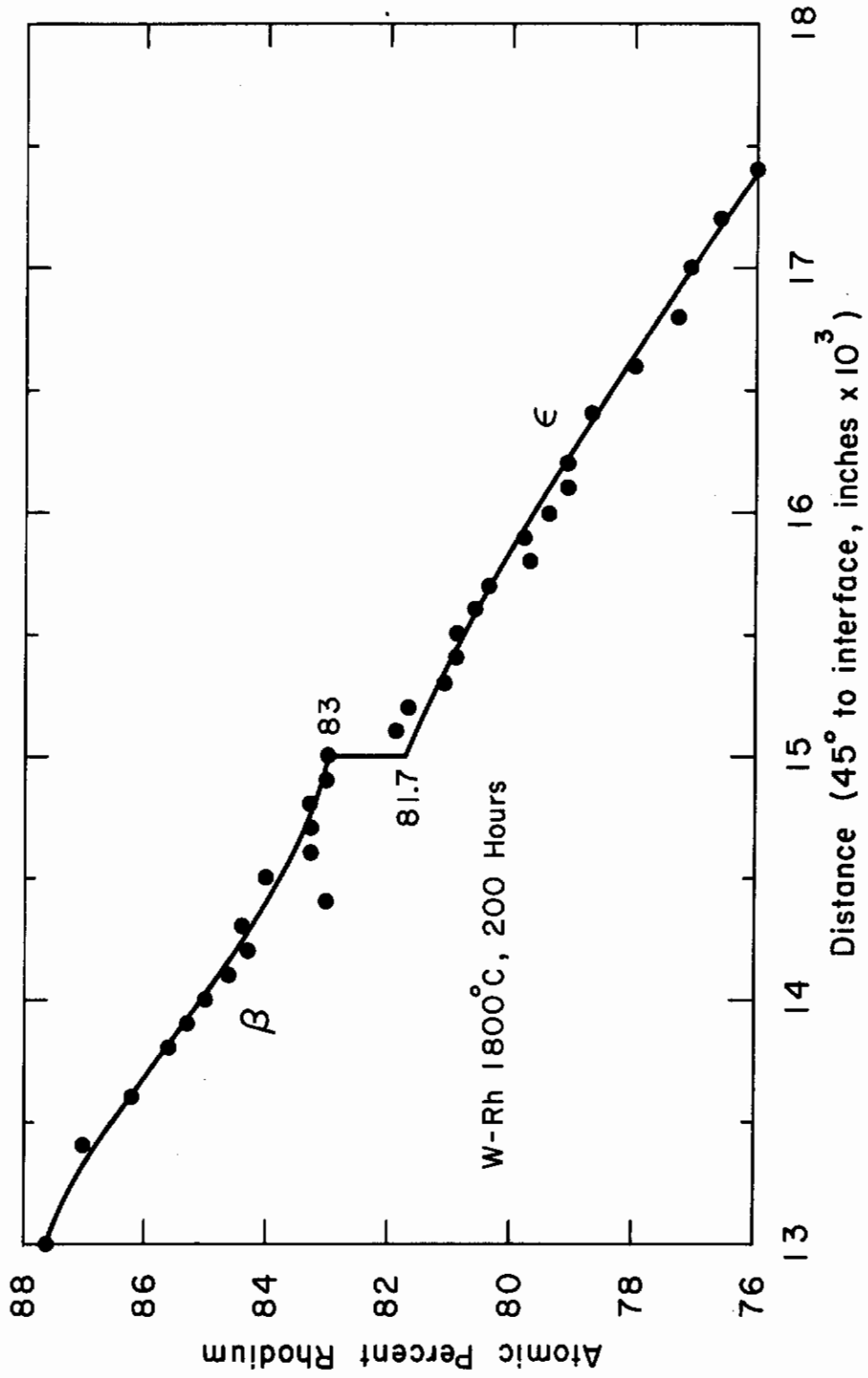

Figure 22. Composition vs Penetration Profile, W-Rh System, 1800°C, 200 hours, Exploded View.

Approved for Public Release

Contrails

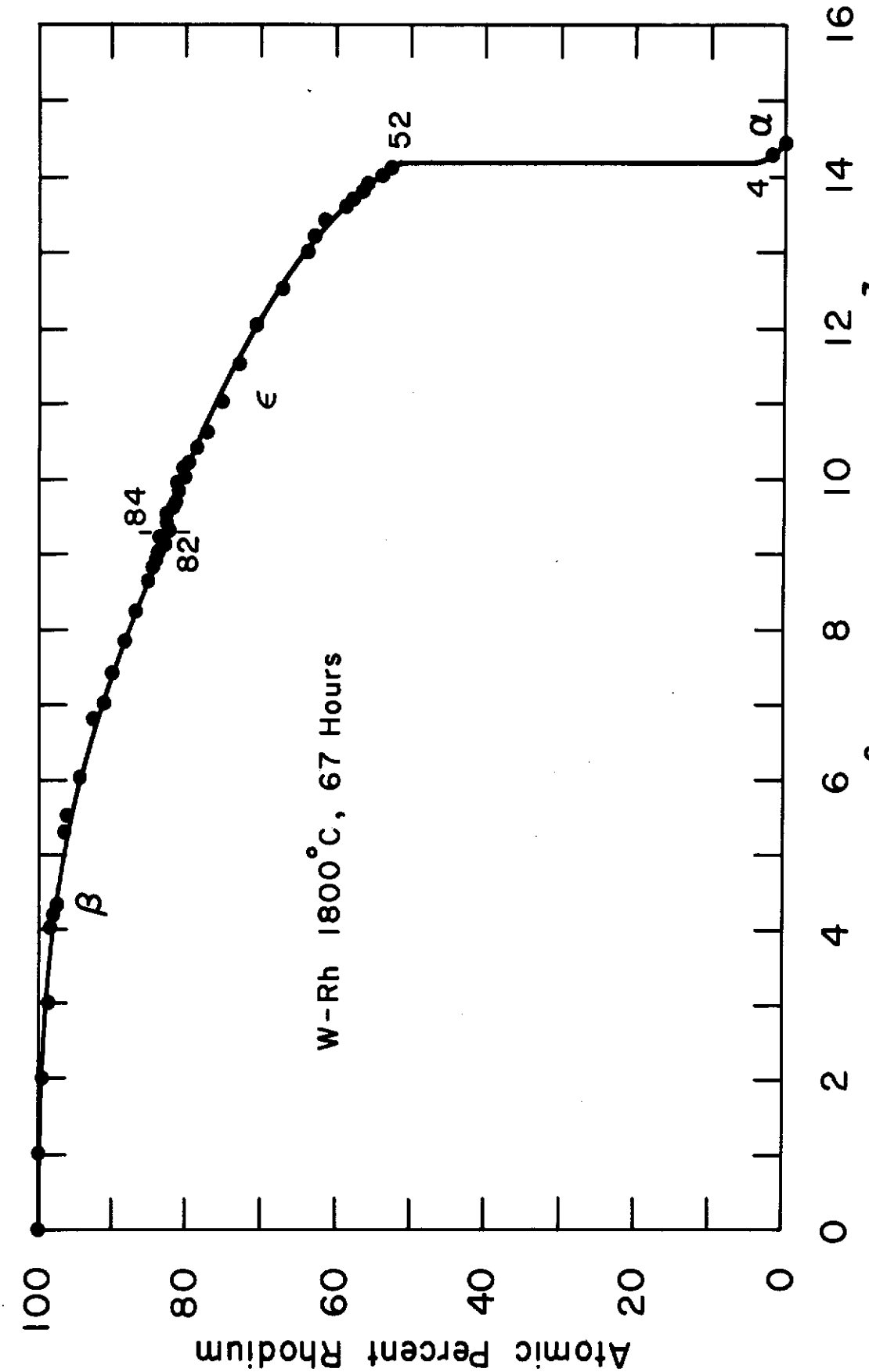

Figure 23. Composition vs Penetration Profile. W-Rh System, 1800°C, 67 hours.

Approved for Public Release

Contrails

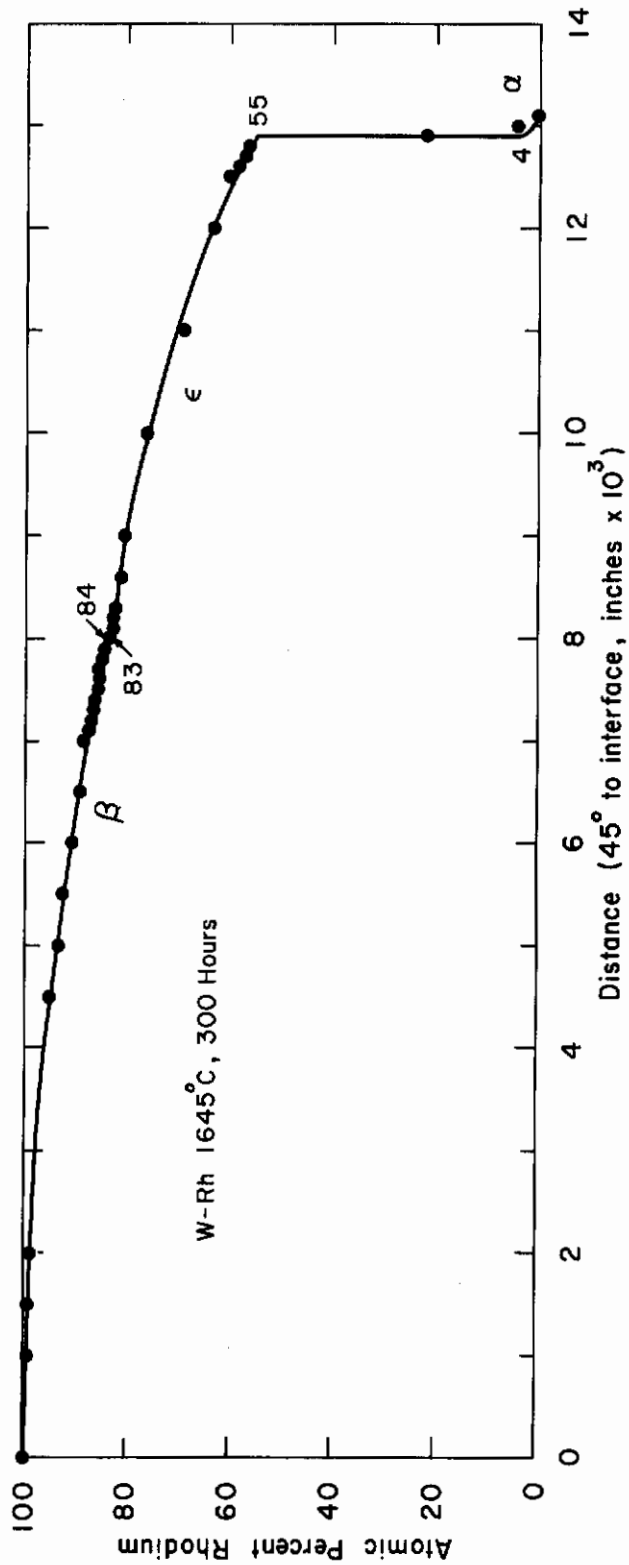

Figure 24. Composition vs Penetration Profile, W-Rh System, 1645°C.

Approved for Public Release

Contrails

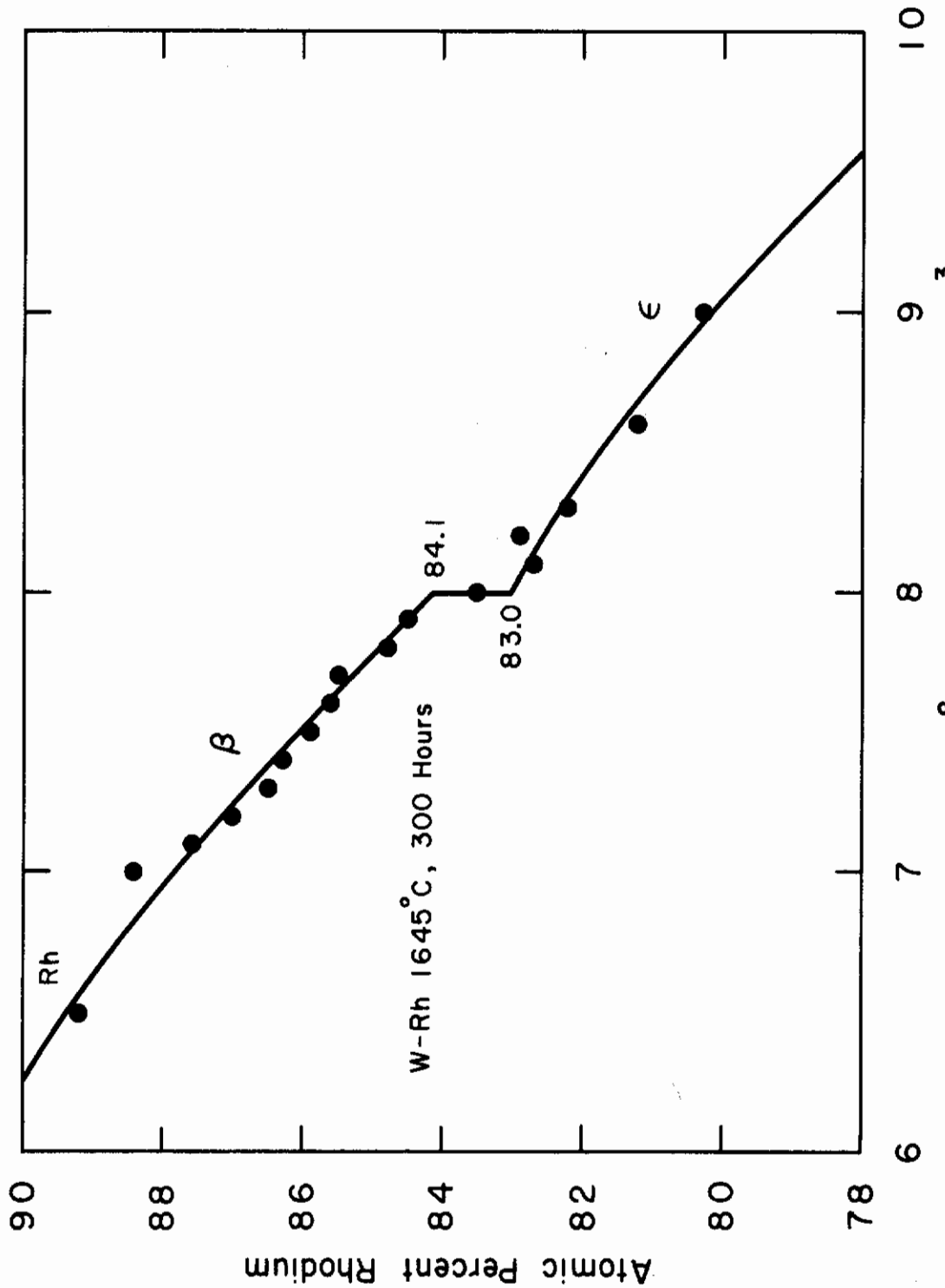

Figure 25. Composition vs. Penetration Profile, W-Rh System, 1645°C, Exploded View.

Approved for Public Release

Contrails

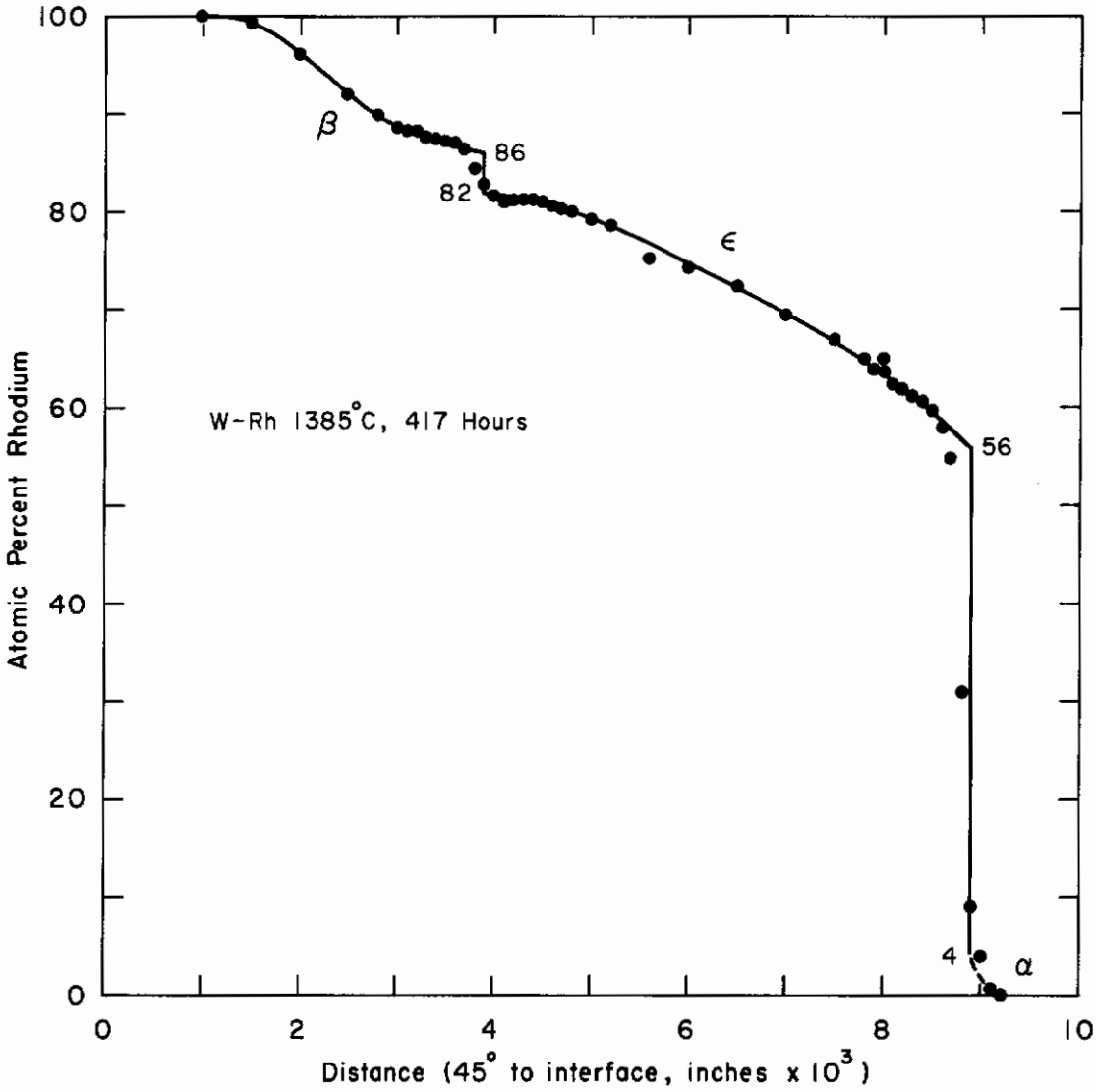

Figure 26. Composition vs. Penetration Profile, W-Rh System, 1385°C.

Approved for Public Release

Contrails

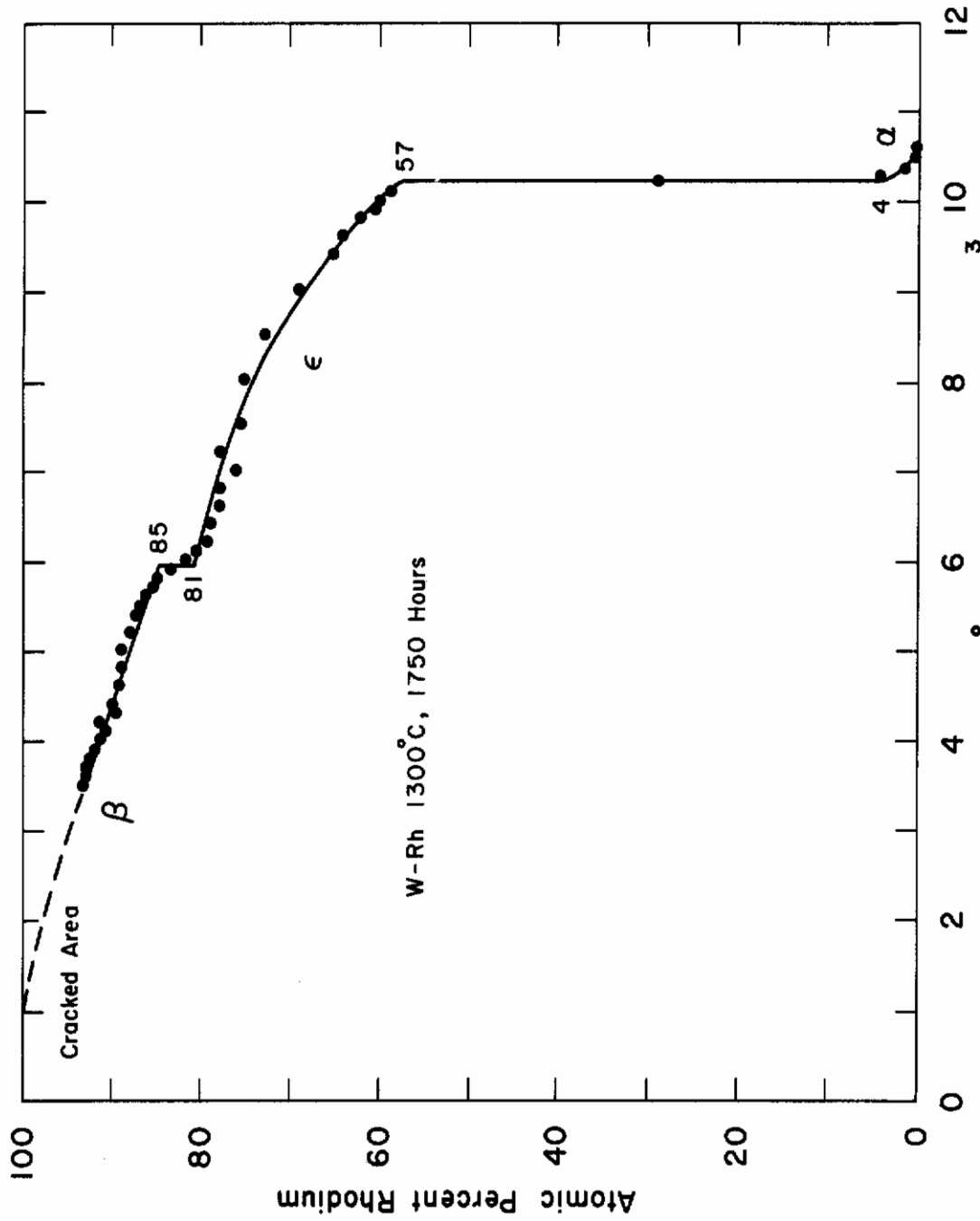

Figure 27. Composition vs Penetration Profile, W-Rh System, 1300°C.

Approved for Public Release

Contrails

TABLE 16

INTERDIFFUSION COEFFICIENTS OF THE W-Rh SYSTEM

FOR DIFFERENT COMPOSITIONS AT SEVERAL TEMPERATURES

Annealing Temperature (°C)	Annealing Time (hrs.)	Phase	Composition (a/o Rh)	Interdiffusion Coefficient, $\tilde{D}$ (cm^2/hr.)
1800	200	βRh	99	2.16×10^{-7}
			98	2.44×10^{-7}
			97	2.66×10^{-7}
			96	2.84×10^{-7}
			95	3.02×10^{-7}
			94	3.20×10^{-7}
			93	3.37×10^{-7}
			92	3.55×10^{-7}
			91	3.73×10^{-7}
			90	3.92×10^{-7}
			89	4.13×10^{-7}
			88	4.35×10^{-7}
			87	4.60×10^{-7}
			86	4.88×10^{-7}
			85	5.18×10^{-7}
			84	5.54×10^{-7}
		ε + βRh	83-81	2Ø
		ε	80	8.40×10^{-7}
			79	7.08×10^{-7}
			78	6.22×10^{-7}
			77	5.60×10^{-7}
			76	5.12×10^{-7}
			75	4.74×10^{-7}
			74	4.42×10^{-7}
			73	4.15×10^{-7}
			72	3.92×10^{-7}
			71	3.71×10^{-7}
			70	3.53×10^{-7}
			69	3.36×10^{-7}
			68	3.21×10^{-7}
			67	3.07×10^{-7}
			66	2.94×10^{-7}
			65	2.83×10^{-7}
			64	2.72×10^{-7}

(Table continued on next page.)

Approved for Public Release

Contrails

TABLE 16 (continued)

Annealing Temperature (°C)	Annealing Time (hrs.)	Phase	Composition (a/o Rh)	Interdiffusion Coefficient, $\tilde{D}$ (cm^2/hr.)
1800	200	ε	63	2.62×10^{-7}
			62	2.52×10^{-7}
			61	2.43×10^{-7}
			60	2.34×10^{-7}
			59	2.26×10^{-7}
			58	2.18×10^{-7}
			57	2.11×10^{-7}
			56	2.04×10^{-7}
			55	1.97×10^{-7}
			54	1.90×10^{-7}
			53	1.84×10^{-7}
		αW + ε	52-3	2Ø
		αW	2	2.63×10^{-9}
			1	2.43×10^{-9}
1800	67	βRh	99	--
			98	4.73×10^{-7}
			97	4.75×10^{-7}
			96	4.71×10^{-7}
			95	4.68×10^{-7}
			94	4.63×10^{-7}
			93	4.58×10^{-7}
			92	4.53×10^{-7}
			91	4.48×10^{-7}
			90	4.44×10^{-7}
			89	4.39×10^{-7}
			88	4.35×10^{-7}
			87	4.30×10^{-7}
			86	4.26×10^{-7}
			85	4.21×10^{-7}
			84	4.16×10^{-7}
			83	4.12×10^{-7}
		ε + βRh	82	--
		ε	81	4.77×10^{-7}
			80	4.71×10^{-7}
			79	4.66×10^{-7}
			78	4.60×10^{-7}
			77	4.54×10^{-7}
			76	4.48×10^{-7}

(Table continued on next page.)

Approved for Public Release

Contrails

TABLE 16 (continued)

Annealing Temperature (°C)	Annealing Time (hrs.)	Phase	Composition (a/o Rh)	Interdiffusion Coefficient, $\tilde{D}$ (cm^2/hr.)
1800	67	ε	75	4.41×10^{-7}
			74	4.34×10^{-7}
			73	4.28×10^{-7}
			72	4.21×10^{-7}
			71	1.87×10^{-7}
			70	1.84×10^{-7}
			69	1.81×10^{-7}
			68	1.78×10^{-7}
			67	1.75×10^{-7}
			66	1.72×10^{-7}
			65	1.70×10^{-7}
			64	1.67×10^{-7}
			63	1.64×10^{-7}
			62	1.61×10^{-7}
			61	1.59×10^{-7}
			60	1.56×10^{-7}
			59	1.54×10^{-7}
			58	1.51×10^{-7}
			57	1.48×10^{-7}
			56	1.46×10^{-7}
			55	1.43×10^{-7}
			54	1.41×10^{-7}
			53	1.38×10^{-7}
			52	1.35×10^{-7}
		αW + ε	51-6	2Ø
		αW	5	5.72×10^{-9}
			4	5.56×10^{-9}
			3	5.38×10^{-9}
			2	5.17×10^{-9}
			1	4.89×10^{-9}
1645	300	βRh	99	6.23×10^{-8}
			98	6.37×10^{-8}
			97	6.47×10^{-8}
			96	1.26×10^{-7}
			95	1.26×10^{-7}
			94	1.26×10^{-7}
			93	1.26×10^{-7}
			92	1.25×10^{-7}

(Table continued on next page.)

Approved for Public Release

Contrails

TABLE 16 (continued)

Annealing Temperature (°C)	Annealing Time (hrs.)	Phase	Composition (a/o Rh)	Interdiffusion Coefficient, $\tilde{D}$ (cm^2/hr.)
1645	300	βRh	91	1.24×10^{-7}
			90	1.23×10^{-7}
			89	1.23×10^{-7}
			88	1.22×10^{-7}
			87	1.21×10^{-7}
			86	1.20×10^{-7}
			85	1.19×10^{-7}
		ε + βRh	84	2Ø
		ε	83	1.17×10^{-7}
			82	1.16×10^{-7}
			81	1.19×10^{-7}
			80	1.18×10^{-7}
			79	1.16×10^{-7}
			78	1.15×10^{-7}
			77	1.14×10^{-7}
			76	1.12×10^{-7}
			75	1.11×10^{-7}
			74	1.10×10^{-7}
			73	1.08×10^{-7}
			72	1.07×10^{-7}
			71	1.06×10^{-7}
			70	1.04×10^{-7}
			69	1.03×10^{-7}
			68	1.01×10^{-8}
			67	9.98×10^{-8}
			66	9.68×10^{-8}
			65	9.68×10^{-8}
			64	9.52×10^{-8}
			63	9.36×10^{-8}
			62	9.20×10^{-8}
			61	9.03×10^{-8}
			60	8.86×10^{-8}
			59	8.68×10^{-8}
			58	8.50×10^{-8}
		αW + ε	57-6	2Ø
		αW	5	5.67×10^{-10}
			4	5.46×10^{-10}
			3	5.22×10^{-10}
			2	4.94×10^{-10}
			1	4.55×10^{-10}

(Table continued on next page.)

Approved for Public Release

Contrails

TABLE 16 (continued)

Annealing Temperature (°C)	Annealing Time (hrs.)	Phase	Composition (a/o Rh)	Interdiffusion Coefficient, $\tilde{D}$ ($cm^2/hr.$)
1385	417	βRh	99	7.78×10^{-9}
			98	8.99×10^{-9}
			97	1.02×10^{-8}
			96	1.15×10^{-8}
			95	1.30×10^{-8}
			94	1.46×10^{-8}
			93	1.64×10^{-8}
			92	1.88×10^{-8}
			91	2.18×10^{-8}
			90	2.60×10^{-8}
			89	3.31×10^{-8}
		ε + βRh	88-83	2Ø
		ε	82	1.04×10^{-7}
			81	9.90×10^{-8}
			80	9.49×10^{-8}
			79	9.13×10^{-8}
			78	8.79×10^{-8}
			77	8.49×10^{-8}
			76	8.20×10^{-8}
			75	7.93×10^{-8}
			74	7.68×10^{-8}
			73	7.44×10^{-8}
			72	7.21×10^{-8}
			71	6.99×10^{-8}
			70	6.78×10^{-8}
			69	6.58×10^{-8}
			68	6.39×10^{-8}
			67	6.16×10^{-8}
			66	5.98×10^{-8}
			65	5.81×10^{-8}
			64	5.64×10^{-8}
			63	5.48×10^{-8}
			62	5.31×10^{-8}
			61	5.15×10^{-8}
			60	5.00×10^{-8}
			59	4.84×10^{-8}
			58	4.69×10^{-8}
			57	4.55×10^{-8}
		αW + ε	56-9	2Ø

(Table continued on next page.)

Approved for Public Release

Contrails

TABLE 16 (continued)

Annealing Temperature (°C)	Annealing Time (hrs.)	Phase	Composition (a/o Rh)	Interdiffusion Coefficient, $\tilde{D}$ (cm^2/hr.)
1385	417	αW	8	5.40×10^{-10}
			7	5.25×10^{-10}
			6	5.10×10^{-10}
			5	4.94×10^{-10}
			4	4.75×10^{-10}
			3	4.55×10^{-10}
			2	4.33×10^{-10}
			1	3.99×10^{-10}
1300	1750	βRh	99	1.92×10^{-8}
			98	1.93×10^{-8}
			97	1.92×10^{-8}
			96	1.91×10^{-8}
			95	1.89×10^{-8}
			94	1.88×10^{-8}
			93	1.86×10^{-8}
			92	1.84×10^{-8}
			91	1.82×10^{-8}
			90	1.81×10^{-8}
			89	1.79×10^{-8}
			88	1.77×10^{-8}
			87	1.76×10^{-8}
			86	1.74×10^{-8}
		ε + βRh	85-80	2Ø
		ε	79	5.05×10^{-8}
			78	3.55×10^{-8}
			77	2.88×10^{-8}
			76	2.48×10^{-8}
			75	2.20×10^{-8}
			74	1.99×10^{-8}
			73	1.83×10^{-8}
			72	1.69×10^{-8}
			71	1.58×10^{-8}
			70	1.48×10^{-8}
			69	1.39×10^{-8}
			68	1.32×10^{-8}
			67	1.25×10^{-8}
			66	1.19×10^{-8}
			65	1.13×10^{-8}

(Table continued on next page.)

Approved for Public Release

Contrails

TABLE 16 (continued)

Annealing Temperature (°C)	Annealing Time (hrs.)	Phase	Composition (a/o Rh)	Interdiffusion Coefficient, $\tilde{D}$ (cm^2/hr.)
1300	1750	ε	64	1.08×10^{-8}
			63	1.03×10^{-8}
			62	9.85×10^{-9}
			61	9.43×10^{-9}
			60	9.04×10^{-9}
			59	8.66×10^{-9}
		αW + ε	58-7	8.31×10^{-9}
		αW	6	9.09×10^{-11}
			5	8.80×10^{-11}
			4	8.47×10^{-11}
			3	8.10×10^{-11}
			2	7.67×10^{-11}
			1	7.06×10^{-11}

Approved for Public Release

Contrails

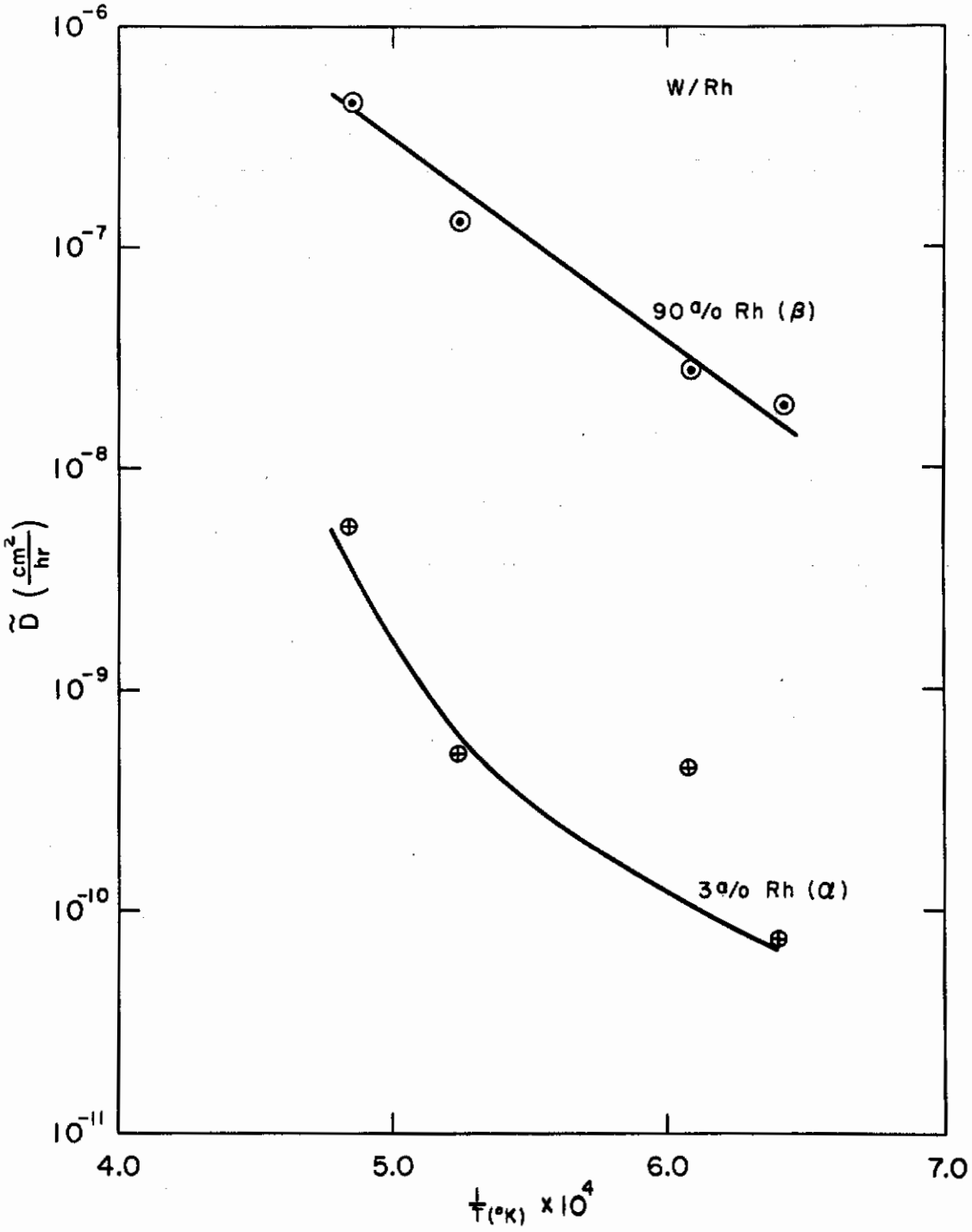

Figure 28. Plot of Logarithm of the Interdiffusion Coefficient vs. Reciprocal Temperature for Couples in the W-Rh System. Compositions from the terminal solid solutions are illustrated.

Approved for Public Release

Contrails

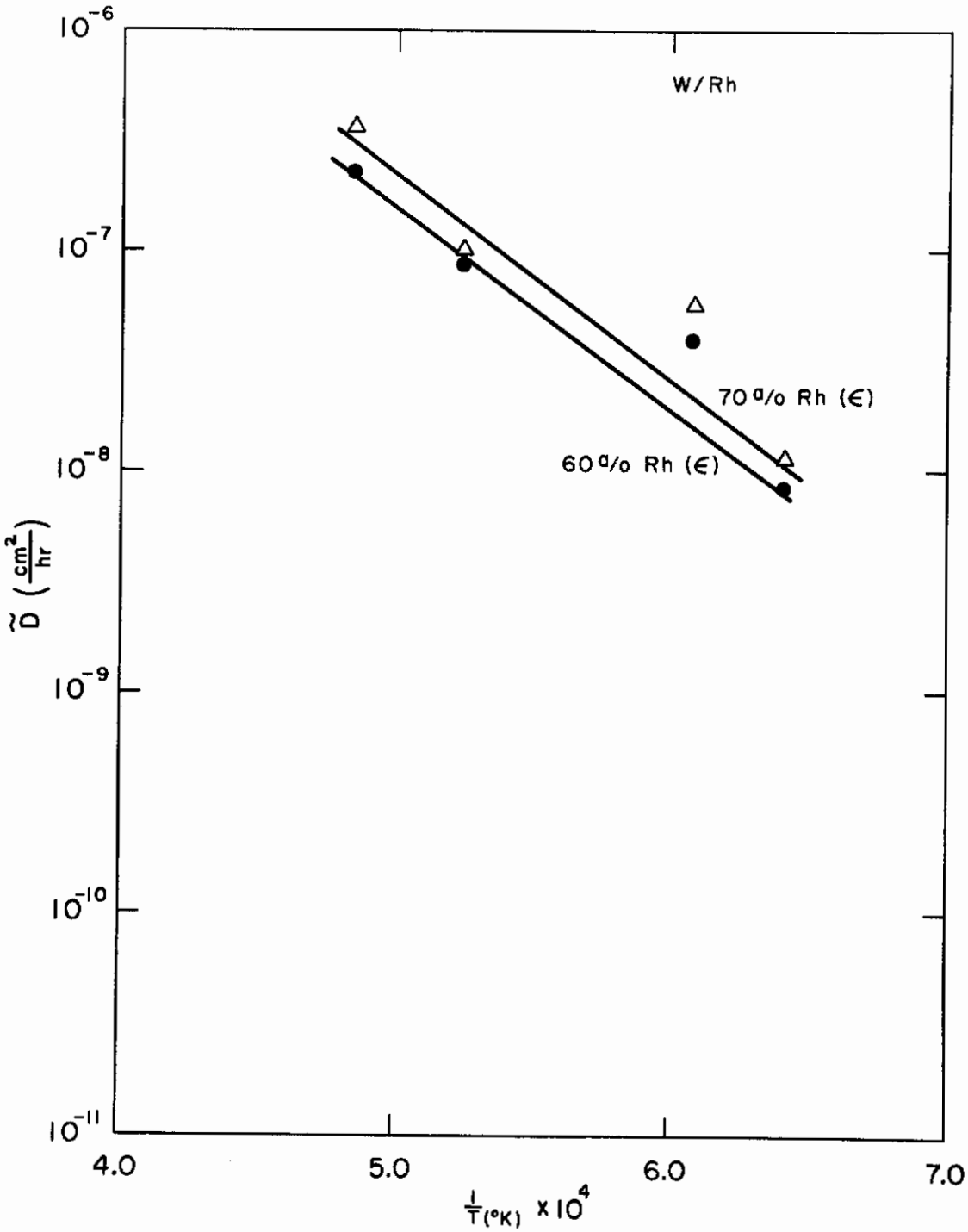

Figure 29. Plot of Logarithm of the Interdiffusion Coefficient vs. Reciprocal Temperature for Couples in the W-Rh System. Compositions in the intermediate hcp phase are illustrated.

Approved for Public Release

TABLE 17

TABULATION OF W-Rh DIFFUSION RESULTS

Temp. (^{o}C)	Time (hrs.)	Grade of Couple*	Interdiffusion Coefficients (cm^2/hr.)				Comments
			3 ^{a}/o Rh α	60 ^{a}/o ϵ	70% ϵ	90% β	
1300	1750	B^{-}	8.1×10^{-11}	9×10^{-9}	1.2×10^{-8}	1.8×10^{-8}	
1385	417	C	4.6×10^{-10}	5×10^{-8}	6.8×10^{-8}	2.6×10^{-8}	Interface is porous and cracked.
1645	300	B	5.2×10^{-10}	8.9×10^{-8}	1.0×10^{-7}	1.2×10^{-7}	
1800	200	B	5.4×10^{-9}	2.3×10^{-7}	3.5×10^{-7}	3.9×10^{-7}	Entry in 3 ^{a}/o column actually is for 2 ^{a}/o.
1800	67	C	5×10^{-9}	2.9×10^{-7}	4.4×10^{-7}	5.0×10^{-7}	Entry in 3 ^{a}/o column actually is for 2 ^{a}/o.
			58,000	41,700	43,400	41,600	Q values, Cal/mole.
			0.00457	0.00525	0.0112	0.00912	D_o values (cm^2/hr.)

* Grades indicate quality of diffusion zones.

Approved for Public Release

Confidential

Contrails

VI. DIFFUSION IN THE SYSTEM TUNGSTEN-PLATINUM

A. Diffusion Couple Preparation and Treatment

1. Material

The platinum used in both standards and the diffusion couples was obtained as a bar of purity greater than 99.9 percent from Metals and Controls, Inc. The tungsten used is that described in Section III.A.1. Typical analyses for the platinum are given in Table 18.

2. Arc-Melting

Arc-melting tungsten powders into buttons to be used for diffusion specimens and standard alloys has already been described in Section III.A.2. Pieces from the platinum bar were arc-melted with the tungsten buttons to make up standard alloys at compositions across the phase diagram. Diffusion specimens were fabricated directly from the platinum as-received bar. It was unnecessary to arc-melt the platinum into buttons.

The alloy standards necessary for the determination of composition in the diffusion couples had previously been found to be inhomogeneous. This situation arose from a compromise in which the melting time during arc-melting was minimized in order to minimize the volatization of the lower melting constituent of the composition standards. Thus platinum in the tungsten-platinum standards was found to undergo disproportionate losses during prolonged melting. The segregation of the alloys limited their usefulness as microbeam probe standards and it was decided to prolong the melting process to produce homogeneous alloys and to resolve the question of the loss of the more volatile substance by subsequent direct chemical analysis rather than relying upon a materials balance as had previously been done. The results of the wet chemical analyses are presented in Table 19.

3. Bonding of Couples

The couples of the W-Pt system were bonded into three layered sandwiches as described in the section on W-Ru system (III.A.3).

Approved for Public Release

Contrails

TABLE 18

TYPICAL SPECTROSCOPIC ANALYSIS OF PLATINUM USED

Impurity Element	Contents Expressed in Percentage
Rh	N.D. <.005
Pd	N.D. <.005
Ir	.02
Au	N.D. <.01
Ag	.01
Cu	P. <.005
Ni	N.D. <.005
Fe*	.02
Si	N.D. <.005

* The high iron content is believed to be due to pickup during the sectioning operation to obtain a sample of platinum from the rod for analyses. Apparently the etching of the platinum before analysis was inadequate.

N.D. - Not detected, less than the amount specified.

P. - Present, less than the amount specified.

Approved for Public Release

Contrails

TABLE 19

W-Pt STANDARD ALLOY COMPOSITIONS
FOR MICROPROBE ANALYSIS

Nominal Composition (^{a}/o Pt)	Composition as Determined by Wet Chemical Analysis (^{a}/o Pt)	Deviation (%)
15	13.4	± 1
30	27.8	± 1
45	44.0	± 1
60	60.5	± 1
75	73.1	± 1
90	86.9	± 1

Approved for Public Release

Contrails

4. Annealing

The comments of Section III.A.4 on the W-Ru system apply here.

5. Sectioning

The couples of the W-Pt system were sectioned as described in the section on W-Ru system (III.A.5).

B. Determination of Composition Profiles

In almost all details, except as noted below, the techniques and procedures for determination of the W-Pt composition profiles parallel the techniques and procedures for determination of those in the W-Ru system described in Sections III.B.1 and III.B.2.

The exceptions to the details mentioned above were as follows:

(1) The compositions of the standard alloys were determined by wet chemical analysis.

(2) The alloys of Table 19 were utilized as standards by simultaneously determining (on two spectrographs) the intensity of tungsten L_{α_1} and platinum L_{α_1} characteristic radiation from suitably prepared specimens.

(3) All microprobe data on the W-Pt system was taken with 30KV accelerating potential, using a lithium fluoride crystal, a scintillation counter and a take-off angle of about 15.5°.

A plot of the normalized X-ray intensities of the W-Pt standards versus composition is given in Figure 30.

1. Traversing of Couples

The data points of the composition profile were determined by translating the sample continuously with a motorized drive (and simultaneously recording the X-ray intensity on a chart) through the axis of the electron beam so that the beam made a 45° angle of traverse with respect to the diffusion interface. The speed of translating varied from 5 microns

Approved for Public Release

Contrails

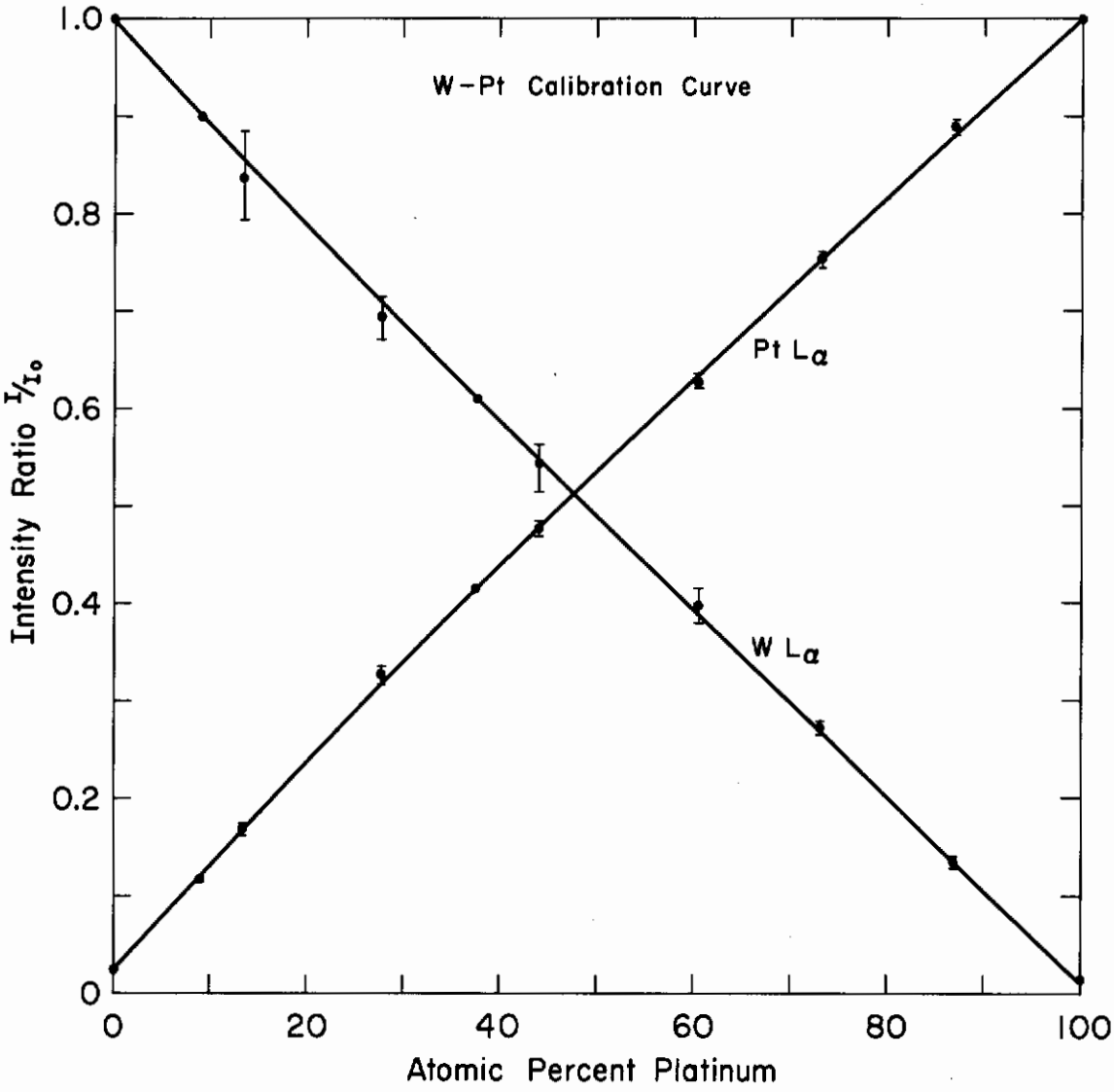

Figure 30. Plot of Normalized Intensity of Characteristic Radiation of W and Pt vs. Composition. The L_{α_1} X-ray lines of both elements were used.

Approved for Public Release

Contrails

per minute to 20 microns per minute depending on the diffusion zone width. For wide zones, the higher translating speeds were used. The calibration curve of Figure 30 was then used to obtain composition-distance profiles from the recorded X-ray intensity charts.

2. Composition-Penetration Profiles

Five temperatures were used for diffusion treatments in this work. The times and temperature of these treatments are given in Table 20. The composition-penetration profiles found on the five annealed specimens are given in Figures 31, 32, 33, 34 and 35. These figures contain the data points taken with respect to only one of the constituents. In nearly all cases, the sum of the compositions of tungsten and platinum taken independently at a single point add to percentages between 99 and 101. Thus, only one set of data points is given. The composition-distance profiles of Figures 31, 32, 33, 34 and 35 were presented as step points by reading at specific increments on the continuous scan-X-ray intensity recording mentioned in the previous section.

There are some uncertainties regarding the location of the phases in the composition versus penetration profiles of Figures 34 and 35. The ε and γ phases (discussed in detail later and clearly delineated in Figures 31, 32 and 33) in the diffusion couples annealed at 1300°C, 1373°C and 1645°C, had wide zones (each greater than 25 microns) enabling one to obtain sufficient data points within each one phase region. However, the zone widths (measurements were made with a filar eyepiece placed in the metallograph) of the ε and γ phase in the diffusion couples annealed at 1700°C and 1743°C were about 5 microns each, making it difficult to obtain sufficient data on each phase. For this reason there were large uncertainties as to the locations of the ε and γ phases in the composition vs. penetration profiles for the two highest temperature anneals. The uncertainties as to the location of the two phases are so indicated by question marks in Figures 34 and 35.

Approved for Public Release

Contrails

TABLE 20

TIMES AND TEMPERATURES OF ANNEALING TREATMENTS
OF W-Pt COUPLES

Nominal Temperature (°C)	Temperature Deviation (°C)	Time of Anneal (hours)
1300	± 20	1750
1473	± 12	432
1645	± 15	300
1700	± 11	96
1743	± 10	24

Approved for Public Release

Contrails

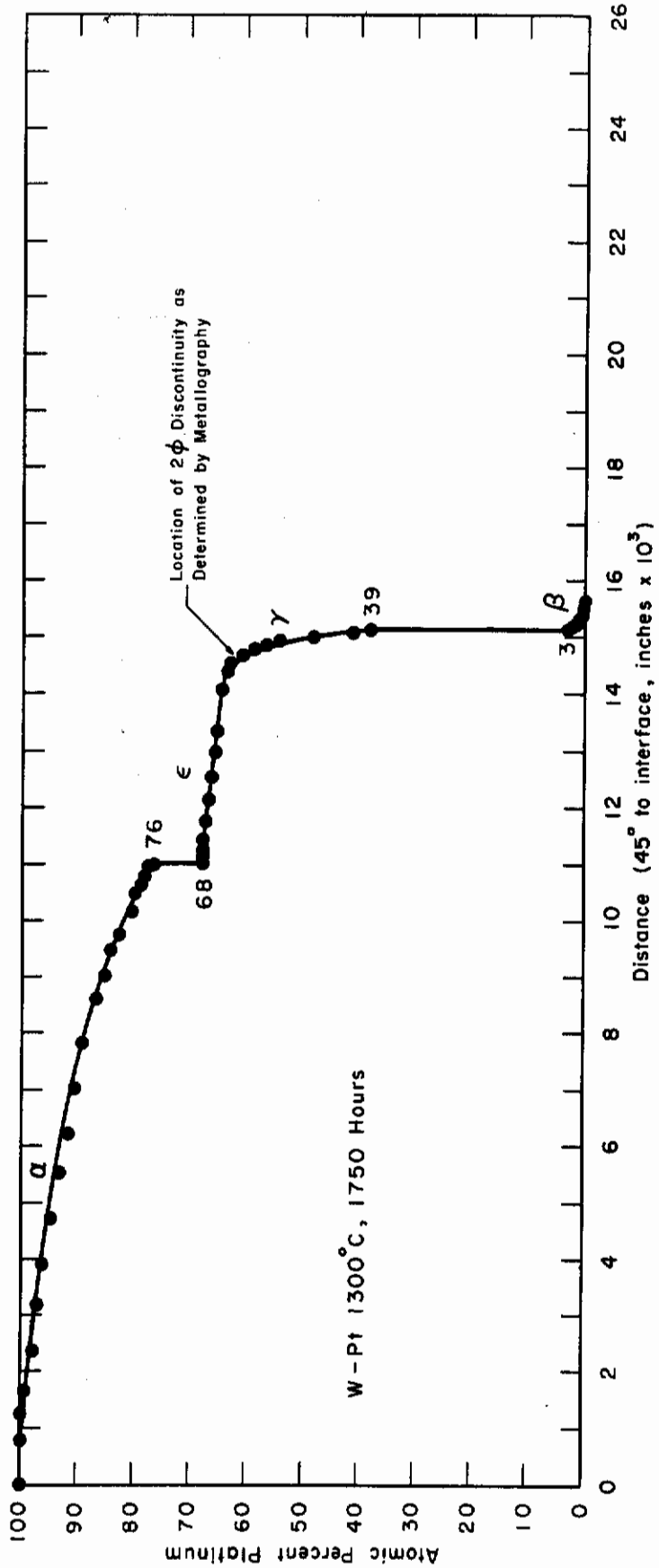

Figure 31. Composition vs Penetration Profile, W-Pt System, 1300°C.

Approved for Public Release

Contrails

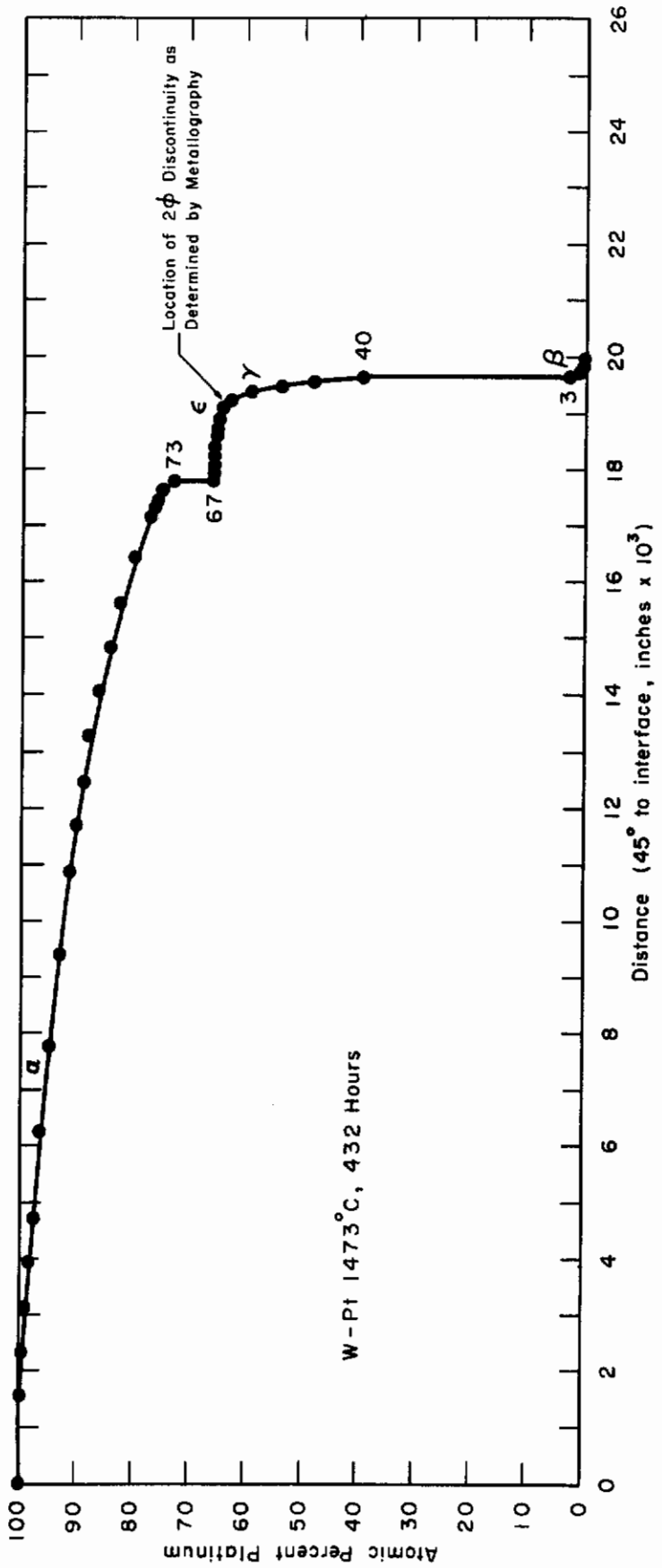

Figure 32. Composition vs Penetration Profile, W-Pt System, 1473°C.

Approved for Public Release

Contrails

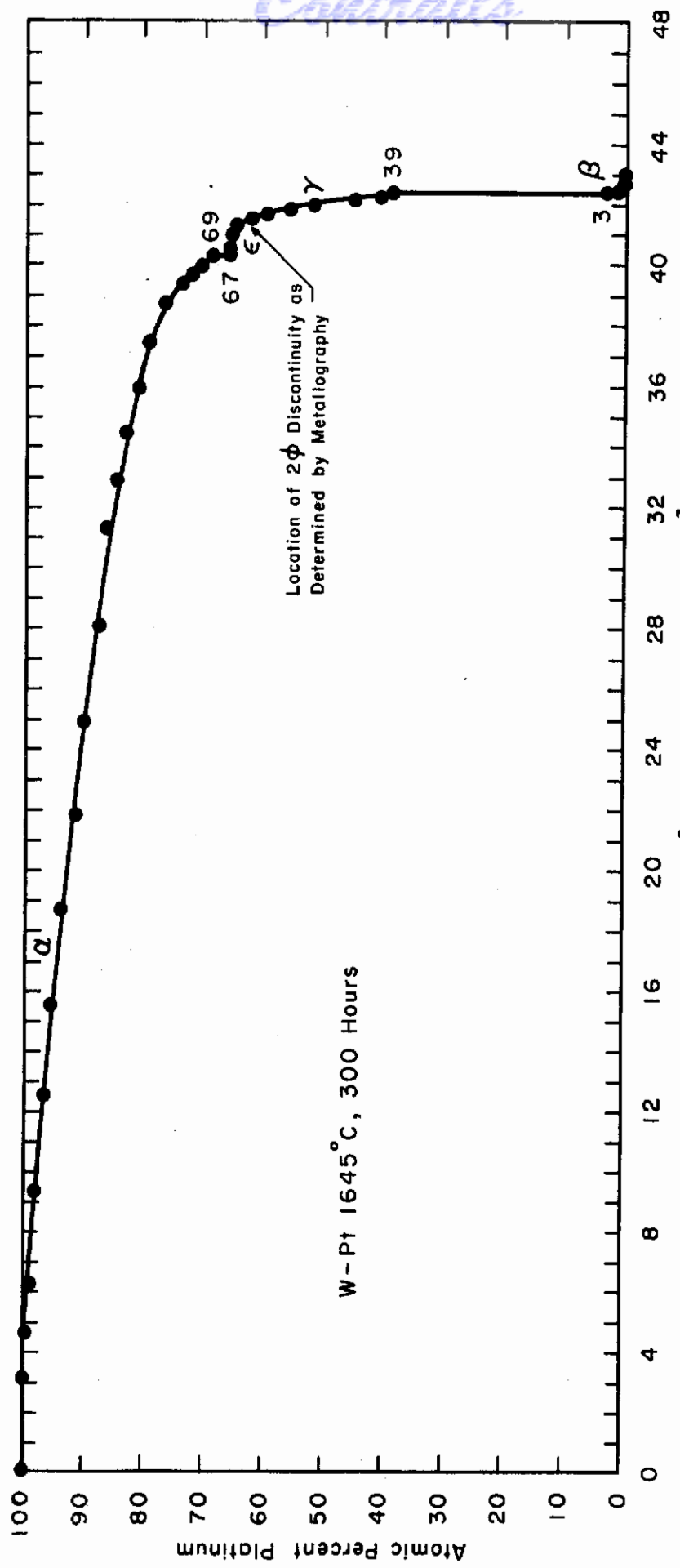

Figure 33. Composition vs Penetration Profile, W-Pt System, 1645°C.

Approved for Public Release

Contrails

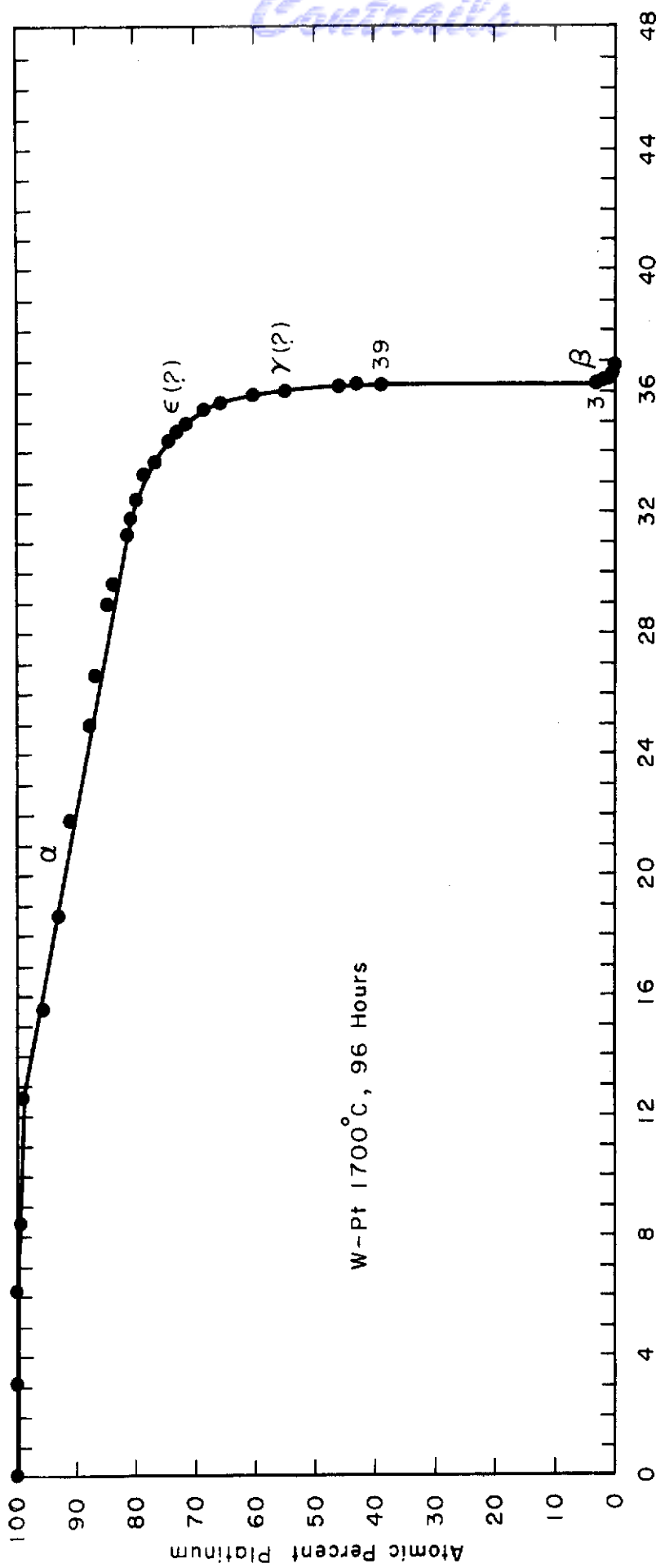

Figure 34. Composition vs Penetration Profile, W-Pt System, 1700°C.

Approved for Public Release

Contrails

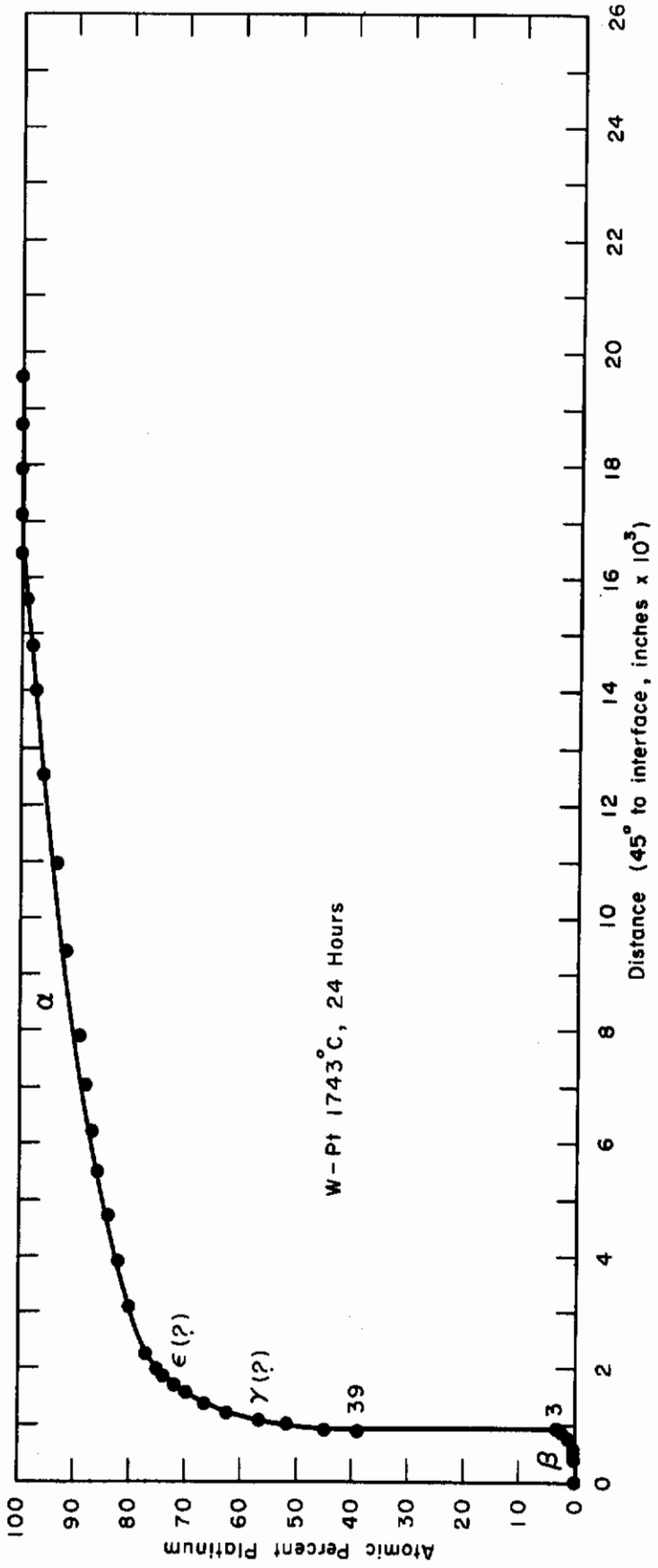

Figure 35. Composition vs Penetration Profile, W-Pt System, 1743°C.

Approved for Public Release

Contrails

C. Interdiffusion Coefficient Determinations

The comments of Section III.C.1 on the W-Ru system apply here also. The computer methods for solving the Boltzmann-Matano expression for the interdiffusion coefficient as described in Section III.C.2 for the W-Ru system were also employed on the profiles of the W-Pt couples.

D. Results and Discussion

1. Interdiffusion Coefficient as a Function of Composition

The data points of Figures 31 through 35 were processed in a computer to yield the interdiffusion coefficient as a function of composition in each of the phases of this system. Interdiffusion coefficients versus composition are tabulated in Table 21 for the profiles of Figures 31, 32, 33, 34 and 35. Discontinuities of the interdiffusion coefficients within a single phase region have been discussed in Section III.D.1 of the W-Ru system.

2. Variation of Interdiffusion Coefficients with Temperature

Plots of the logarithm of the interdiffusion coefficient versus reciprocal temperature were made for various compositions across the phase diagram. These are presented for compositions in each phase field in Figures 36 through 42. It is to be noted that the data of Figures 36 through 42 do not all fall on straight lines. Reasons for this have already been stated in Section III.D.2 of the W-Ru system. A summary of the interdiffusion coefficient values for selected compositions in each phase field is given in Table 22. The activation energies, Q, and the frequency factors, D_o, that are listed in this table were obtained from the slopes of plots such as are given in Figures 36 through 42. The slopes of these curves were taken at the high temperature regions in all cases. From the way the curves are formed, it should be noted that such a procedure gives a maximum value of both Q and D_o for the temperature interval studied.

Approved for Public Release

Contrails

TABLE 21

INTERDIFFUSION COEFFICIENTS OF THE W-Pt SYSTEM
FOR DIFFERENT COMPOSITIONS AT SEVERAL TEMPERATURES

Annealing Temperature (°C)	Annealing Time (hrs.)	Phase	Composition (a/o Pt)	Interdiffusion Coefficient, $\tilde{D}$ ($cm^2/hr.$)
1743	24	αPt	99	1.93×10^{-6}
			98	2.26×10^{-6}
			97	2.05×10^{-6}
			96	2.88×10^{-6}
			95	3.25×10^{-6}
			94	3.63×10^{-6}
			93	4.39×10^{-6}
			92	4.34×10^{-6}
			91	4.28×10^{-6}
			90	4.21×10^{-6}
			89	4.14×10^{-6}
			88	4.06×10^{-6}
			87	3.98×10^{-6}
			86	3.90×10^{-6}
			85	3.82×10^{-6}
			84	3.74×10^{-6}
			83	3.65×10^{-6}
			82	3.57×10^{-6}
			81	3.48×10^{-6}
			80	3.39×10^{-6}
			79	3.30×10^{-6}
			78	3.21×10^{-6}
			77	5.61×10^{-7}
			76	5.19×10^{-7}
			75	4.84×10^{-7}
			74	4.53×10^{-7}
			73	4.26×10^{-7}
			72	4.02×10^{-7}
		?($\epsilon + \alpha$)	71	3.80×10^{-7}
			70	3.61×10^{-7}
			69	3.43×10^{-7}
			68	3.27×10^{-7}
		?(ϵ)	67	3.13×10^{-7}
			66	2.99×10^{-7}

(Table continued on next page.)

Approved for Public Release

Contrails

TABLE 21 (continued)

Annealing Temperature (°C)	Annealing Time (hrs.)	Phase	Composition (a/o Pt)	Interdiffusion Coefficient, $\tilde{D}$ (cm^2/hr.)
1743	24	?(ε)	65	2.87×10^{-7}
			64	2.75×10^{-7}
		?(ε + γ)	63	2.64×10^{-7}
		?(γ)	62	2.54×10^{-7}
			61	2.45×10^{-7}
			60	2.36×10^{-7}
			59	2.28×10^{-7}
			58	2.20×10^{-7}
			57	2.12×10^{-7}
			56	2.05×10^{-7}
			55	1.99×10^{-7}
			54	1.92×10^{-7}
			53	1.86×10^{-7}
			52	1.80×10^{-7}
			51	1.75×10^{-7}
			50	1.69×10^{-7}
			49	1.64×10^{-7}
		βW + γPt	48-4	2Ø
		βW	3	2.00×10^{-8}
			2	1.93×10^{-8}
			1	1.82×10^{-8}
1700	96	αPt	99	1.22×10^{-6}
			98	1.32×10^{-6}
			97	1.48×10^{-6}
			96	1.64×10^{-6}
			95	1.86×10^{-6}
			94	2.07×10^{-6}
			93	2.34×10^{-6}
			92	2.71×10^{-6}
			91	3.23×10^{-6}
			90	4.18×10^{-6}
			89	6.85×10^{-6}
			88	--
			87	--
			86	4.49×10^{-6}
			85	3.19×10^{-6}
			84	2.55×10^{-6}
			83	2.15×10^{-6}

(Table continued on next page.)

Approved for Public Release

Contrails

TABLE 21 (continued)

Annealing Temperature (°C)	Annealing Time (hrs.)	Phase	Composition (a/o Pt)	Interdiffusion Coefficient, $\tilde{D}$ (cm^2/hr.)
1700	96	αPt	82	1.87×10^{-6}
			81	1.66×10^{-6}
			80	1.50×10^{-6}
			79	1.36×10^{-6}
			78	1.25×10^{-6}
			77	1.16×10^{-6}
			76	1.08×10^{-6}
			75	1.01×10^{-7}
			74	9.44×10^{-7}
			73	8.87×10^{-7}
			72	8.36×10^{-7}
		?(ε + α)	71	7.90×10^{-7}
			70	7.48×10^{-7}
			69	1.14×10^{-7}
			68	1.11×10^{-7}
		?(ε)	67	1.09×10^{-7}
			66	1.06×10^{-7}
			65	1.04×10^{-7}
			64	1.01×10^{-7}
		?(ε + γ)	63	9.91×10^{-8}
		?(γ)	62	9.70×10^{-8}
			61	9.49×10^{-8}
			60	9.29×10^{-8}
			59	9.10×10^{-8}
			58	8.91×10^{-8}
			57	8.74×10^{-8}
			56	8.56×10^{-8}
			55	8.40×10^{-8}
			54	8.23×10^{-8}
			53	8.07×10^{-8}
			52	7.92×10^{-8}
			51	7.76×10^{-8}
			50	7.62×10^{-8}
			49	7.47×10^{-8}
			48	7.33×10^{-8}
			47	7.20×10^{-8}
		βW + γPt	46-5	2Ø
		βW	4	5.73×10^{-9}
			3	3.93×10^{-9}
			2	3.71×10^{-9}
			1	3.41×10^{-9}

(Table continued on next page.)

Approved for Public Release

Contrails

TABLE 21 (continued)

Annealing Temperature (°C)	Annealing Time (hrs.)	Phase	Composition (a/o Pt)	Interdiffusion Coefficient, $\tilde{D}$ (cm^2/hr.)
1645	300	αPt	99	--
			98	--
			97	1.86×10^{-6}
			96	1.89×10^{-6}
			95	1.88×10^{-6}
			94	1.87×10^{-6}
			93	1.84×10^{-6}
			92	1.81×10^{-6}
			91	1.78×10^{-6}
			90	1.75×10^{-6}
			89	1.72×10^{-6}
			88	1.68×10^{-6}
			87	1.65×10^{-6}
			86	1.61×10^{-6}
			85	1.58×10^{-6}
			84	1.54×10^{-6}
			83	1.50×10^{-6}
			82	1.47×10^{-6}
			81	1.43×10^{-6}
			80	1.39×10^{-7}
			79	4.36×10^{-7}
			78	4.41×10^{-7}
			77	4.46×10^{-7}
			76	4.53×10^{-7}
			75	4.61×10^{-7}
			74	4.71×10^{-7}
			73	4.83×10^{-7}
			72	4.97×10^{-7}
		ε + α	71-67	2Ø
		ε	66	3.94×10^{-8}
			65	3.96×10^{-8}
			64	3.99×10^{-8}
		ε + γ	63	2Ø
		γ	62	4.06×10^{-8}
			61	4.11×10^{-8}
			60	4.18×10^{-8}
			59	4.26×10^{-8}
			58	4.36×10^{-8}
			57	4.47×10^{-8}
			56	4.61×10^{-8}
			55	4.78×10^{-8}

(Table continued on next page.)

Approved for Public Release

Contrails

TABLE 21 (continued)

Annealing Temperature (°C)	Annealing Time (hrs.)	Phase	Composition (a/o Pt)	Interdiffusion Coefficient, $\tilde{D}$ (cm^2/hr.)
1645	300	γ	54	4.99×10^{-8}
			53	5.25×10^{-8}
			52	5.59×10^{-8}
			51	6.05×10^{-8}
			50	6.70×10^{-8}
			49	7.71×10^{-8}
			48	9.57×10^{-8}
			47	1.48×10^{-7}
		βW + γ	46-5	2Ø
		βW	4	5.86×10^{-9}
			3	---
			2	3.49×10^{-9}
			1	3.23×10^{-9}
1473	432	αPt	99	7.61×10^{-8}
			98	1.72×10^{-7}
			97	1.95×10^{-7}
			96	2.41×10^{-7}
			95	2.39×10^{-7}
			94	2.37×10^{-7}
			93	2.33×10^{-7}
			92	2.30×10^{-7}
			91	2.26×10^{-7}
			90	2.23×10^{-7}
			89	2.19×10^{-7}
			88	2.15×10^{-7}
			87	2.12×10^{-7}
			86	2.08×10^{-7}
			85	2.04×10^{-7}
			84	2.00×10^{-7}
			83	1.96×10^{-7}
			82	1.92×10^{-7}
			81	1.88×10^{-7}
			80	1.84×10^{-7}
			79	1.80×10^{-7}
			78	1.76×10^{-7}
			77	1.72×10^{-7}
		ε + αPt	76-68	2Ø

(Table continued on next page.)

Approved for Public Release

Contrails

TABLE 21 (continued)

Annealing Temperature (°C)	Annealing Time (hrs.)	Phase	Composition (a/o Pt)	Interdiffusion Coefficient, $\tilde{D}$ (cm^2/hr.)
1473	432	ε	67	4.96×10^{-7}
			66	4.87×10^{-7}
		ε + γ	65	2Ø
		γ	64	1.09×10^{-8}
			63	1.06×10^{-8}
			62	1.04×10^{-8}
			61	1.01×10^{-8}
			60	9.90×10^{-9}
			59	9.67×10^{-9}
			58	9.44×10^{-9}
			57	9.23×10^{-9}
			56	9.02×10^{-9}
			55	8.82×10^{-9}
			54	8.62×10^{-9}
			53	8.43×10^{-9}
			52	8.25×10^{-9}
			51	8.07×10^{-9}
			50	7.88×10^{-9}
			49	7.70×10^{-9}
		β + γ	48-6	2Ø
		β	5	1.46×10^{-6}
			4	6.44×10^{-7}
			3	7.42×10^{-8}
			2	--
			1	6.25×10^{-10}
1300	1750	αPt	99	1.10×10^{-8}
			88	1.43×10^{-8}
			97	1.75×10^{-8}
			96	2.07×10^{-8}
			95	2.42×10^{-8}
			94	2.81×10^{-8}
			93	3.21×10^{-8}
			92	3.60×10^{-8}
			91	3.93×10^{-8}
			90	4.14×10^{-8}
			89	4.17×10^{-8}
			88	4.05×10^{-8}
			87	3.83×10^{-8}

(Table continued on next page.)

Approved for Public Release

Contrails

TABLE 21 (continued)

Annealing Temperature (°C)	Annealing Time (hrs.)	Phase	Composition (a/o Pt)	Interdiffusion Coefficient, $\tilde{D}$ (cm^2/hr.)
1300	1750	αPt	86	3.56×10^{-8}
			85	3.29×10^{-8}
			84	3.04×10^{-8}
			83	2.55×10^{-8}
			82	2.61×10^{-8}
			81	2.43×10^{-8}
			80	2.27×10^{-8}
			79	2.13×10^{-8}
			78	2.01×10^{-8}
			77	1.90×10^{-8}
		ε + αPt	76-69	2Ø
		ε	68	1.22×10^{-8}
			67	1.21×10^{-8}
			66	1.20×10^{-8}
		ε + γ	65	2Ø
		γ	64	3.66×10^{-9}
			63	3.59×10^{-9}
			62	3.52×10^{-9}
			61	3.45×10^{-9}
			60	3.39×10^{-9}
			59	3.32×10^{-9}
			58	3.26×10^{-9}
			57	3.21×10^{-9}
			56	3.15×10^{-9}
			55	3.10×10^{-9}
			54	3.04×10^{-9}
			53	2.99×10^{-9}
			52	2.94×10^{-9}
			51	2.89×10^{-9}
			50	2.84×10^{-9}
			49	2.80×10^{-9}
			48	2.75×10^{-9}
			47	2.75×10^{-9}
			46	2.66×10^{-9}
		βW + γ	45-4	2Ø
		βW	3	3.79×10^{-10}
			2	3.57×10^{-10}
			1	3.26×10^{-10}

Approved for Public Release

Contrails

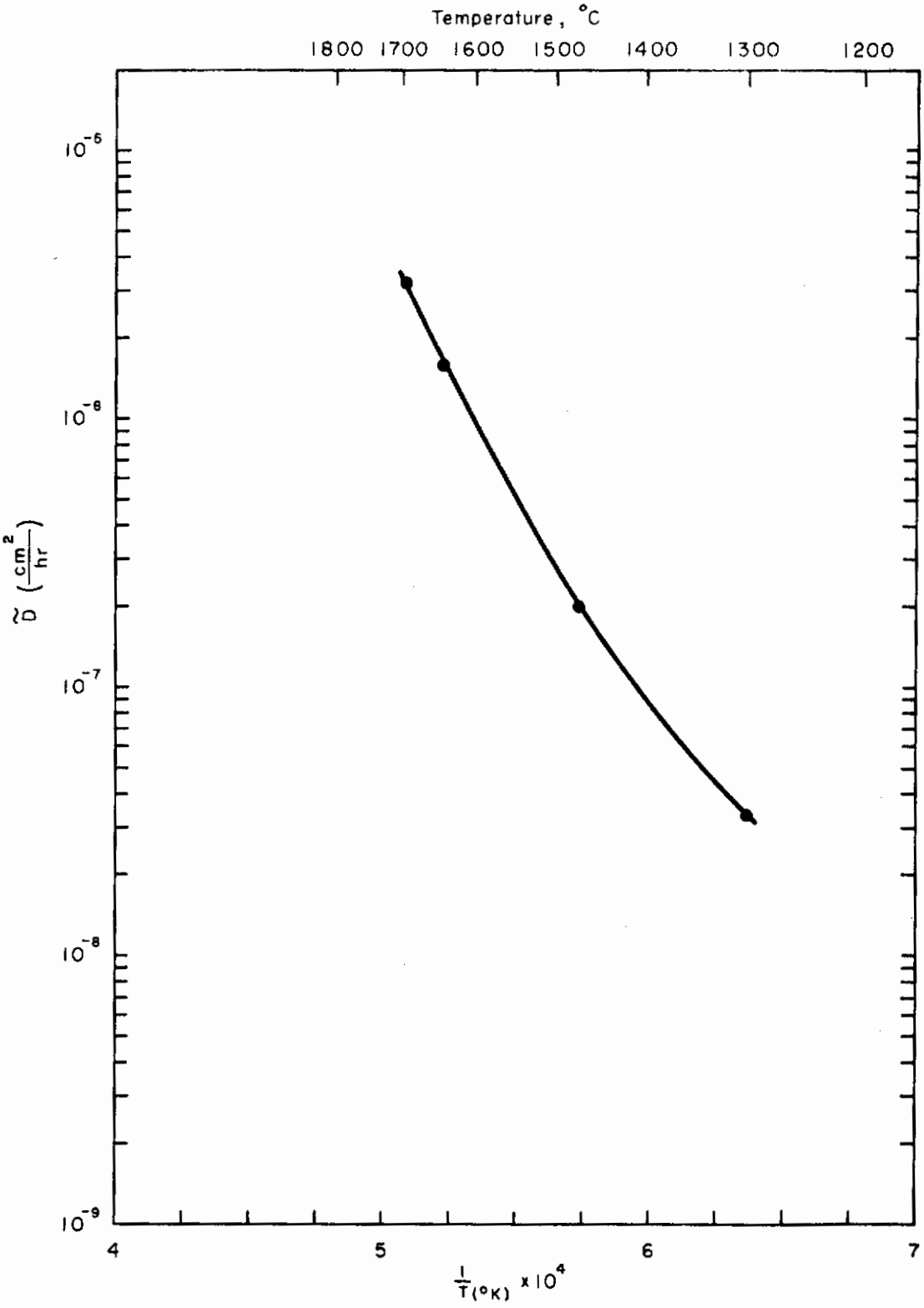

Figure 36. Plot of Logarithm of the Interdiffusion Coefficient vs. Reciprocal Temperature for Couples in the W-Pt System, 85 a/o Pt (α).

Approved for Public Release

Contrails

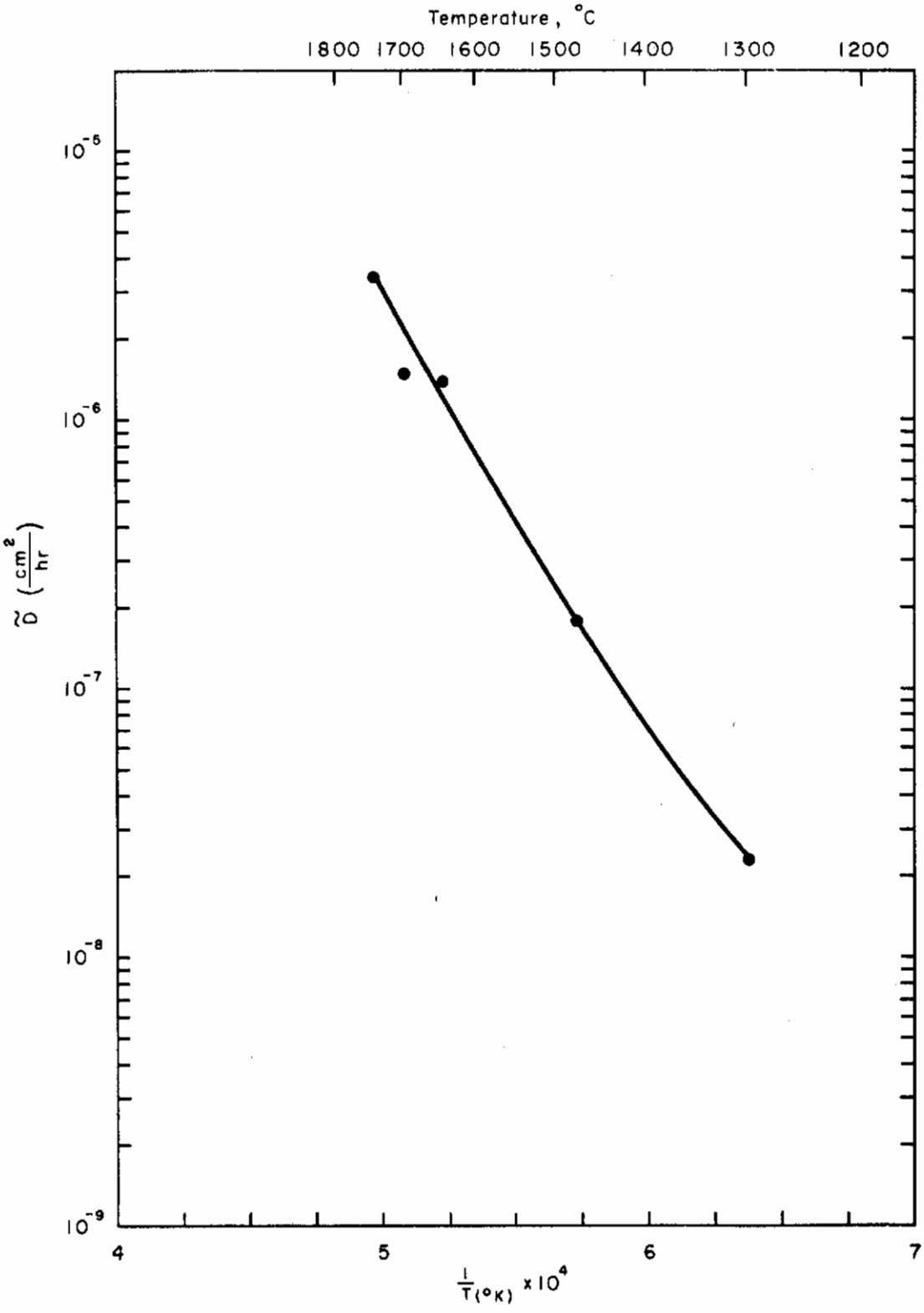

Figure 37. Plot of Logarithm of the Interdiffusion Coefficient vs Reciprocal Temperature for Couples in the W-Pt System, 80 a/o Pt (α).

Approved for Public Release

Contrails

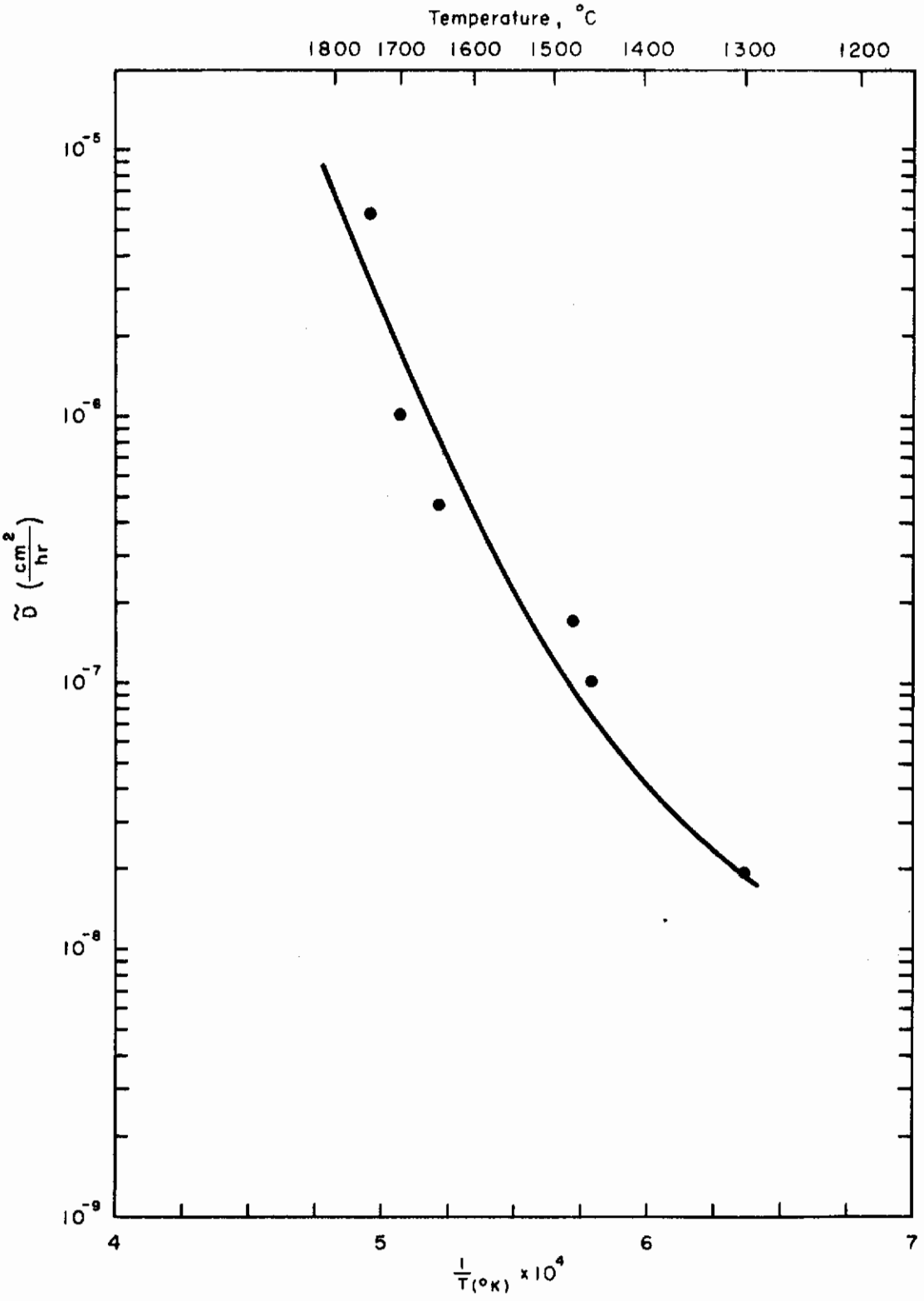

Figure 38. Plot of Logarithm of the Interdiffusion Coefficient vs Reciprocal Temperature for Couples in the W-Pt System, 77 a/o Pt (α).

Approved for Public Release

Contrails

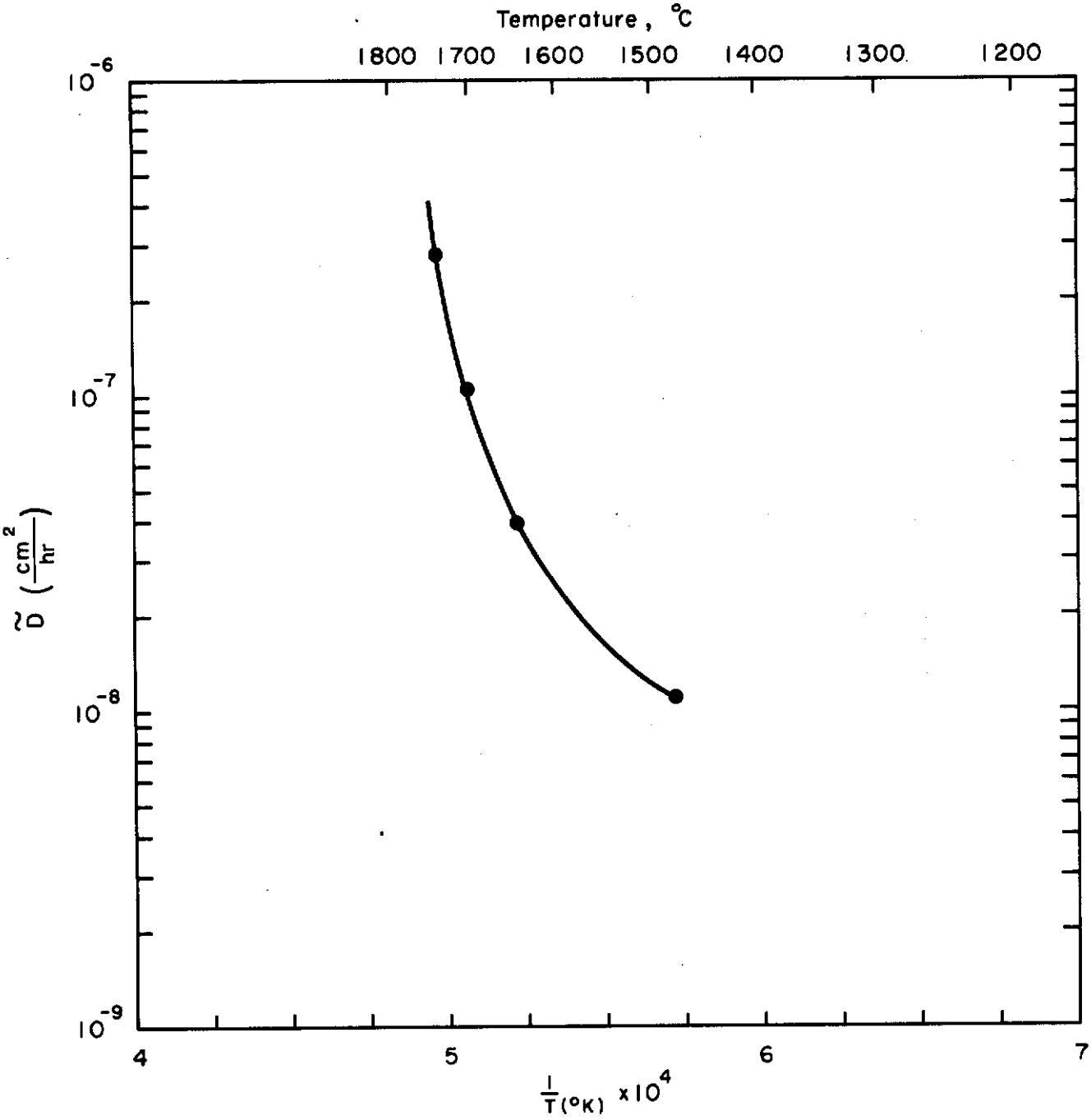

Figure 39. Plot of Logarithm of the Interdiffusion Coefficient vs Reciprocal Temperature for Couples in the W-Pt System, 65 a/o Pt.

Approved for Public Release

Contrails

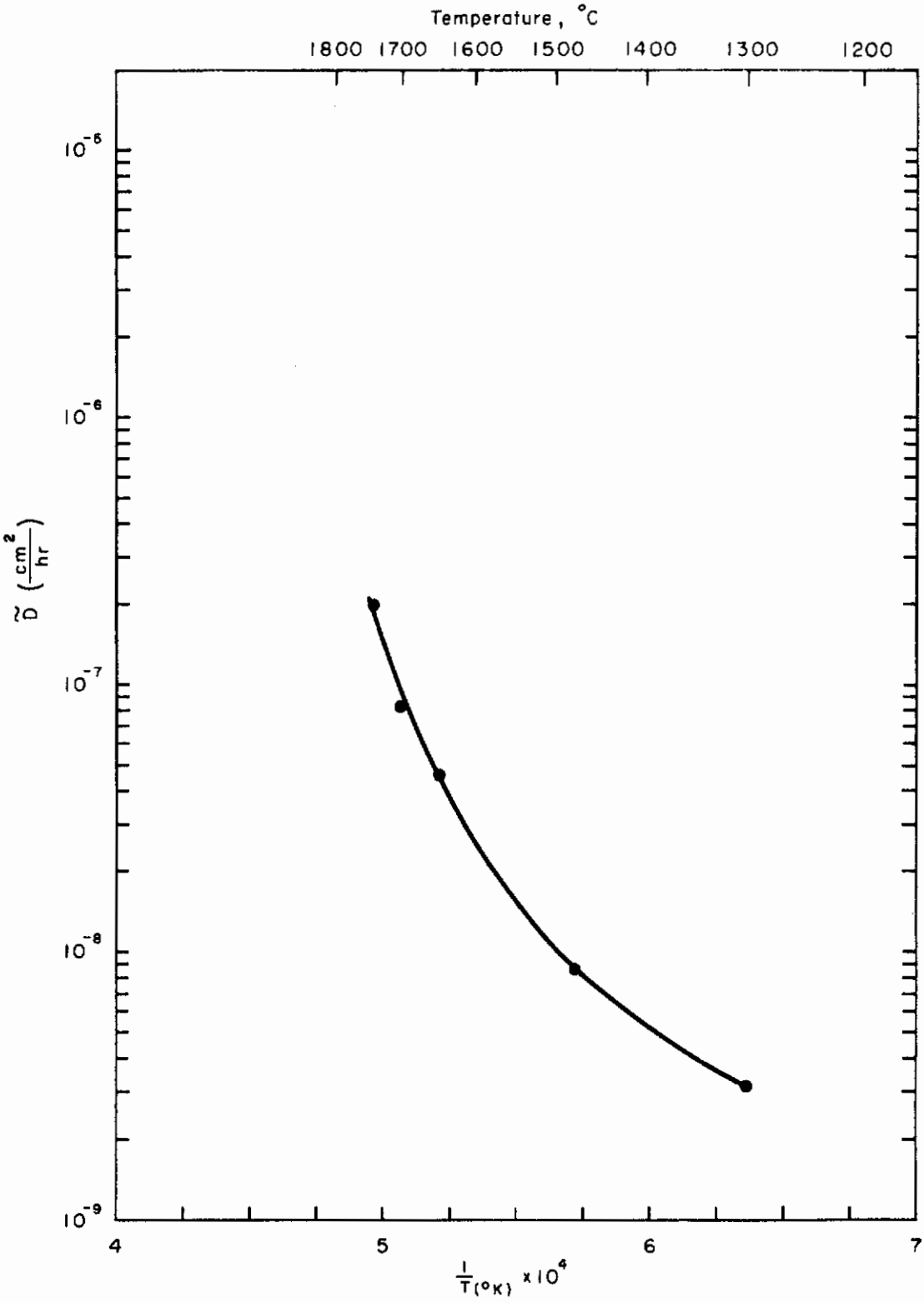

Figure 40. Plot of Logarithm of the Interdiffusion Coefficient vs Reciprocal Temperature for Couples in the W-Pt System, 55 a/o Pt.

Approved for Public Release

Contrails

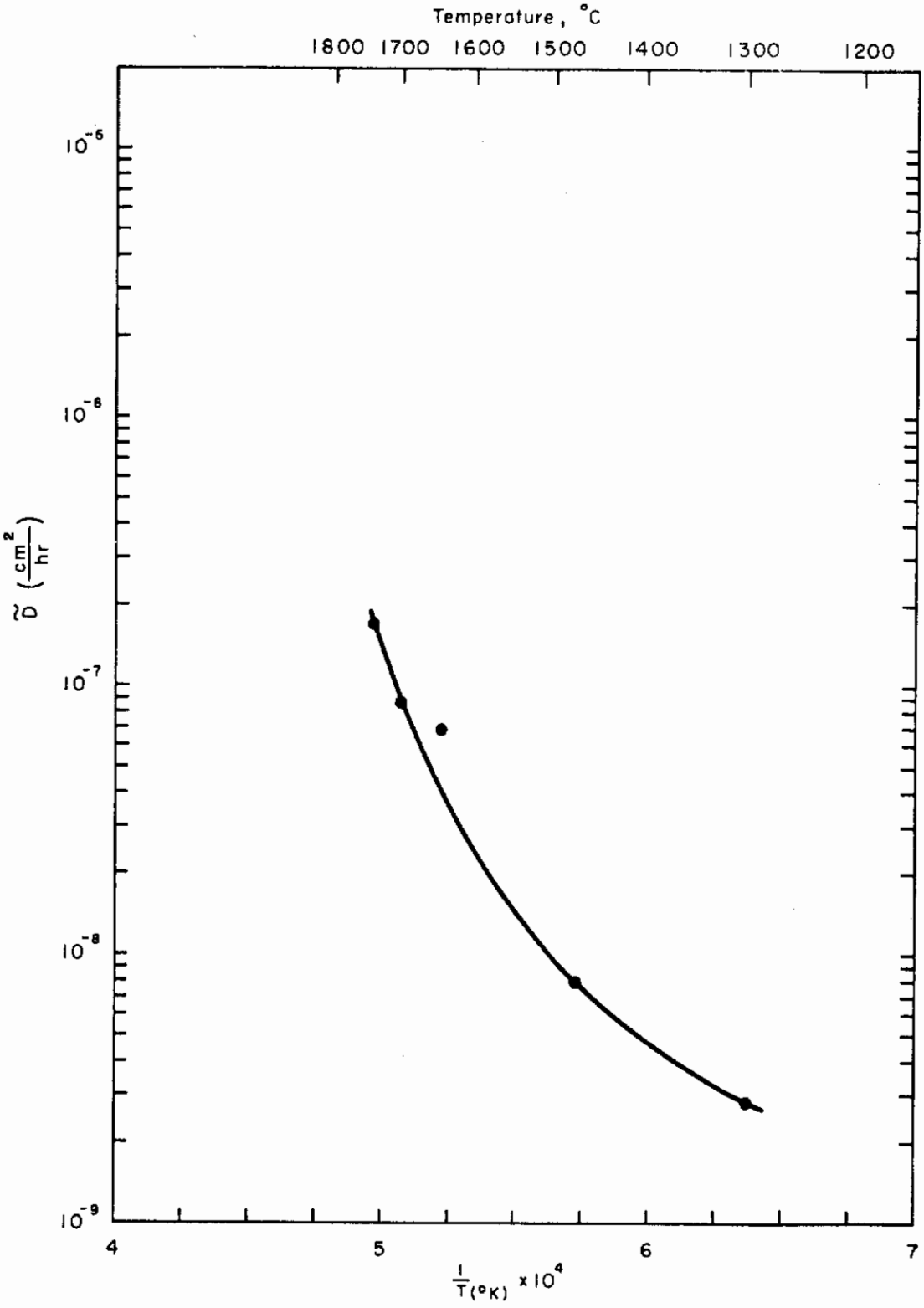

Figure 41. Plot of Logarithm of the Interdiffusion Coefficient vs. Reciprocal Temperature for Couples in the W-Pt System, 50 a/o Pt.

Approved for Public Release

Contrails

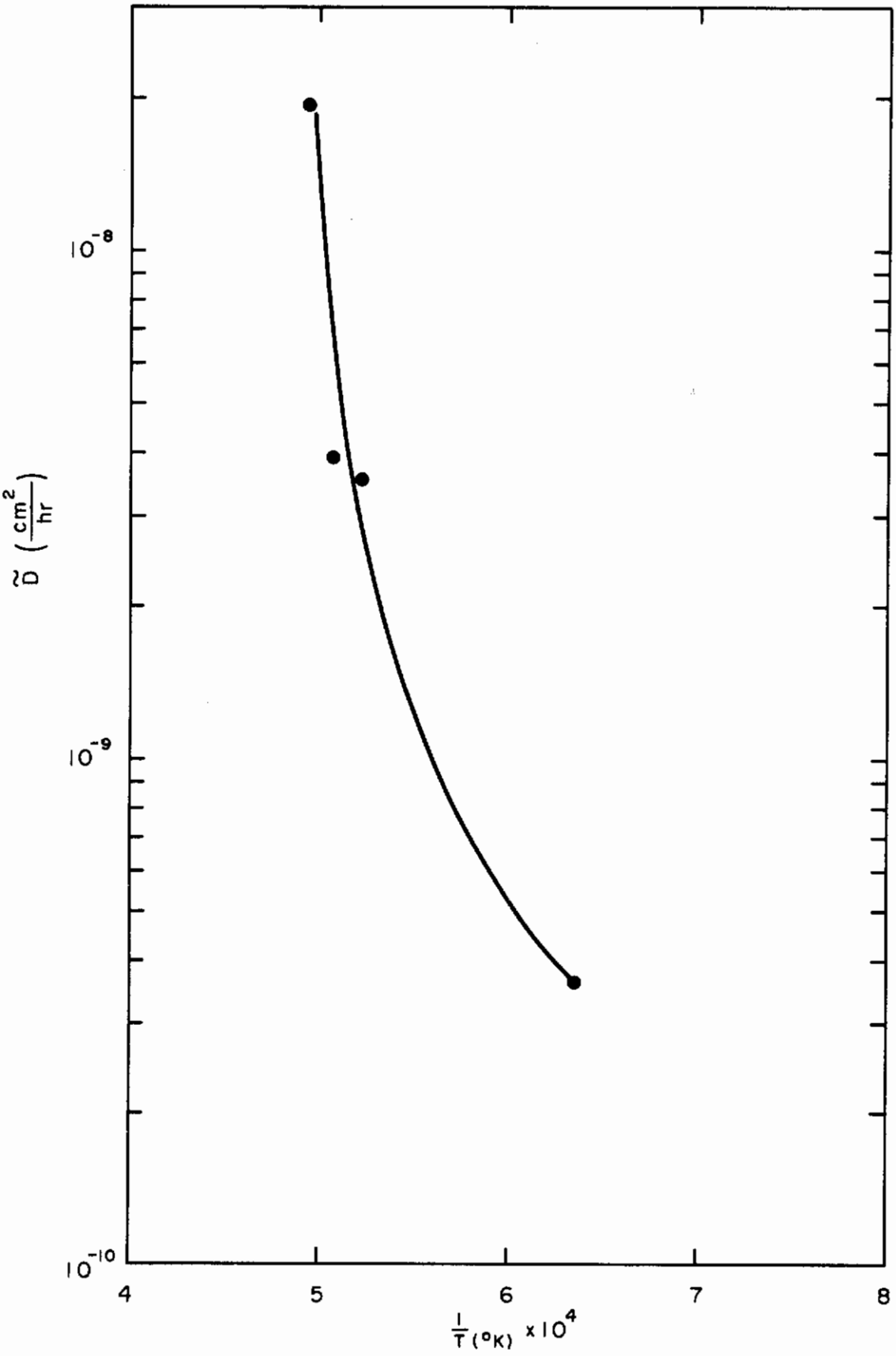

Figure 42. Plot of Logarithm of the Interdiffusion Coefficient vs Reciprocal Temperature for Couples in the W-Pt System, 2 a/o Pt (β).

Approved for Public Release

TABLE 22

TABULATION OF W-Pt DIFFUSION RESULTS

System	Temp (°C)	Time (hrs)	Grade of Couple*	Interdiffusion Coefficients ($cm^2/hr.$)							Comments
				2 a/o Pt (β)	50 a/o γ	55 a/o γ	65 a/o ε	77 a/o α	80 a/o α	85 a/o α	
W-Pt	1300	1750	A	3.6×10^{-10}	$.8 \times 10^{-9}$	3.1×10^{-9}	----	1.9×10^{-8}	2.3×10^{-8}	3.3×10^{-8}	.004 in zone.
	1473	432	A	----	7.9×10^{-9}	8.6×10^{-9}	1.1×10^{-8}	1.7×10^{-7}	1.8×10^{-7}	2.0×10^{-7}	.003 in zone.
	1645	300		3.5×10^{-9}	6.8×10^{-8}	4.6×10^{-8}	4.0×10^{-8}	4.7×10^{-7}	1.4×10^{-6}	1.6×10^{-6}	.0025 in zone.
	1700	96	A		7.6×10^{-8}	8.2×10^{-8}	1.0×10^{-7}	1.0×10^{-6}	1.5×10^{-6}	3.2×10^{-6}	.002 in zone.
	1743	24	A	1.9×10^{-8}	1.7×10^{-7}	2.0×10^{-7}	2.8×10^{-7}	5.0×10^{-6}	3.4×10^{-6}	----	.0015 in zone.
				139,000	83,600	82,100	92,000	78,000	75,400	74,200	Q cal/mole.
				11×10^5	17	12	158	63	43	46	D_o values ($cm^2/hr.$).

* Grades indicate quality of diffusion zones.

Approved for Public Release

Contrails

3. The ε and γ Phases

A check of the W-Pt phase diagram in Appendix II and reported in the literature as recently as 1961 shows below the solidus curves, a simple diagram of two terminal solid solutions and a two-phase region between them. However, electron microprobe data and metallographic examination indicate two additional single-phase and corresponding two-phase regions within the reported wide platinum terminal solid solution phase. The two single-phase regions have been designated in the present work as ε and γ as shown in Figure 68 of Appendix II. The ε phase polarizes and can readily be observed under polarized light.

Approved for Public Release

Contrails

VII. DIFFUSION IN THE SYSTEM COLUMBIUM-CHROMIUM

A. Diffusion Couple Preparation and Treatment

1. Material

The electron beam melted columbium utilized for both the diffusion couples and standard alloys was obtained as a rod of purity greater than 99.8%. The iodide chromium single crystal utilized for diffusion couples only was obtained as lenticular pieces (about 3/8 inch long by 1/4 inch at the widest part) of purity greater than 99.99%. Chromium metal pellets about 99.999 pure (refers to metallic content) obtained from United Mineral and Chemical Corporation were used for making standard alloys. The columbium was obtained from Wah Chang Corporation, and the iodide chromium crystals were generously supplied by Mr. C. S. Wukusick, High Temperature Materials Department of the Nuclear Materials and Propulsion Operation of General Electric Corporation. Typical analysis for these elements are given in Table 23. It is probable that the purity of the arc-melted materials was increased during the arc-melting consolidation above the figures given in Table 23. (See Section III.A.1)

2. Arc-Melting

Arc-melting was performed under conditions virtually identical to those described in Section III.A.2 on the W-Ru system and was utilized in the Cb-Cr study for making standard alloys only.

Diffusion specimens were fabricated directly from the electron beam melted as-received columbium stock and as-received iodide chromium crystals.

As with the W-Pt system (see Section IV.A.2), a wet chemical analysis was performed to establish the compositions qf the Cb-Cr standard alloys. The problems of inhomogenity and prolonged melting paralleled those of the W-Pt system. The results of the wet chemical analysis are presented in Table 24.

Approved for Public Release

Contrails

TABLE 23

TYPICAL ANALYSES OF COLUMBIUM AND CHROMIUM USED

Material	Impurity Element	Contents (ppm)
Columbium	Al, Co, Cr, Mg, Mn, Mo, Ni, Pb, Sn, V, Zn	each <20
	Fe, Si	each <100
	C	<30
	Cd	<5
	Cu	<40
	H	3
	N	56
	O	<55
	Ta	<590
	Ti	<150
	W	<200
Iodide Chromium	O, S	each 8
	N	2
	H, Al	each 1
	C	40
	Fe	30
	Ni	4
	Si	14
	Ca	3
Chromium pellets	Bi, Li, K, Mg, Ca, Sr, Ba, Al, Ti, V, Nb, Sb, Pb, Mo, W, Mn, Fe, Co, Ni, Ir, Cu, Ag, Zn, Cd, Ga, Sn	Total Metallic 10
	S, N	each 10
	C	80
	H	300
	O	3400

Approved for Public Release

Contrails

TABLE 24

Cb-Cr STANDARD ALLOY COMPOSITIONS FOR MICROPROBE ANALYSIS

Nominal Composition (^{a}/o Cr)	Composition as Determined by Wet Chemical Analysis (^{a}/o Cr)	Deviation (%)
16.6	0.7	± 1
51.9	31.3	± 1
65.8	50.4	± 1
81.7	74.3	± 1
95.1	88.4	± 1

Approved for Public Release

Contrails

3. Bonding of Couples

The couples of the Cb-Cr system were bonded into three-layered sandwiches as described in Section III.A.3 of the W-Ru system.

4. Annealing

All the columbium-chromium diffusion runs were conducted in purified argon under a pressure of 1.33 atmosphere in order to suppress the volatization of chromium. For this purpose the tantalum tube resistance furnace was used exclusively since the furnace was readily adaptable to pressurization.

The comments of Section III.A.4 on the W-Ru system regarding measurements of temperature in the tantalum tube furnace apply here also.

5. Sectioning

The couples of the Cb-Cr system were sectioned as described in Section III.A.5 of the W-Ru system.

B. Determination of Composition Profiles

In almost all details, except as noted below, the techniques and procedures for determination of the Cb-Cr composition of profiles parallel that of the W-Ru system described in Section III.B.1 and Section III.B.2.

The exceptions to the details mentioned above were as follows:

(1) The composition of the standard alloys were determined by wet chemical analysis.

(2) The alloys of Table 24 were utilized as standards by simultaneously determining (on two spectrographs) the intensity of columbium L_{α_1} and chromium K_{α_1} characteristic radiation from suitably prepared specimens.

A plot of the normalized X-ray intensities of the Cb-Cr standards vs composition is given in Figure 43.

Approved for Public Release

Contrails

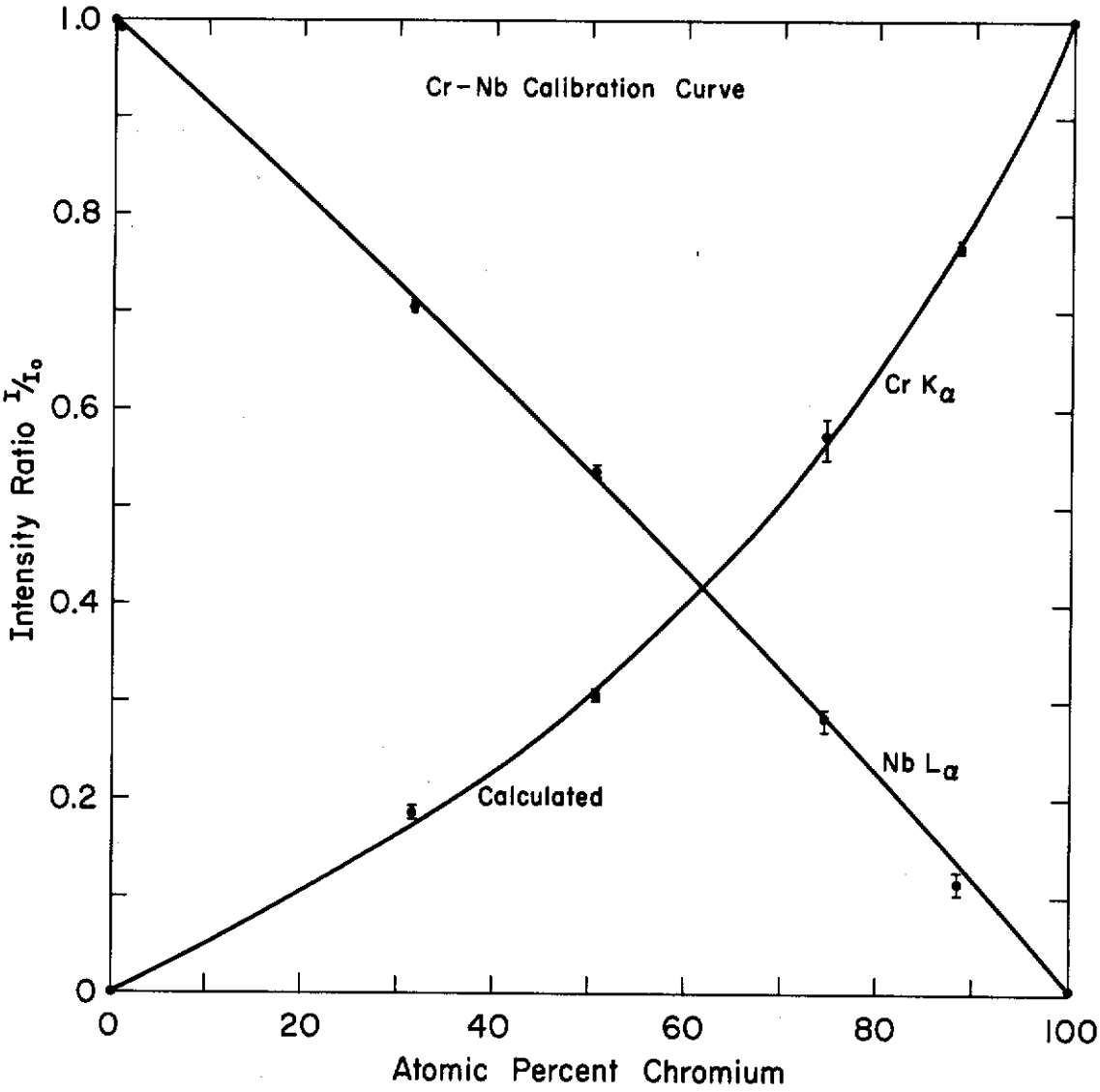

Figure 43. Plot of Normalized Intensity of Characteristic Radiation of Cb and Cr vs Composition. The Cr K_{α_1} and Cb L_{α_1} X-ray lines were used.

Approved for Public Release

Contrails

1. Traversing of Couples

The techniques and procedures used to determine the composition profiles for the Cb-Cr system were virtually identical to that of the W-Pt system described in Section VI.B.1.

2. Composition-Penetration Profiles

Six temperatures were used for diffusion treatments in this work. The times and temperature of these treatments are given in Table 25. The composition-penetration profiles found on the six annealed specimens are given in Figures 44, 45, 46, 47, 48 and 49. These figures contain the data points taken with respect to only one of the constituents. In nearly all cases the sum of the compositions of columbium and chromium taken independently at a single point add to percentages between 99 and 101. Thus, only one set of data points is given. The composition-penetration profiles of Figure 44, 45, 46, 47, 48 and 49 were presented as step points by reading at specific increments on the continuous scan-X-ray intensity recording mentioned in the previous section.

C. Interdiffusion Coefficient Determinations

The comments of Section III.C.1 on the W-Ru system apply here also. The computer methods for solving the Boltzmann-Matano expression for the interdiffusion coefficient as described in Section III.C.2 for the W-Ru system were also employed on the profiles of the W-Pt couple.

D. Results and Discussion

1. Interdiffusion Coefficient as a Function of Composition

The data points of Figures 44 through 49 were processed in a computer to yield the interdiffusion coefficient as a function of composition in each of the phases (except the β phase which is discussed below) of this system. Interdiffusion coefficient vs. composition are tabulated in Table 26 for the profiles of Figures 44, 45, 46, 47, 48 and 49. Discontinuities of the interdiffusion coefficients within

Approved for Public Release

Contrails

TABLE 25

TIME AND TEMPERATURES OF ANNEALING TREATMENTS
OF COLUMBIUM-CHROMIUM COUPLES

Nominal Temperature (°C)	Temperature Deviation (°C)	Time of Anneal (hours)
1101	± 20	432
1251	± 10	342
1400	± 9	168
1502	± 10	95
1575	± 10	24
1624	± 8	9

Approved for Public Release

Contrails

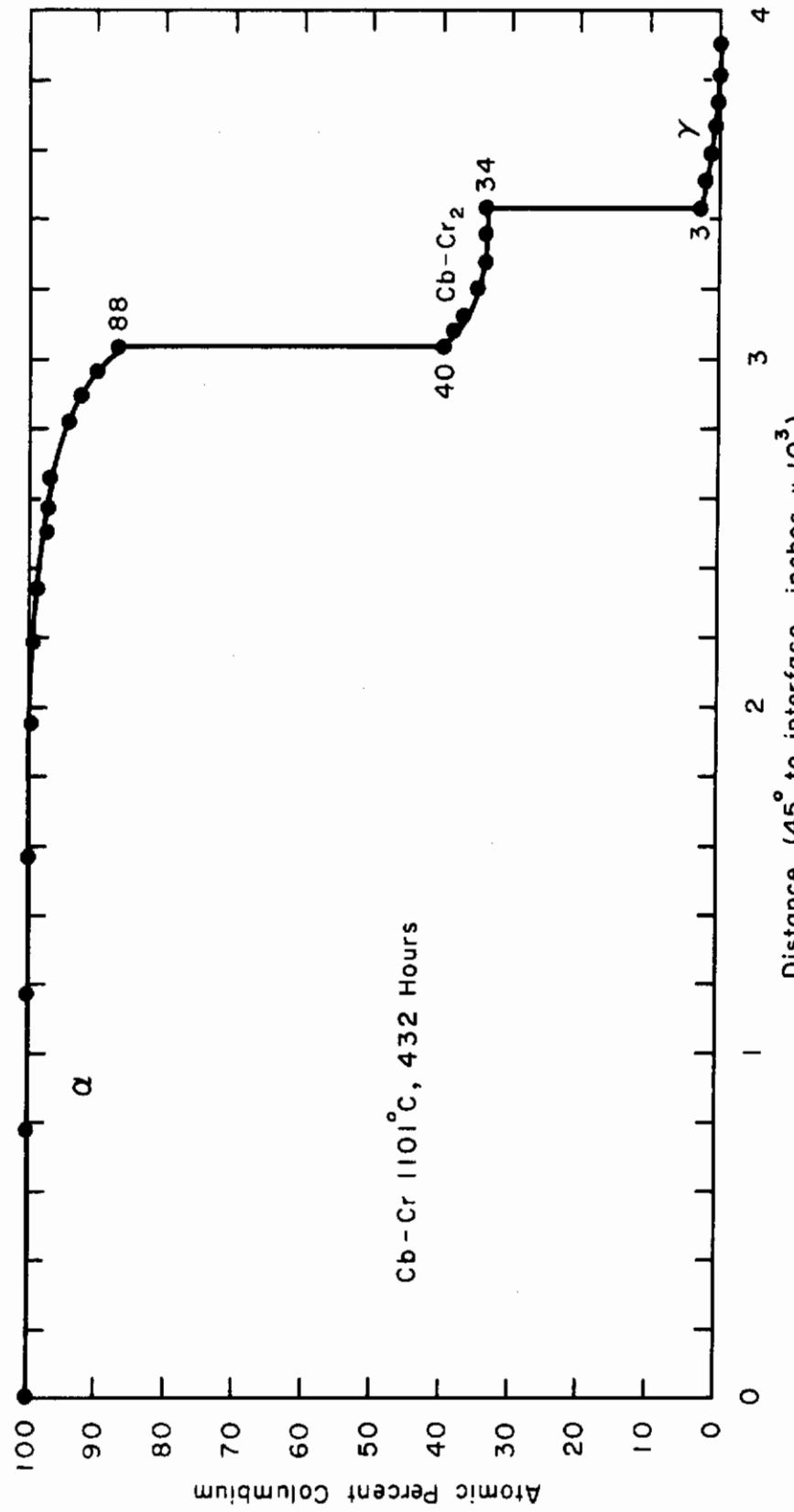

Figure 44. Composition vs Penetration Profile, Cb-Cr System, 1101°C.
Drawing No. RA-2723.

Approved for Public Release

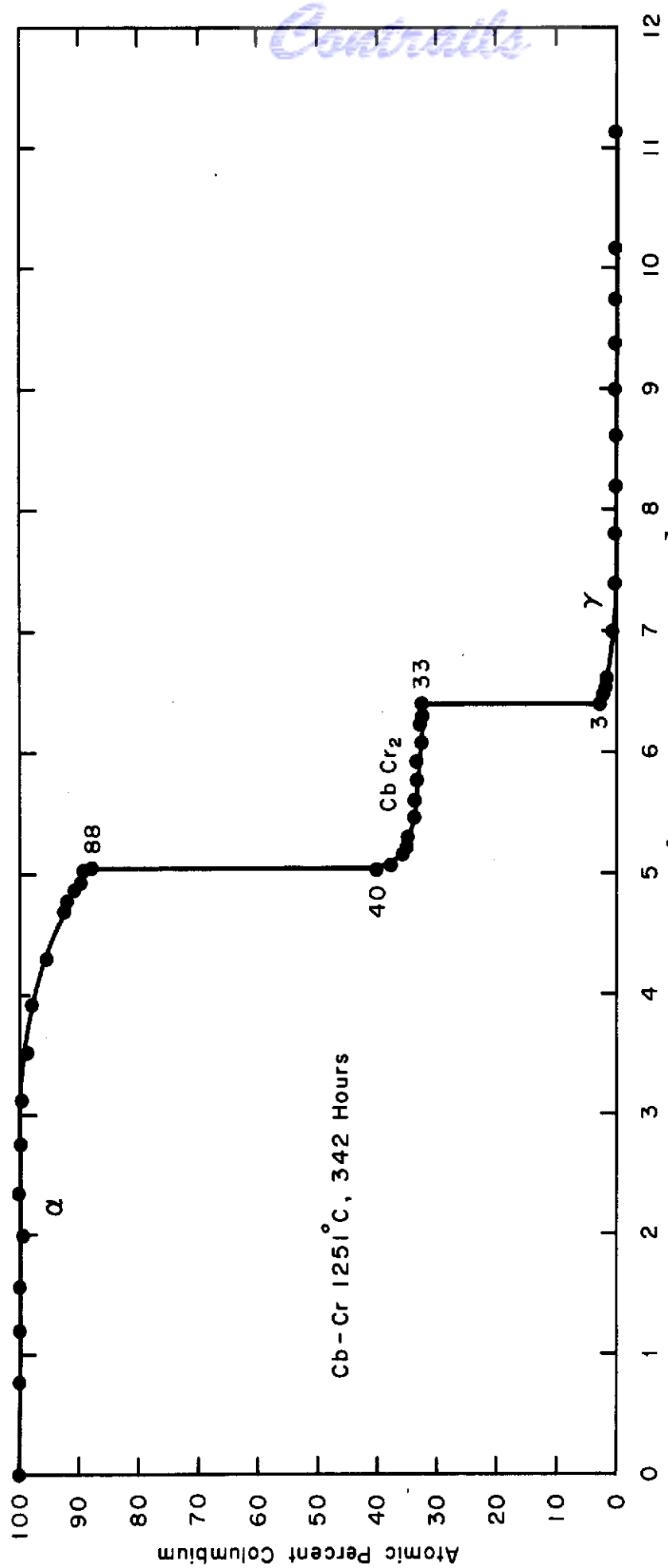

Figure 45. Composition vs Penetration Profile, Cb-Cr System, 1251°C.

Approved for Public Release

Contrails

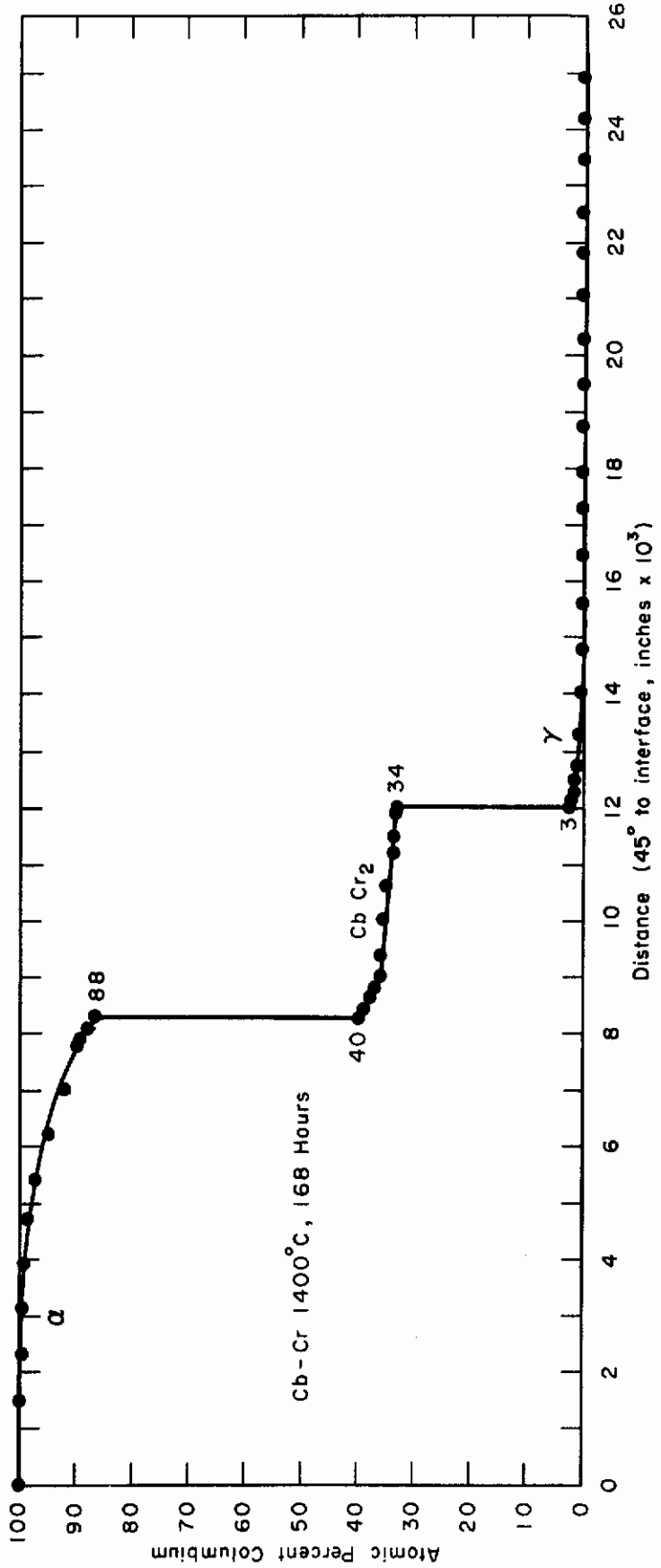

Figure 46. Composition vs. Penetration Profile, Cb-Cr System, 1400°C.

Approved for Public Release

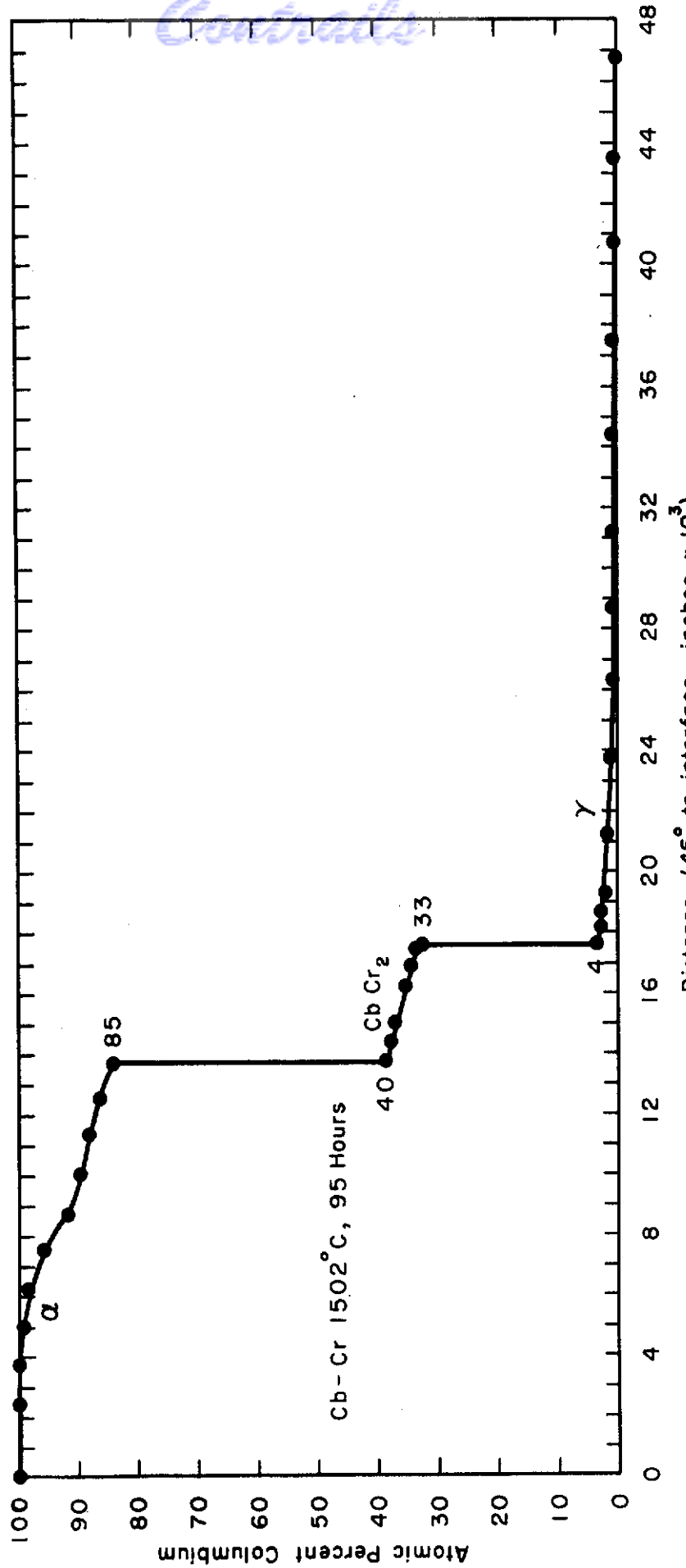

Figure 47. Composition vs Penetration Profile, Cb-Cr System, 1502°C.

Approved for Public Release

Contrails

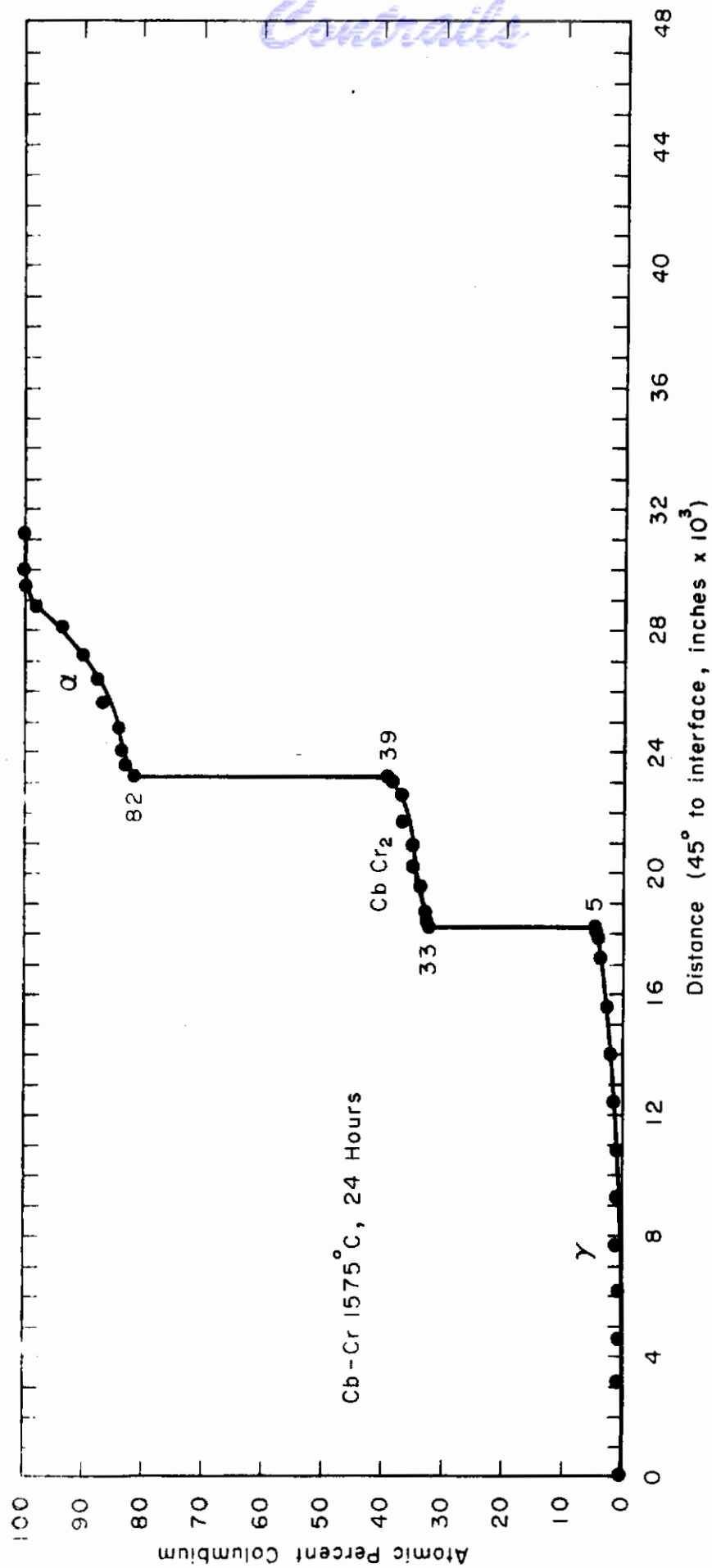

Figure 48. Composition vs Penetration Profile, Cb-Cr System, 1575°C.

Approved for Public Release

Contrails

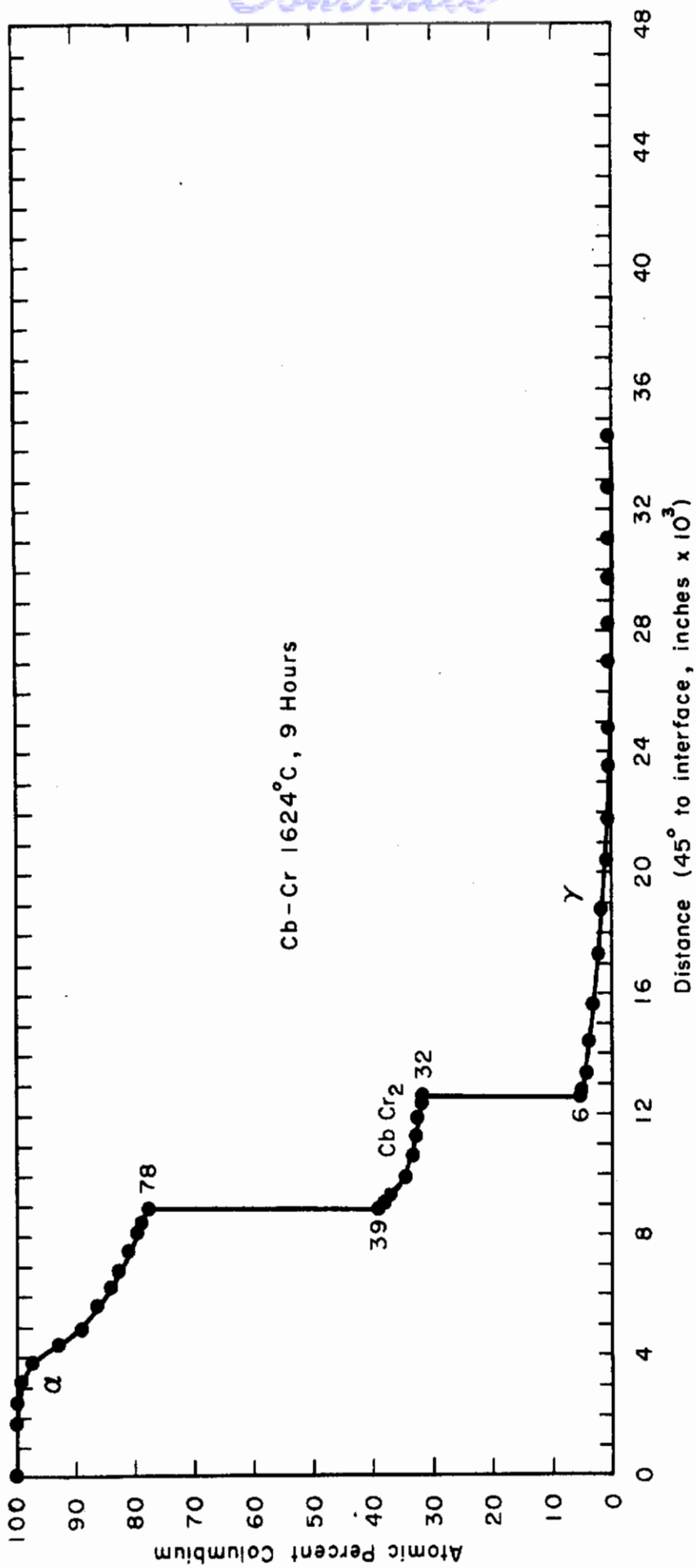

Figure 49. Composition vs Penetration Profile, Cb-Cr System, 1624°C.

Approved for Public Release

Contrails

TABLE V-26

INTERDIFFUSION COEFFICIENTS OF THE Cb-Cr SYSTEM FOR DIFFERENT COMPOSITIONS AT SEVERAL TEMPERATURES

Annealing Temperature (°C)	Annealing Time (hrs.)	Phase	Composition (^{a}/o Cb)	Interdiffusion Coefficient, $\tilde{D}$ (cm^2/hr.)
1624	9	αCb	99	5.19×10^{-6}
			98	6.37×10^{-6}
			97	7.45×10^{-6}
			96	8.49×10^{-6}
			95	9.54×10^{-6}
			94	1.07×10^{-6}
			93	1.19×10^{-6}
			92	1.33×10^{-6}
			91	1.49×10^{-6}
			90	1.68×10^{-6}
			89	1.90×10^{-6}
			88	2.18×10^{-6}
			87	2.55×10^{-6}
			86	3.04×10^{-6}
			85	3.76×10^{-6}
			84	4.90×10^{-6}
			83	6.90×10^{-6}
			82	9.83×10^{-6}
			81	9.16×10^{-6}
			80	6.37×10^{-6}
			79	4.67×10^{-6}
		$\alpha + CbCr_2$	78-39	2Ø
		$CbCr_2$	38	7.12×10^{-6}
			37	7.30×10^{-6}
			36	9.08×10^{-6}
			35	1.08×10^{-5}
			34	1.39×10^{-5}
			33	2.40×10^{-5}
		$CbCr_2+\gamma$ or $\beta\gamma$	32-6	2Ø
			5	8.59×10^{-6}
			4	9.23×10^{-6}
			3	9.96×10^{-6}
			2	1.08×10^{-5}
			1	1.19×10^{-5}
1575	24	αCb	99	3.37×10^{-7}
			98	4.00×10^{-7}
			97	4.52×10^{-7}
			96	5.02×10^{-7}
			95	5.53×10^{-7}

(Table continued on next page.)

Approved for Public Release

Contrails

TABLE 26 (continued)

Annealing Temperature (°C)	Annealing Time (hrs.)	Phase	Composition (^{a}/o Cb)	Interdiffusion Coefficient, $\tilde{D}$ (cm^2/hr.)
1575	24	αCb	94	6.05×10^{-7}
			93	6.61×10^{-7}
			92	7.22×10^{-7}
			91	7.90×10^{-7}
			90	8.69×10^{-7}
			89	9.63×10^{-7}
			88	1.08×10^{-6}
			87	1.23×10^{-6}
			86	1.45×10^{-6}
			85	1.79×10^{-6}
		αCb+$CbCr_2$	84-39	2Ø
		$CbCr_2$	38	8.73×10^{-6}
			37	8.84×10^{-6}
			36	8.90×10^{-6}
			35	8.92×10^{-6}
			34	8.90×10^{-6}
			33	8.83×10^{-6}
		$CbCr_2$+γ or β	32-5	2Ø
		γ	4	2.97×10^{-6}
			3	3.90×10^{-6}
			2	5.35×10^{-6}
			1	5.43×10^{-6}
1502	95	αCb	99	2.27×10^{-7}
			98	2.62×10^{-7}
			97	2.93×10^{-7}
			96	3.22×10^{-7}
			95	3.52×10^{-7}
			94	3.85×10^{-7}
			93	4.22×10^{-7}
			92	4.66×10^{-7}
			91	5.22×10^{-7}
			90	5.96×10^{-7}
			89	7.06×10^{-7}
			88	9.08×10^{-7}
			87	1.53×10^{-6}
		α Cb+$CbCr_2$	86-40	2Ø
		$CbCr_2$	39	2.04×10^{-6}
			38	1.69×10^{-6}
			37	1.47×10^{-6}
			36	1.32×10^{-6}
			35	1.20×10^{-6}
			34	1.10×10^{-6}
		$CbCr_2$ + γ	33-4	2Ø

(Table continued on next page.)

Approved for Public Release

Contrails

TABLE 26 (continued)

Annealing Temperature (°C)	Annealing Time (hrs.)	Phase	Composition (a/o Cb)	Interdiffusion Coefficient, $\tilde{D}$ ($cm^2/hr.$)
1502	95	γ	3	1.52×10^{-6}
			2	1.78×10^{-6}
			1	2.14×10^{-6}
1400	168	αCb	99	8.14×10^{-7}
			98	7.85×10^{-7}
			97	7.60×10^{-7}
			96	7.38×10^{-7}
			95	7.20×10^{-7}
			94	7.06×10^{-7}
			93	6.88×10^{-7}
			92	6.73×10^{-7}
			91	6.61×10^{-7}
			90	6.47×10^{-7}
			89	6.34×10^{-7}
			88	6.21×10^{-7}
			87	6.08×10^{-7}
		αCb+$CbCr_2$	86-39	2Ø
		$CbCr_2$	38	5.05×10^{-7}
			37	5.47×10^{-7}
			36	6.32×10^{-7}
			35	8.65×10^{-7}
		$CbCr_2$ + γ	34-3	2Ø
		γ	2	1.53×10^{-7}
			1	2.69×10^{-7}
1251	342	αCb	99	8.10×10^{-9}
			98	6.91×10^{-9}
			97	6.23×10^{-9}
			96	5.76×10^{-9}
			95	5.44×10^{-9}
			94	5.15×10^{-9}
			93	4.90×10^{-9}
			92	4.68×10^{-9}
			91	4.46×10^{-9}
			90	4.28×10^{-9}
			89	4.10×10^{-9}
		αCb+$CbCr_2$	88-39	2Ø
		$CbCr_2$	38	1.01×10^{-8}
			37	1.03×10^{-8}
			36	1.05×10^{-8}
			35	4.45×10^{-8}
			34	6.60×10^{-8}

(Table continued on next page.)

Approved for Public Release

Contrails

TABLE 26 (continued)

Annealing Temperature (°C)	Annealing Time (hrs.)	Phase	Composition (a/o Cb)	Interdiffusion Coefficient, D (cm^2/hr.)
1251	342	$CbCr_2$ + γ	33-3	2Ø
		γ	2	5.06×10^{-9}
			1	6.71×10^{-9}
1101	432	αCb	99	1.70×10^{-9}
			98	1.10×10^{-9}
			97	1.06×10^{-9}
			96	9.47×10^{-10}
			95	8.60×10^{-10}
			94	7.92×10^{-10}
			93	7.34×10^{-10}
			92	6.88×10^{-10}
			91	6.48×10^{-10}
			90	6.12×10^{-10}
			89	5.76×10^{-10}
		αCb+$CbCr_2$	88-41	2Ø
		$CbCr_2$	40	8.10×10^{-10}
			39	8.96×10^{-10}
			38	1.02×10^{-7}
			37	1.18×10^{-7}
			36	1.46×10^{-7}
		$CbCr_2$+ γ	35-3	2Ø
		γ	2	4.54×10^{-10}
			1	2.63×10^{-10}

Approved for Public Release

Contrails

a single phase region have been discussed in Section III.D.1 of the W-Ru system.

2. Variation of Interdiffusion Coefficients with Temperature

Plots of the logarithm of the interdiffusion coefficient versus reciprocal temperature were made for various compositions across the phase diagram. These are presented for a composition in each phase field in Figures 50, 51, 52, 53 and 54. It is to be noted that the data of Figures 50, 51, 52, 53 and 54 do not all fall on straight lines. Reasons for this have already been stated in Section III.D.2 of the W-Ru system. A summary of the interdiffusion coefficient values for selected compositions in each phase field is given in Table 27. The activation energies, Q, and the frequency factors, D_o, that are listed in this table were obtained from the slopes of plots such as are given in Figures 50, 51, 52, 53 and 54. The slopes of these curves were taken at the high temperature regions in all cases, as the diffusion zones were broader and considered somewhat more reliable. From the way the curves are formed, it should be noted that such a procedure gives a maximum value of both Q and D_o.

3. The β and $CbCr_2$ Phases

According to the Cb-Cr phase diagram in Appendix II, the appearance of the βCr phase occurs at 1550°C up to the melting point of Cr. Therefore, one might expect that the diffusion couples heat treated at 1575°C and 1624°C would show the presence of the β phase in the composition vs distance profile in Figures 48 and 49. The fact that no such indication occurred in the profiles suggests two possible explanations. One explanation is that the β phase exists but that it was suppressed. In a technical paper on the growth of diffusion layers in binary systems, Kidson[8] shows how the apparent absence of certain phases implies that the rate constants are too small to permit detection of the phase layers by ordinary microscopic techniques, and that the appearance or non-

Approved for Public Release

Contrails

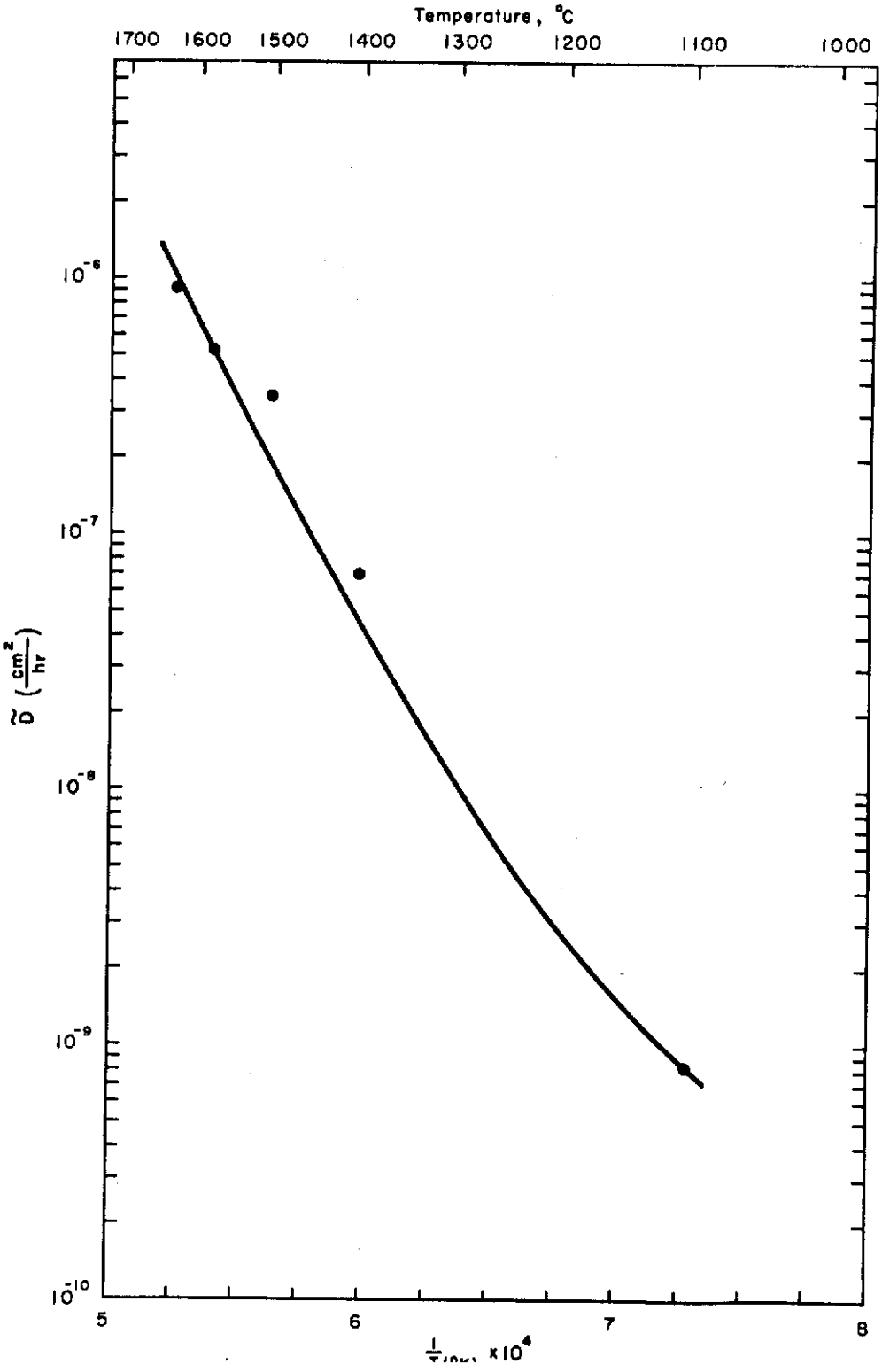

Figure 50. Plot of Logarithm of the Interdiffusion Coefficient vs Reciprocal Temperature for Couples in the Cb-Cr System, 95[a]/o Cb (α).

Approved for Public Release

Contrails

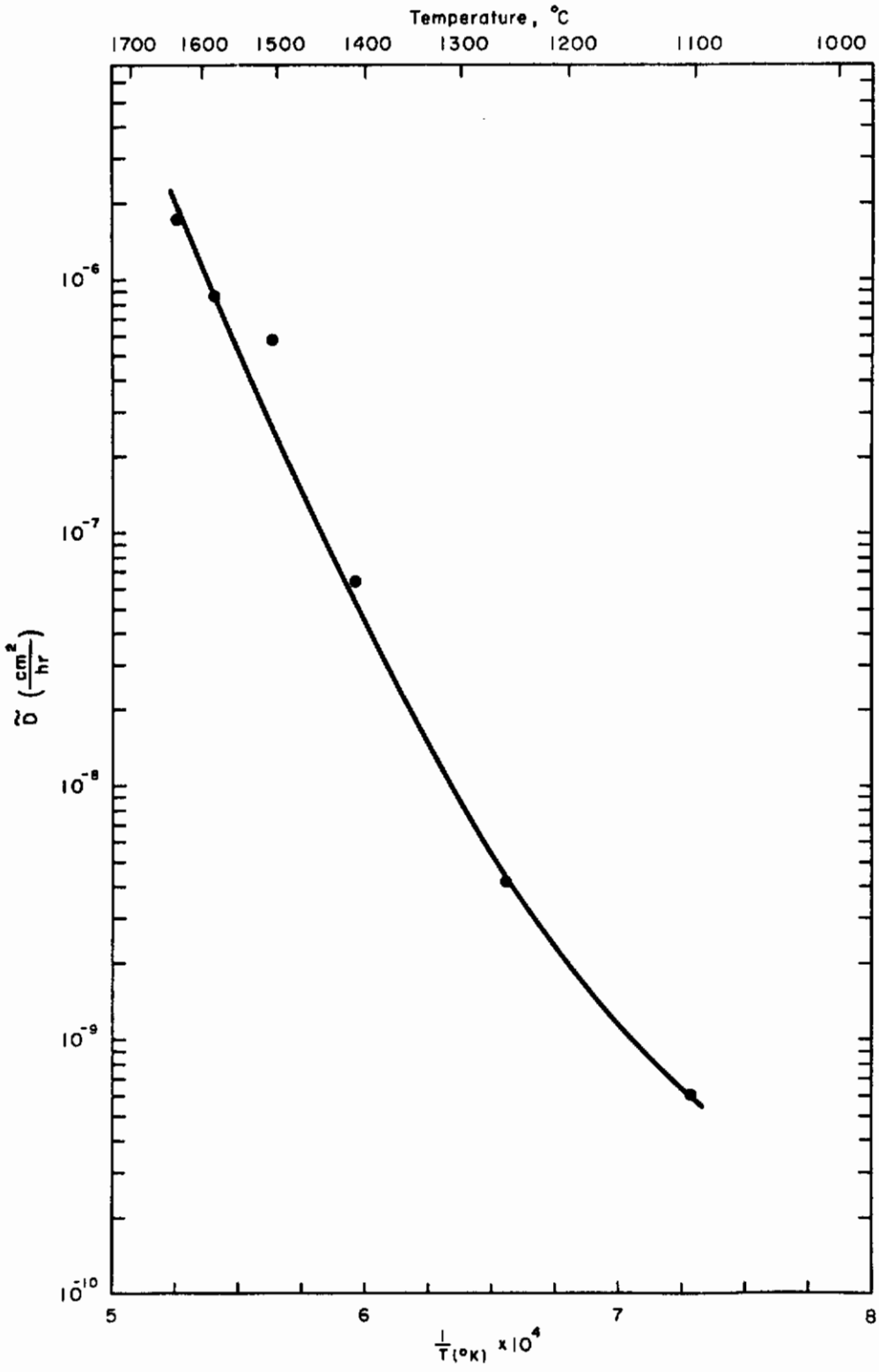

Figure 51. Plot of Logarithm of the Interdiffusion Coefficient vs Reciprocal Temperature for Couples in the Cb-Cr System, 90 a/o Cb (α).

Approved for Public Release

Contrails

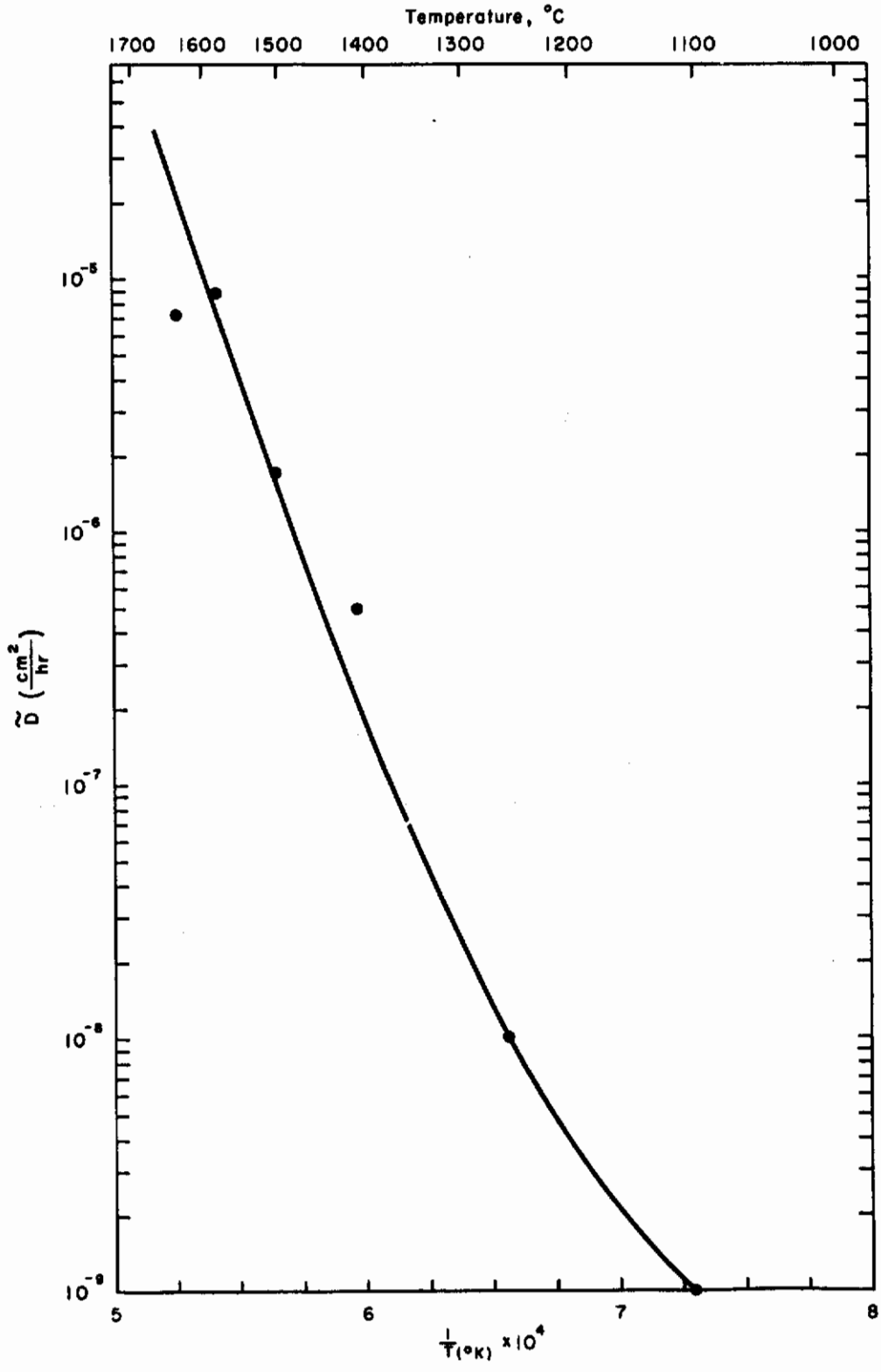

Figure 52. Plot of Logarithm of the Interdiffusion Coefficient vs Reciprocal Temperature for Couples in the Cb-Cr System, 38 a/o Cb ($CbCr_2$).

Approved for Public Release

Contrails

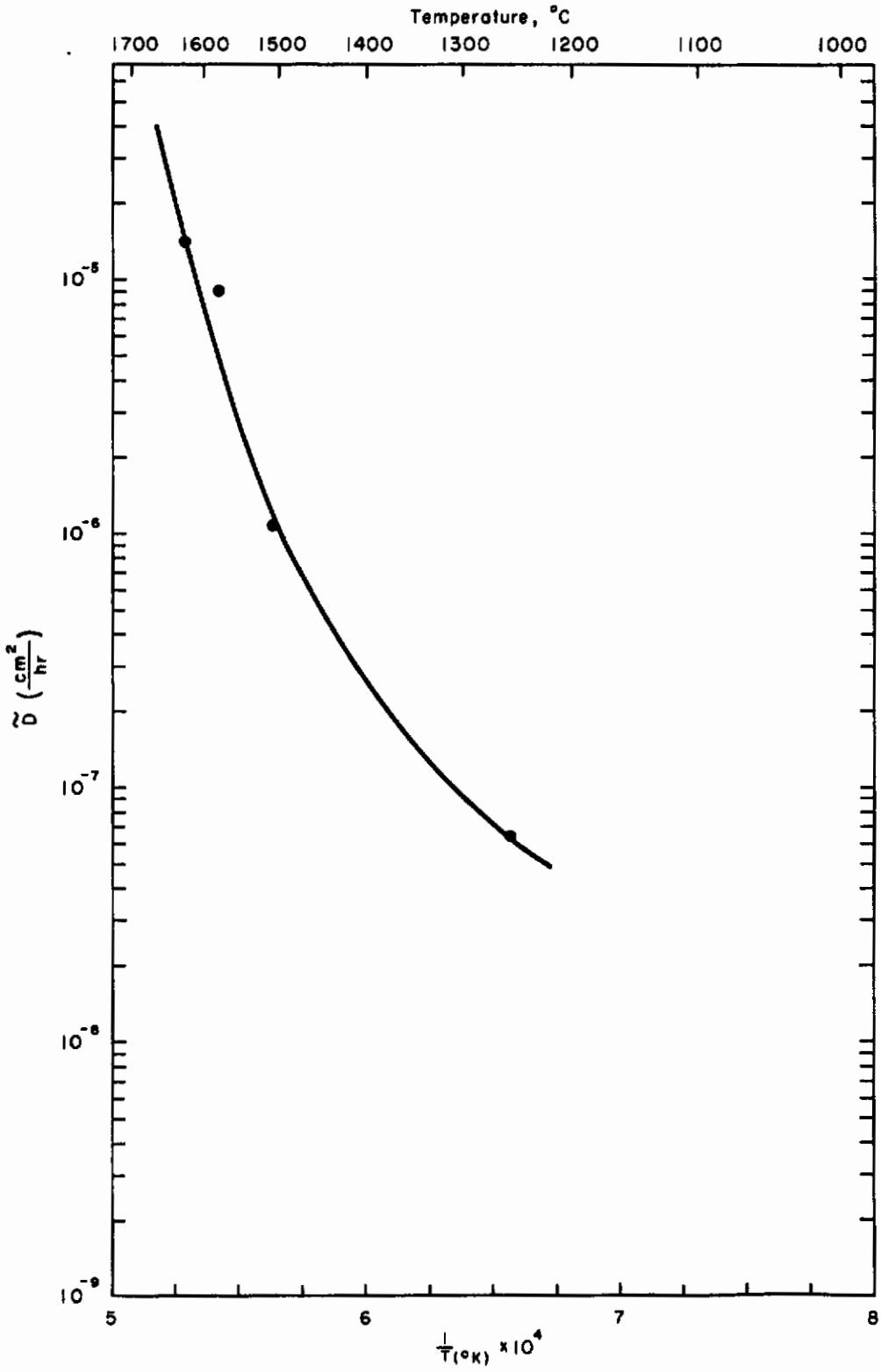

Figure 53. Plot of Logarithm of the Interdiffusion Coefficient vs Reciprocal Temperature for Couples in the Cb-Cr System, 34 a/o Cb ($CbCr_2$)

Approved for Public Release

Contrails

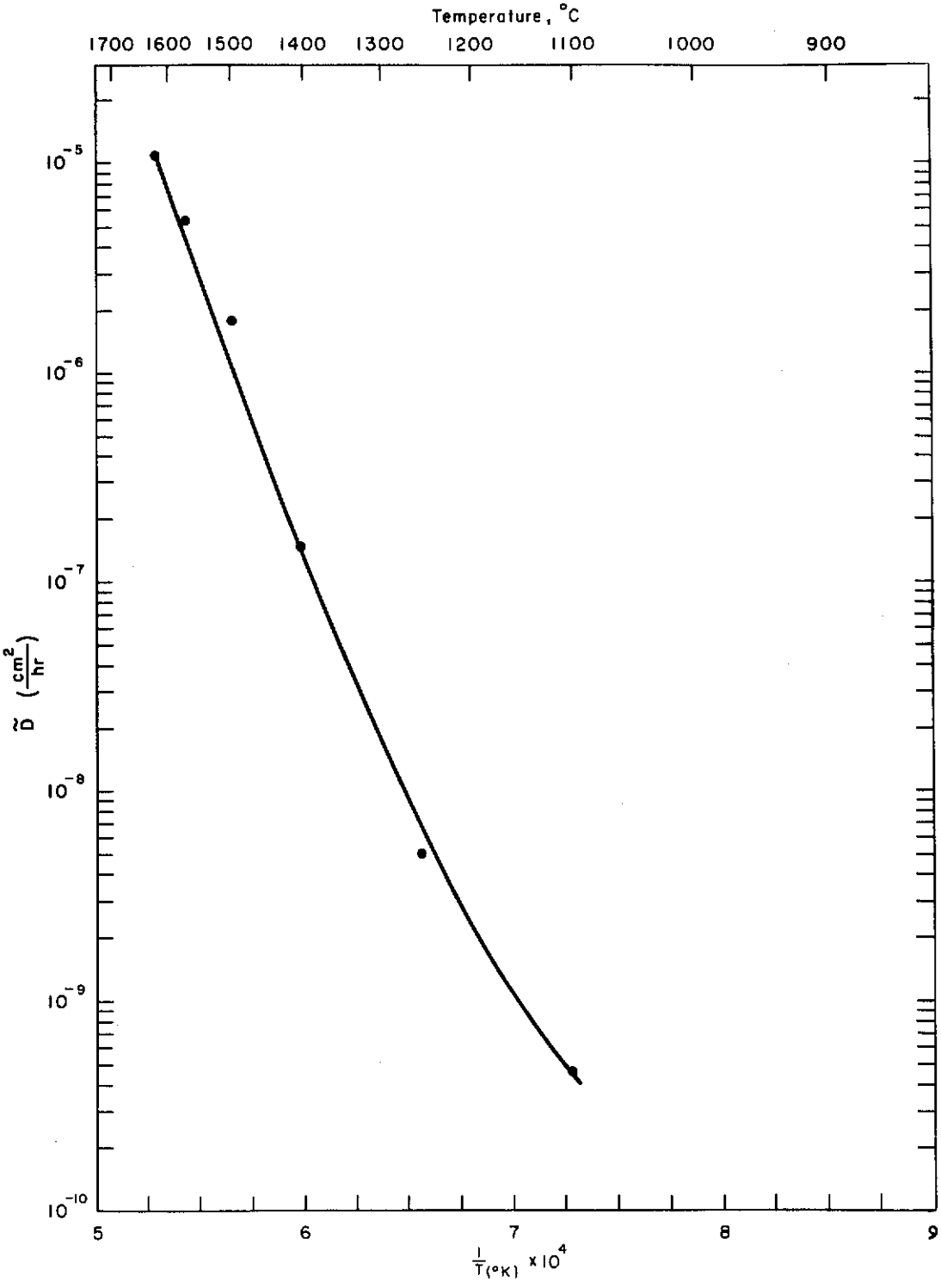

Figure 54. Plot of Logarithm of the Interdiffusion Coefficient vs Reciprocal Temperature for Couples in the Cb-Cr System, 2 a/o Cb (α).

Approved for Public Release

TABLE 27

TABULATION OF Cb-Cr DIFFUSION RESULTS

System	Temp. (°C)	Time (hrs.)	Grade of Couple*	Interdiffusion Coefficients (cm^2/hr.)					Comments
				2 a/o Cb(γ)	34 a/o Cb($CbCr_2$)	38 a/o ($CbCr_2$)	90 a/o Cb(α)	95 a/o Cb(α)	
Cr-Cb	1101	432	A	4.7×10^{-10}	- - - -	1.0×10^{-9}	6.1×10^{-10}	8.6×10^{-10}	.001 in. zone
	1251	342	A	5.0×10^{-9}	6.5×10^{-8}	1.0×10^{-8}	4.3×10^{-9}	5.4×10^{-9}	.0015 in. zone
	1400	168	C	1.5×10^{-7}	- - - -	5.0×10^{-7}	6.5×10^{-8}	7.2×10^{-8}	Crack at interface, .002 in. zone.
	1502	95	D	1.8×10^{-6}	1.1×10^{-6}	1.7×10^{-6}	5.8×10^{-7}	3.5×10^{-7}	Crack at interface, .0025 in. zone.
	1575	24	C	5.4×10^{-6}	9.0×10^{-6}	8.6×10^{-6}	8.6×10^{-7}	5.4×10^{-7}	Crack at interface, .003 in. zone.
	1624	9	C	1.1×10^{-5}	1.7×10^{-5}	7.2×10^{-6}	1.7×10^{-6}	9.4×10^{-7}	Crack at interface, .0055 in. zone.
				97,900	94,000	94,800	92,000	86,000	Q, cal./mole.
				123,000	93,000	85,100	9,550	1,100	D_o values (cm^2/hr.)

* Grades indicate quality of diffusion zones.

Approved for Public Release

Contrails

appearance of a phase is governed by conditions peculiar to a particular annealing temperature, rather than depending only upon sufficiently high annealing temperatures or long annealing times. The other explanation is that the high temperature β Cr phase does not exist. Pearson[11] in his book questions the existence of the high temperature β phase.

The Cb-Cr phase diagram also shows that the $CbCr_2$ phase is stoichiometric, with no solid solubility, whereas data from the microprobe analysis of the diffusion couples shows the phase to be about 5 a/o in width.

Approved for Public Release

Contrails

VIII. DIFFUSION IN THE SYSTEM MOLYBDENUM-MOLYBDENUM DISILICIDE

A. Diffusion Couple Preparation and Treatment

1. Material

Wrought molybdenum stock, utilized for the diffusion couples and a few of the standard alloys, was obtained as a rod of purity greater than 99.9%. For most of the standards alloys molybdenum powder was obtained of purity greater than 99.9%. The molybdenum disilicide, 95-98% of theoretical density, was obtained as a coating of purity estimated at about 99.8%. The silicon utilized for the standard alloys was obtained as powder of purity greater than 99.9%.

The sintered molybdenum rod was obtained from Climax Molybdenum Company, the molybdenum powder from General Electric Company, the molybdenum disilicide coating from the Pfaudler Company, and the silicon powder from Anderson Laboratories, Inc. Typical analyses for these elements are presented in Table 28. Analysis for the molybdenum disilicide was not available.

2. Arc-Melting

Arc-melting was performed under conditions virtually identical to those described in Section III.A.2 on the W-Ru system and was utilized in the Mo-$MoSi_2$ study for making standard alloys only.

Diffusion specimens were fabricated directly from the sintered molybdenum as-received rod.

As with the W-Pt system (see Section VI.A.2), a wet chemical analysis was performed to establish the compositions of the Mo-Si standard alloys. The problems of inhomogenity and prolong melting paralleled that of the W-Pt system. The results of the wet chemical analysis are presented in Table 29.

3. Bonding of Couples

Twenty-seven molybdenum discs were ground, polished through 3/0 abrasive paper and annealed at 2000°C for two hours in an argon atmosphere.

Approved for Public Release

Contrails

TABLE 28

TYPICAL ANALYSIS OF MOLYBDENUM AND SILICON USED

Material	Impurity Element	Content (PPM)
Mo wrought rod	C	33
	O	< 2
	H	< 3
	N	< 4
	Fe	<20
	Ni	<10
	Si	<30
Mo powder	Al, Ca, Fe, Cr, Ni, Mn, Mg, Sn, C	Each 10
	Cu, W	Each 30
	Si	20
	O	580
Si	Al, Ca	Each m*
	Cu, Mg, Mn, Ag	Each t
	B, Mo, Ni, Pb, Sn, Ti, V, Zn	Each nd

Explanation of symbols used in spectroscoptic analyses of Si:

m = minor

t = trace

nd = not detected

Approved for Public Release

Contrails

TABLE 29

Mo-Si STANDARD ALLOY COMPOSITIONS FOR MICROPROBE ANALYSIS

Nominal Composition (^{a}/o Si)*	Composition as Determined by Wet Chemical Analysis (^{a}/o Si)	Deviation (%)
16.5	17.1	± 1
40	41.4	± 1
55	57.3	± 1
66.9	67.9	± 1

* A Mo - 25 ^{a}/o Si alloy made up for use as a standard was not used because it was found to be contaminated with tungsten presumably from the tungsten electrode during arc-melting.

Approved for Public Release

Contrails

These samples were sent to the Pfaudler Corp., Rochester, N. Y., for deposition of $MoSi_2$ on the specimen surface. The Pfaudler process of deposition involves a siliconizing treatment at approximately 1100°C for a period of time as long as nine hours. Approximately half of the twenty-seven samples were heat treated for nine hours and the other half for seven hours. Metallographic examination of the deposited $MoSi_2$ layer in a sectioned specimen revealed a tightly bonded layer of $MoSi_2$ on the molybdenum with a very small diffusion zone between the molybdenum and the $MoSi_2$. A very small amount of free silicon is evident on the outside surface of the $MoSi_2$ deposit. The thickness of the $MoSi_2$ deposit on the sample examined varied between 0.003 and 0.004 inches after a 7-hour siliconizing treatment. It would be expected that the 9-hour siliconizing treatment would give a somewhat thicker $MoSi_2$ layer. The personnel at Pfaudler advised against longer siliconizing treatments for thicker $MoSi_2$ layers for fear of having the deposit spall off. In the as-bonded condition, the samples sometimes showed as much as 10 microns of Mo_3Si_2 present as an intermediate phase but most often there was only one to two microns of this compound.

4. Annealing

All of the Mo-$MoSi_2$ diffusion runs were conducted in 1.33 atmospheres of purified argon. For this purpose the tantalum tube resistance furnace was used exclusively since the furnace was readily adaptable to pressurization.

The comments of Section III.A.4 on the W-Ru system regarding measurements of temperature in the tantalum tube furnace apply here also.

5. Sectioning

The couples of the Mo-$MoSi_2$ system were sectioned as described in Section III.A.5 of the W-Ru system.

Approved for Public Release

Contrails

B. Determination of Composition Profiles

In almost all details, except as noted below, the techniques and procedures for determination of the Mo-$MoSi_2$ composition profiles parallel that of the W-Ru system described in Section III.B.1 and Section III.B.2.

The exceptions to the details mentioned above were as follows:

(1) The composition of the standard alloys were determined by wet chemical analysis.

(2) The alloys of Table 29 were utilized as standards by simultaneously determining (on two spectrographs) the intensity of molybdenum L_{α_1} and silicon K_{α_1} characteristic radiation from suitably prepared specimens.

A plot of the normalized X-ray intensities of the Mo-Si standards vs. composition is given in Figure 55.

1. Traversing of Couples

The techniques and procedures used to determine the composition profiles for the Mo-$MoSi_2$ system were virtually identical to that of the W-Pt system described in Section VI.B.1.

2. Composition-Penetration Profiles

Six temperatures were used for diffusion treatments in this work. The times and temperature of these treatments are given in Table 30. The composition-penetration profiles found on the six annealed specimens are given in Figures 56, 57, 58, 59 and 60. These figures contain the data points taken with respect to only one of the constituents. In nearly all cases the sum of the compositions of molybdenum and silicon taken independently at a single point add to percentages between 99 and 101. Thus, only one set of data points is given. The composition-penetration profiles of Figures 56, 57, 58, 59 and 60 were presented as step points by reading at specific increments on the continuous scan-X-ray intensity recording.

Approved for Public Release

Contrails

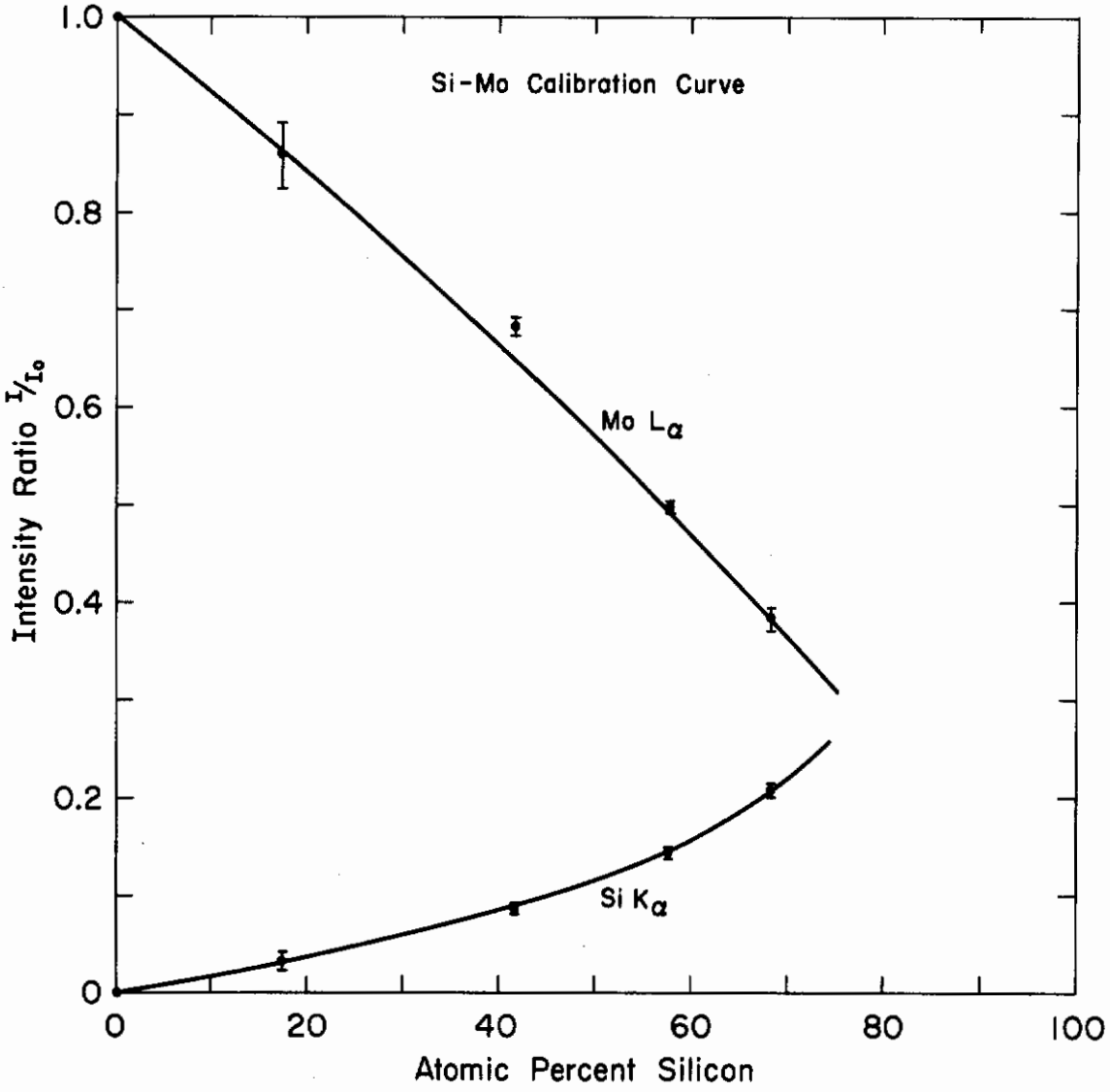

Figure 55. Plot of Normalized Intensity of Characteristic Radiation of Mo and Si vs Composition. The Mo L_{α_1} and Si K_{α_1} X-ray lines were used.

Approved for Public Release

Contrails

TABLE 30

TIMES AND TEMPERATURES OF ANNEALING TREATMENTS
OF MOLYBDENUM-MOLYBDENUM DISILICIDE COUPLES

Nominal Temperature (°C)	Temperature Deviation (°C)	Time of Anneal (hours)
904	± 6	700
1098	± 6	500
1365	± 10	44
1626	± 4	2.5
1715	± 7	1

Approved for Public Release

Contrails

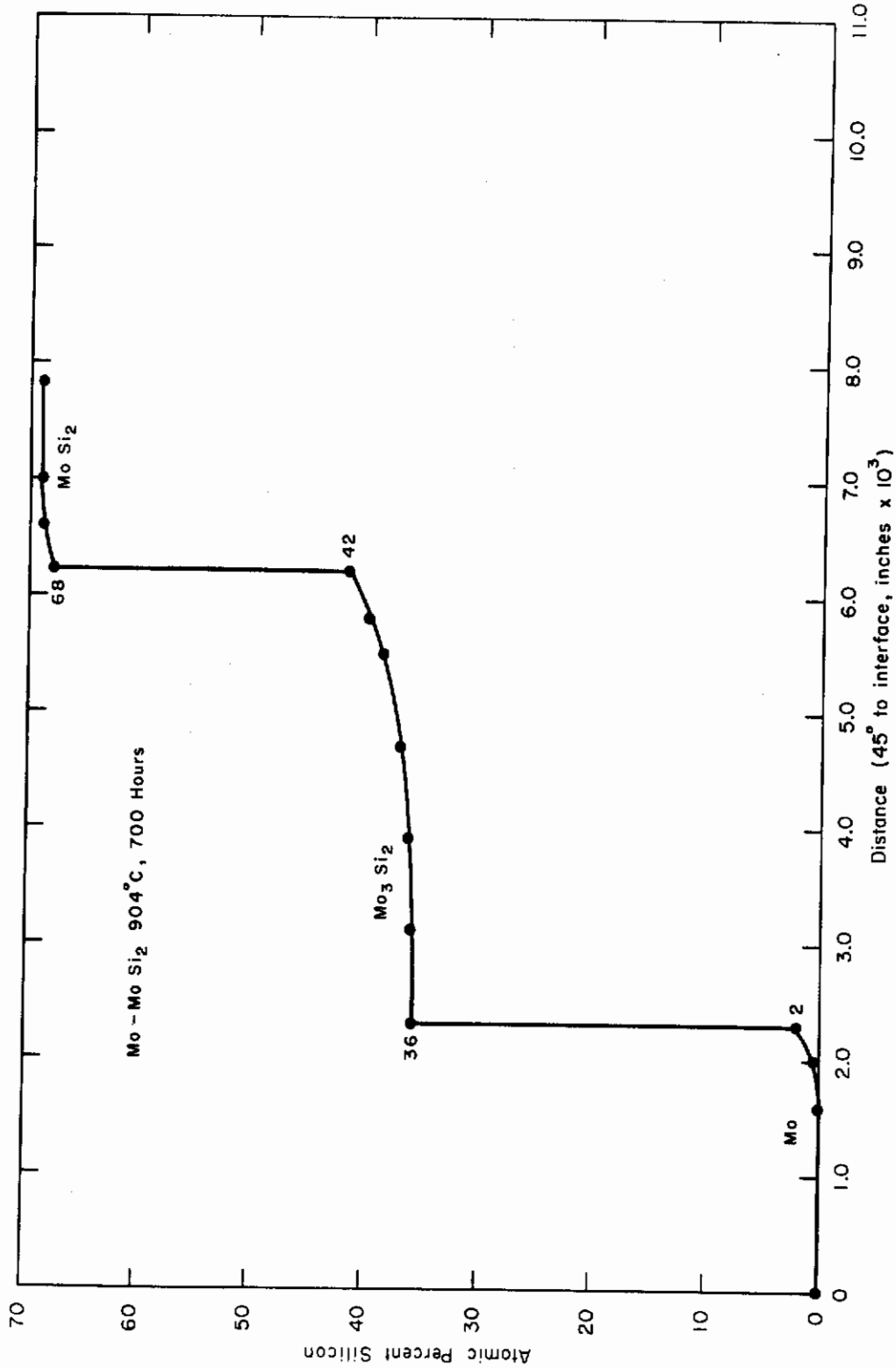

Figure 56. Composition vs. Penetration Profile, Mo-$MoSi_2$ System, 904°C.

Approved for Public Release

Contrails

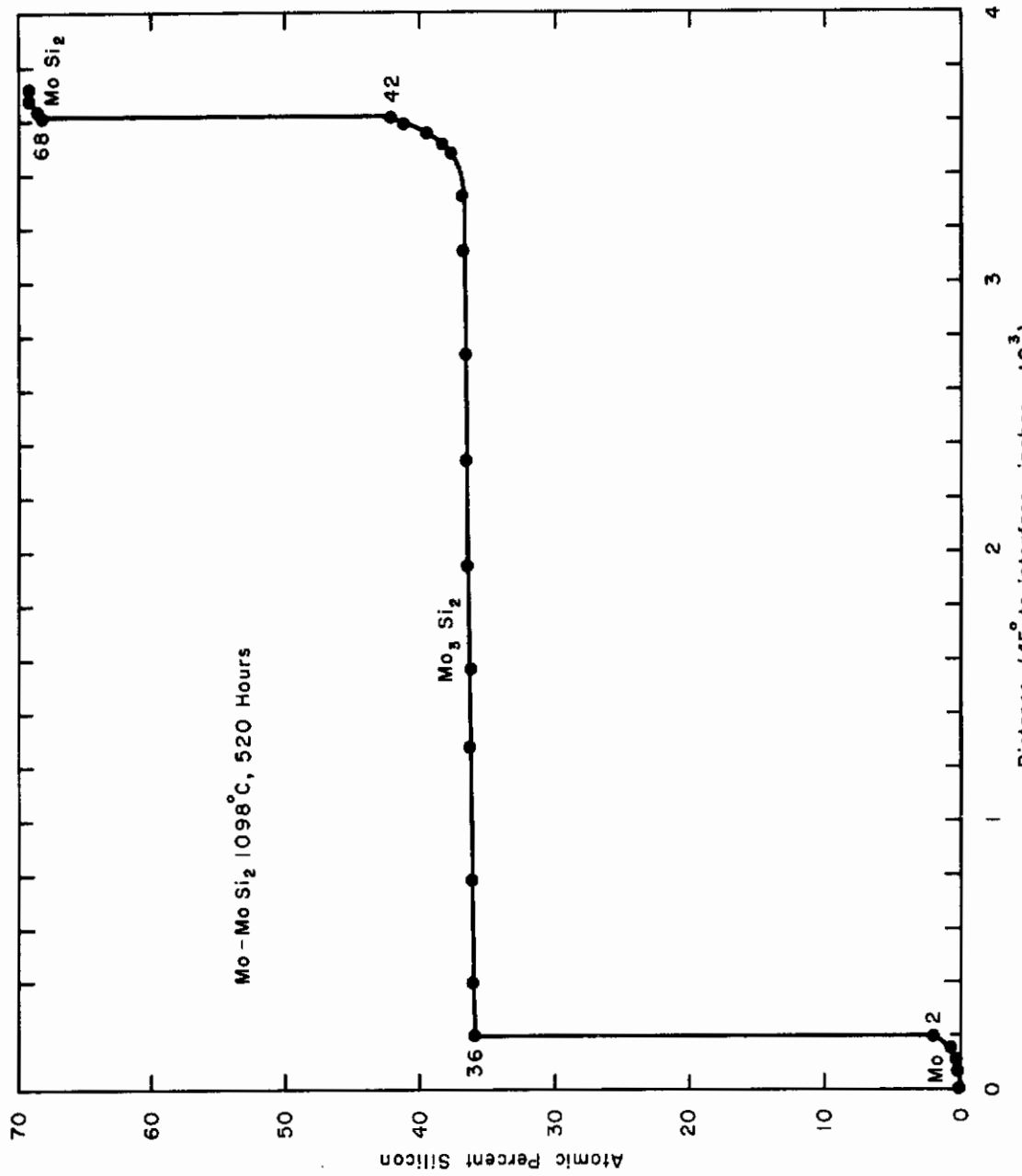

Figure 57. Composition vs Penetration Profile, Mo-$MoSi_2$ System, 1098°C.

Approved for Public Release

Contrails

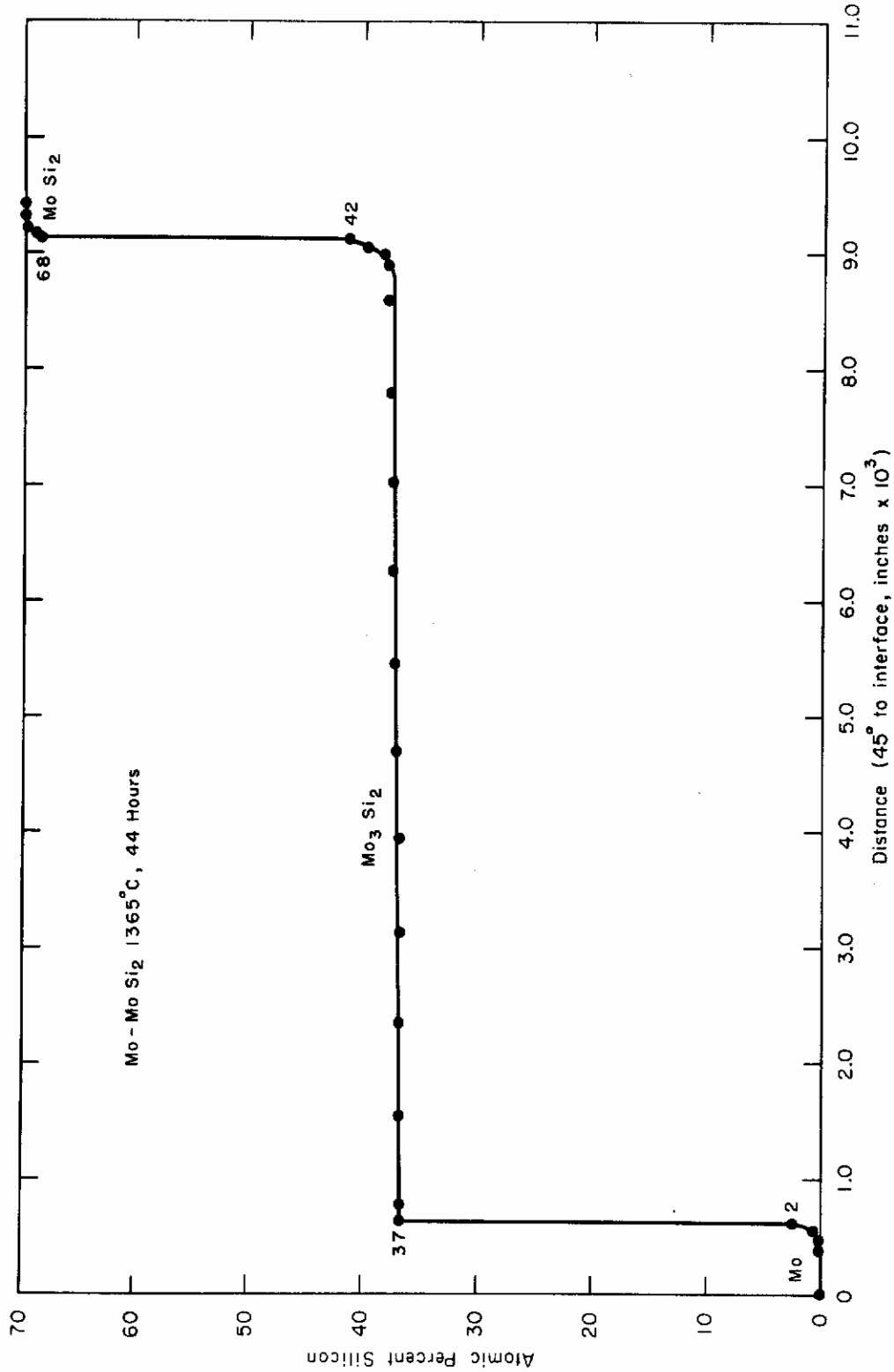

Figure 58. Composition vs Penetration Profile, Mo-$MoSi_2$ System, 1365°C.

Approved for Public Release

Contrails

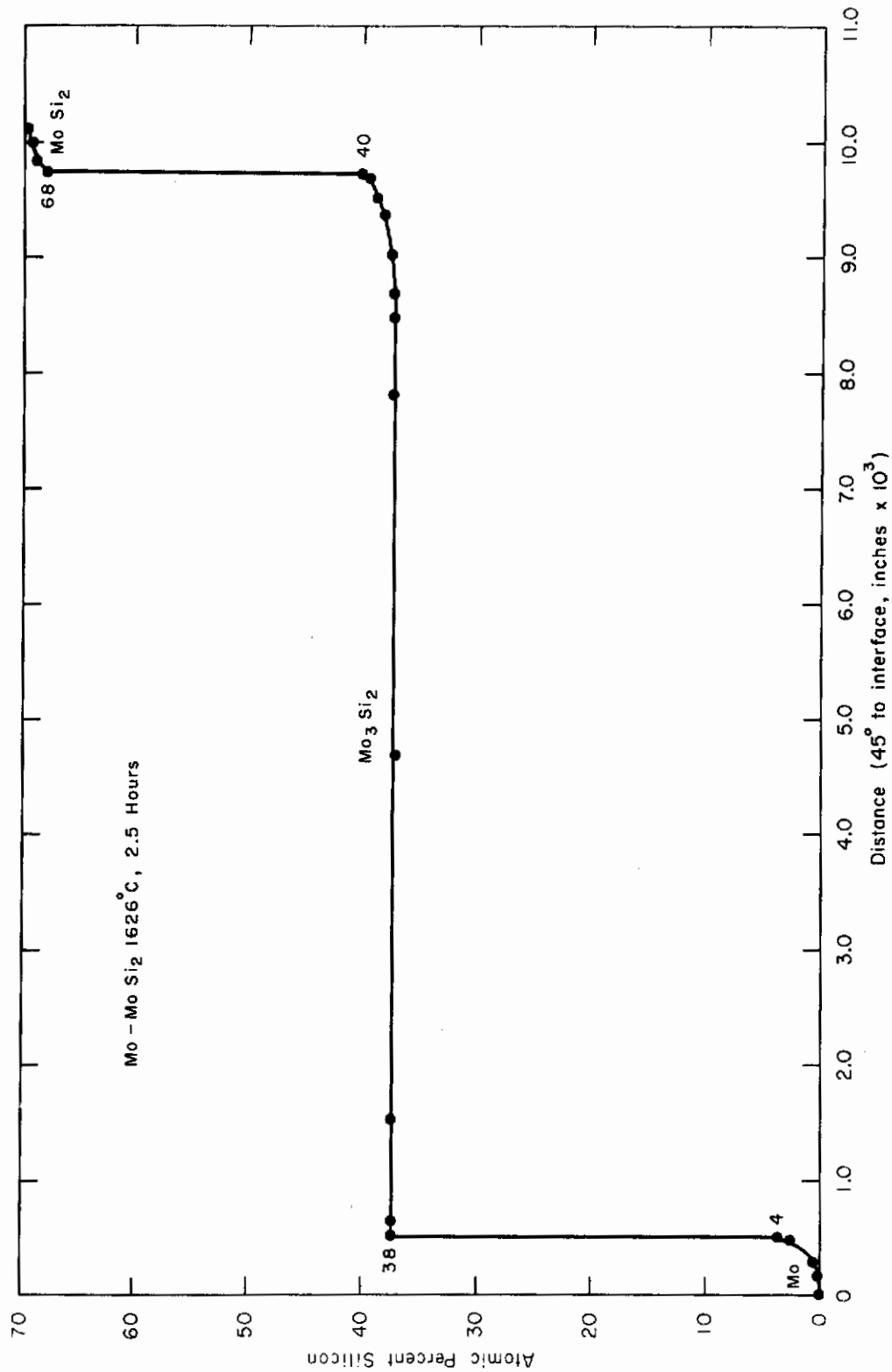

Figure 59. Composition vs Penetration Profile, Mo-$MoSi_2$ System, 1626°C.

Approved for Public Release

Contrails

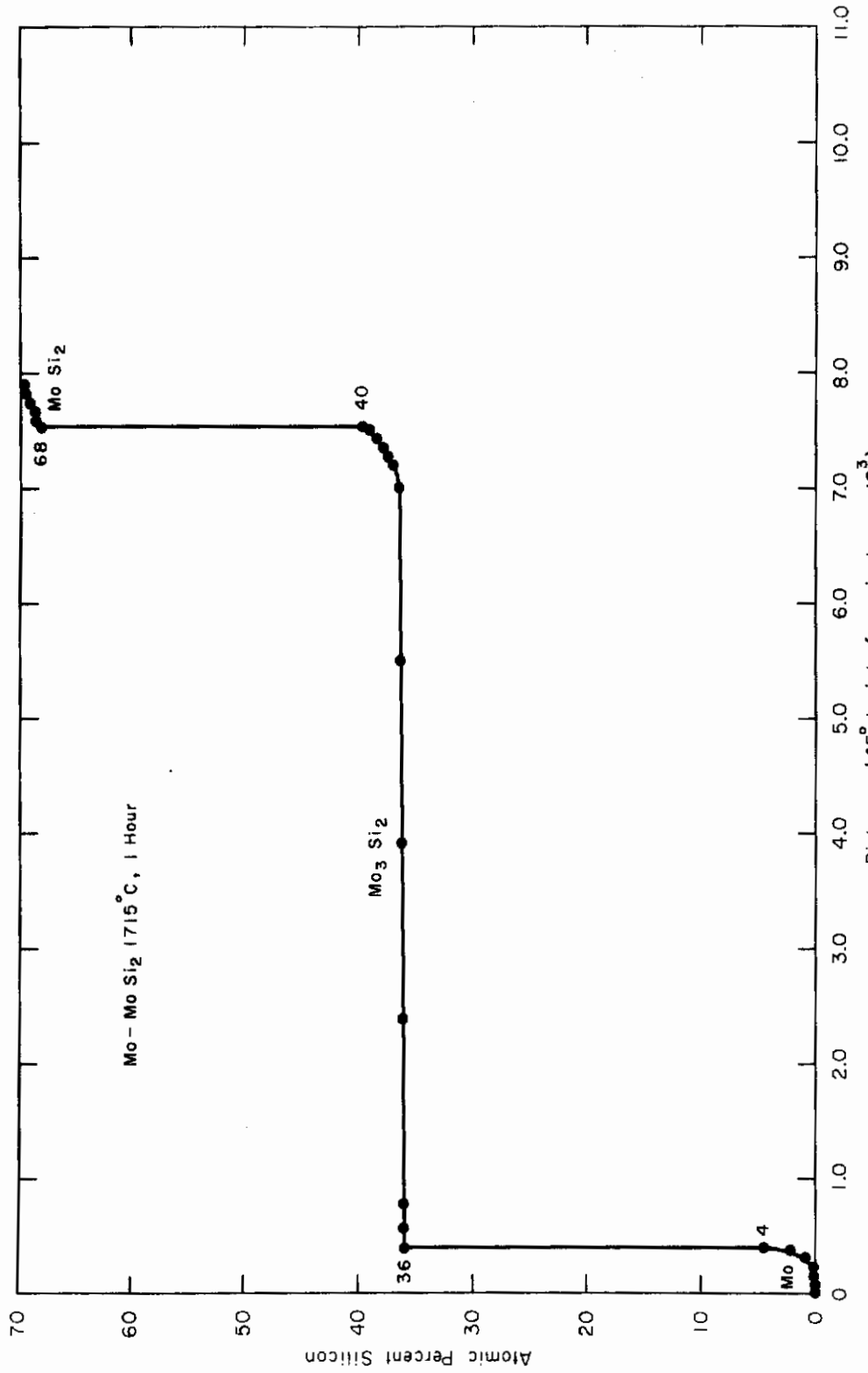

Figure 60. Composition vs Penetration Profile, Mo-$MoSi_2$ System, 1715°C.

Approved for Public Release

Contrails

C. Interdiffusion Coefficient Determinations

The comments of Section III.C.1 on the W-Ru system apply here also. The computer methods for solving the Boltzmann-Matano expression for the interdiffusion coefficient as described in Section III.C.2 for the W-Ru system were also employed on the profiles of the Mo-$MoSi_2$ couple.

D. Results and Discussion

1. Interdiffusion Coefficient as a Function of Composition

The data points of Figures 56 through 60 were processed in a computer to yield the interdiffusion coefficient as a function of composition in each of the phases (except the Mo_3Si which will be discussed later) of this system. Interdiffusion coefficients vs. composition are tabulated in Table 31 for the profiles of Figures 56, 57, 58, 59 and 60. Discontinuities of the interdiffusion coefficients within a single phase region have been discussed in Section III.D.1 of the W-Ru system.

2. Variation of Interdiffusion Coefficients with Temperature

Plots of the logarithm of the interdiffusion coefficient versus reciprocal temperature were made for various compositions across the phase diagram. These are presented for a composition in each phase field (except the Mo_3Si phase field) in Figures 61, 62 and 63. It is to be noted that the data of Figures 61, 62 and 63 do not all fall on straight lines. Reasons for this have already been stated in Section III.D.2 of the W-Ru system. A summary of the interdiffusion coefficient values for selected compositions in each phase field is given in Table 32. The activation energies, Q, and the frequency factors, D_o, that are listed in this table were obtained from the slopes of plots such as are given in Figures 36, 37 and 38. The slopes of these curves were taken at the high temperature regions in all cases, as the diffusion zones were broader and considered somewhat more reliable. From the way the curves are formed, it should be noted that such a procedure gives a maximum value of both Q and D_o.

Approved for Public Release

Contrails

TABLE 31

INTERDIFFUSION COEFFICIENTS OF THE Mo-$MoSi_2$ SYSTEM FOR DIFFERENT COMPOSITIONS AT SEVERAL TEMPERATURES

Annealing Temperature (°C)	Annealing Time (hrs.)	Phase	Composition (a/o Si)	Interdiffusion Coefficient, $\tilde{D}$ (cm^2/hr.)
1715	1	$MoSi_2$	69	6.44×10^{-6}
		$MoSi_2+Mo_3Si_2$	68-40	2Ø
		Mo_3Si_2	39	2.76×10^{-5}
			38	2.59×10^{-5}
			37	2.47×10^{-5}
		$Mo_3Si_2+\alpha Mo$	36-4	2Ø
		αMo	3	2.80×10^{-7}
			2	2.61×10^{-7}
			1	2.36×10^{-7}
1626	2.5	$MoSi_2$	69	5.11×10^{-7}
		$MoSi_2+Mo_3Si_2$	68-41	2Ø
		Mo_3Si_2	40	2.37×10^{-5}
			39	3.42×10^{-5}
			38	1.38×10^{-4}
		$Mo_3Si_2+\alpha Mo$	37-4	2Ø
		αMo	3	3.35×10^{-7}
			2	3.15×10^{-7}
			1	2.88×10^{-7}
1365	44	$MoSi_2$	69	6.91×10^{-9}
		$MoSi_2+Mo_3Si_2$	68-41	2Ø
		Mo_3Si_2	40	3.92×10^{-6}
			39	4.00×10^{-6}
			38	6.26×10^{-6}
			37	6.30×10^{-6}
		$Mo_3Si_2+\alpha Mo$	36-3	2Ø
		αMo	2	7.63×10^{-9}
			1	6.91×10^{-9}
1098	500	$MoSi_2$	69	------
			68	1.40×10^{-8}
		$MoSi_2+Mo_3Si_2$	67-42	2Ø
		Mo_3Si_2	41	5.51×10^{-9}
			40	5.76×10^{-9}
			39	6.05×10^{-9}
			38	6.34×10^{-9}
			37	6.62×10^{-9}
		$Mo_3Si_2+\alpha Mo$	36-2	2Ø
		αMo	1	1.52×10^{-10}

(Table continued on next page.)

Approved for Public Release

Contrails

TABLE 31 (continued)

Annealing Temperature (°C)	Annealing Time (hrs.)	Phase	Composition (a/o Si)	Interdiffusion Coefficient, $\tilde{D}$ (cm^2/hr.)
904	700	$MoSi_2$	69	-----
			68	1.87×10^{-11}
		$MoSi_2$+Mo_3Si_2	67-42	2Ø
		Mo_3Si_2	41	2.60×10^{-10}
			40	3.20×10^{-10}
			39	4.57×10^{-10}
			38	9.11×10^{-10}
			37	2.13×10^{-9}
			36	2.12×10^{-9}
		Mo_3Si_2+αMo	35-2	2Ø
		αMo	1	8.64×10^{-12}

Approved for Public Release

Contrails

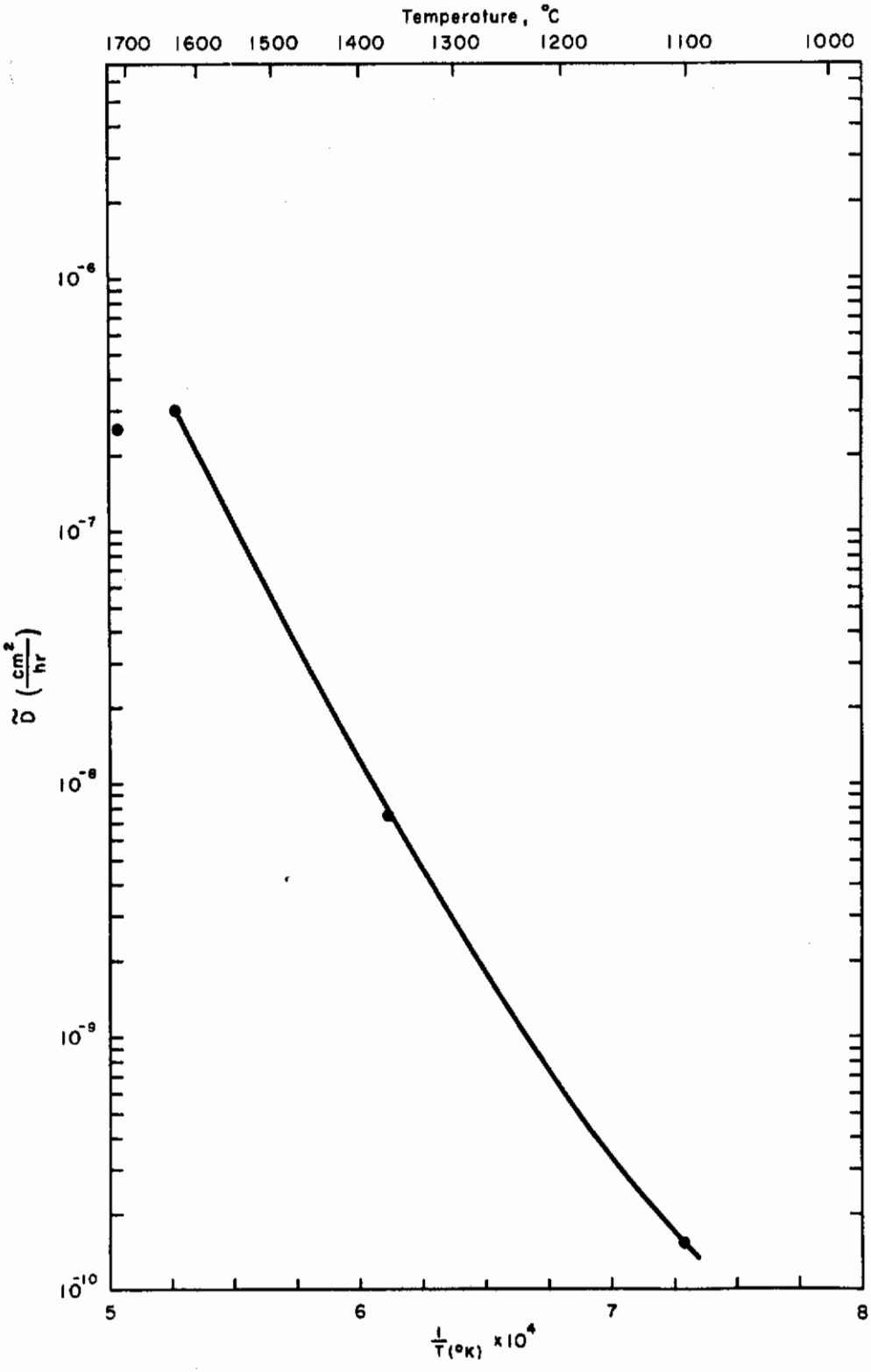

Figure 61. Plot of Logarithm of the Interdiffusion Coefficient vs Reciprocal Temperature for Couples in the Mo-$MoSi_2$ System, 98 a/o Mo (α).

Approved for Public Release

Contrails

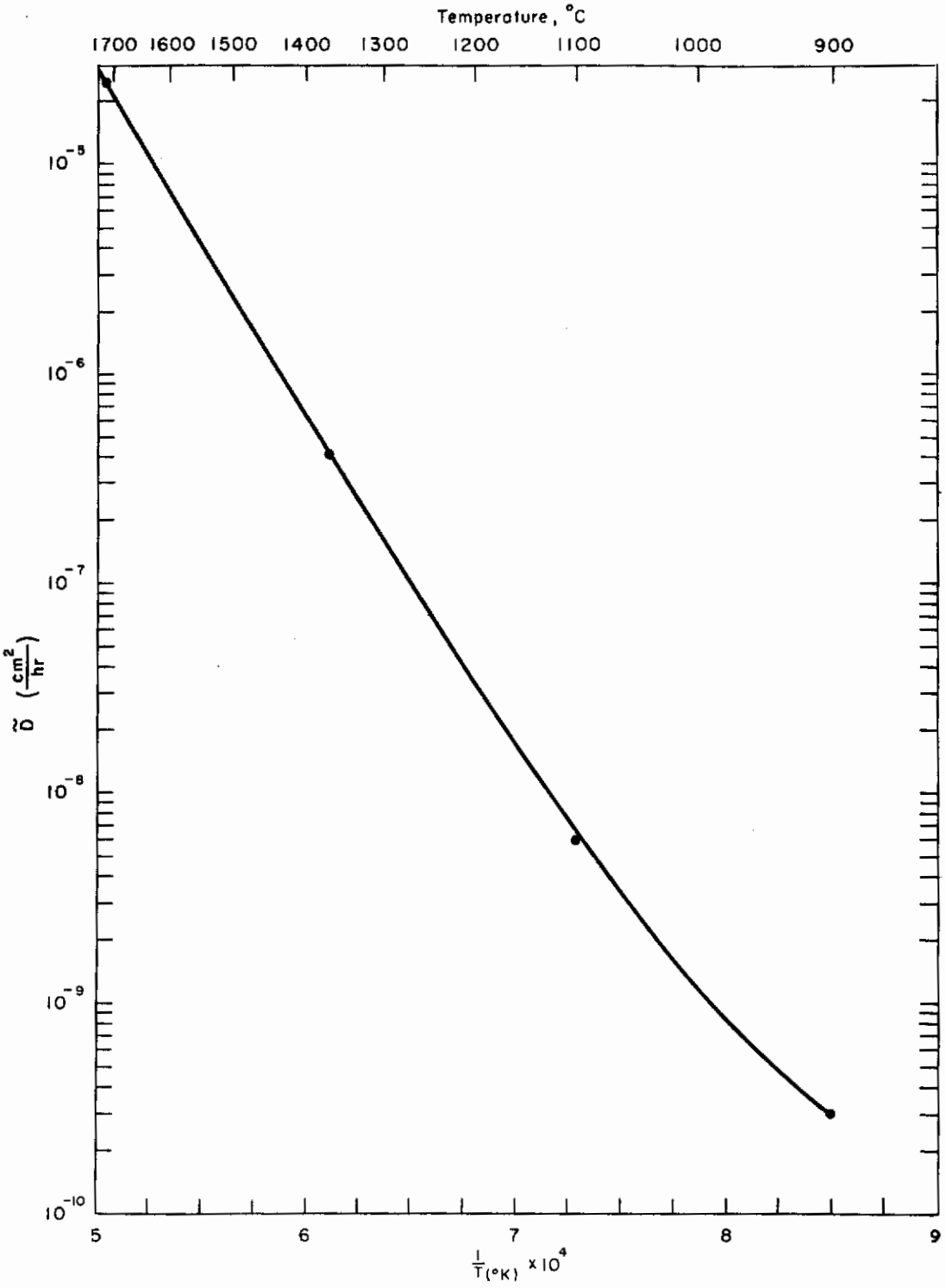

Figure 62. Plot of Logarithm of the Interdiffusion Coefficient vs Reciprocal Temperature for Couples in the Mo-$MoSi_2$ System, 61 a/o Mo (Mo_3Si_2).

Approved for Public Release

Contrails

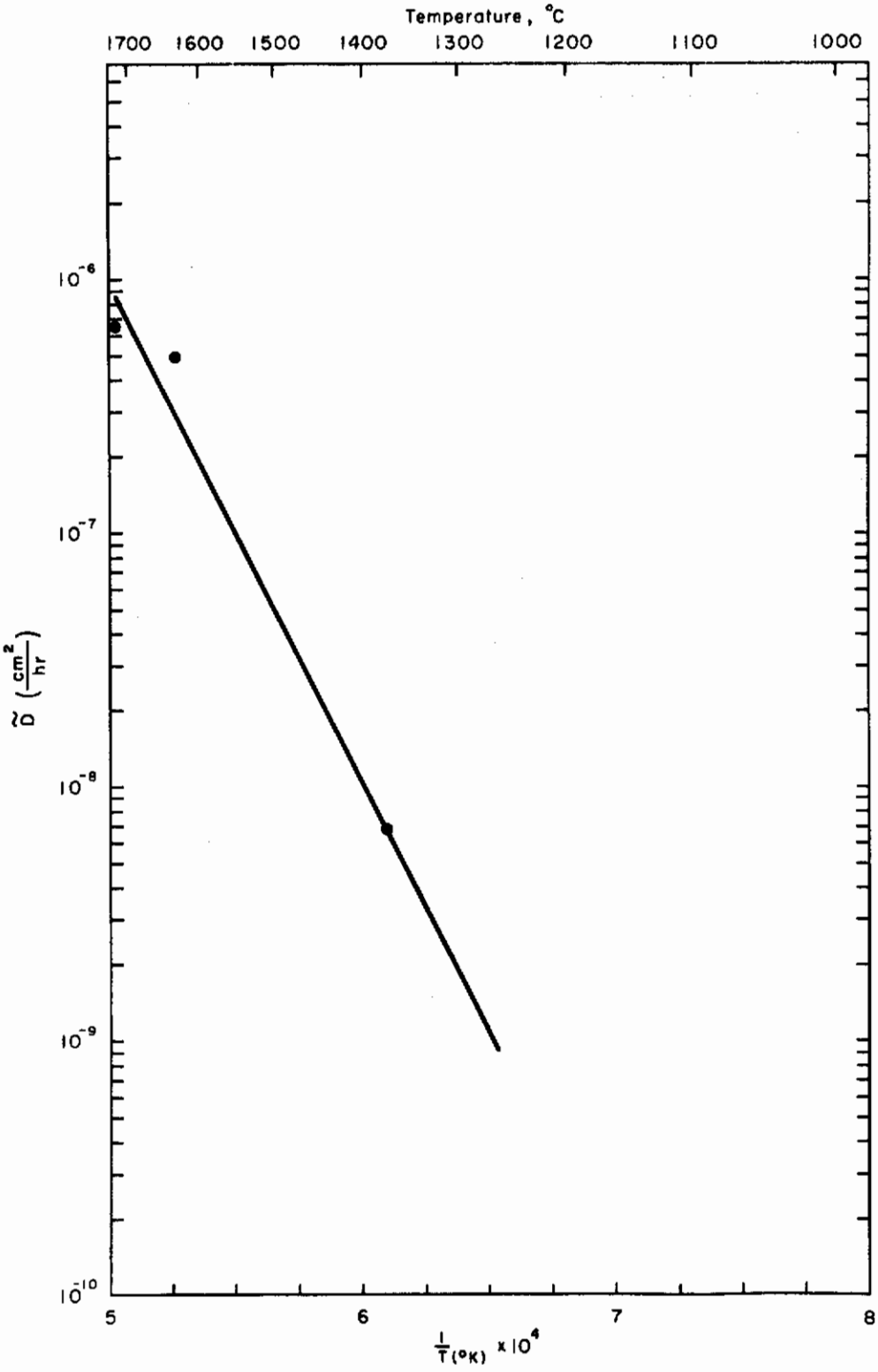

Figure 63. Plot of Logarithm of the Interdiffusion Coefficient vs Reciprocal Temperature for Couples in the Mo-$MoSi_2$ System, 31 a/o Mo ($MoSi_2$).

Approved for Public Release

TABLE 32

TABULATION OF Mo-$MoSi_2$ DIFFUSION RESULTS

Temp.	Time (hrs.)	Grade of Couple*	Interdiffusion Coefficients ($cm^2/hr.$)				Comments
			31[a]/o Mo($MoSi_2$)	60[a]/o Mo(Mo_3Si_2)	Mo_3Si	98[a]/o Mo(α)	
904	700	B	----	3.2×10^{-10}		----	.003 in. zone.
1098	500	A	----	5.8×10^{-9}		1.7×10^{-9}	.002 in. zone.
1365	44	B	6.8×10^{-9}	4.0×10^{-7}		7.6×10^{-9}	.005 in. zone.
1626	2.5	B	5.0×10^{-7}	2.4×10^{-5}	Phase suppressed	3.1×10^{-7}	.006 in. zone.
1715	1	A	6.5×10^{-7}			2.6×10^{-7}	.006 in. zone.
			88,500	74,300		78,000	Q, cal/mole.
			347	302		16.2	D_o values ($cm^2/hr.$).

* Grades indicate quality of diffusion zones.

Approved for Public Release

Contrails

3. The Mo_3Si and Mo_3Si_2 Phases

The Mo-Si phase diagram shown in Figure 70 in Appendix II presents the Mo_3Si_2 phase as stoichiometric with no solid solubility, whereas data from the microprobe analysis of the diffusion couples shows the phase to be about 5 $^{a}/_{o}$ in width.

The phase diagram also shows a Mo_3Si phase which was not ascertained by the microprobe data. The reason for the apparent absence of this phase can be explained by Kidson's[8] work briefly discussed in Section VII.D.3.

Approved for Public Release

Contrails

REFERENCES

1. N. L. Peterson, "Diffusion in Refractory Metals," WADD Technical Report 60-793, 1960.

2. E. J. Rapperport and M. F. Smith, "The Constitution Diagram Tungsten-Ruthenium," to be published in the Transactions of the Metallurgical Society of AIME.

3. W. E. Forsythe, Ed., Smithsonian Physical Tables, 9th revised Edition, Smithsonian Institute, Washington, D. C., 1959.

4. R. Castaing, Advances in Electronics and Electron Physics, Vol. XIII, Academic Press, Inc., New York, 1960, pp. 317-386.

5. E. J. Rapperport and C. S. Hartley, "Diffusion in Refractory Metals," Refractory-Metals and Alloys II, Interscience Publishers (J. Wiley), New York, 1963.

6. W. Jost, Diffusion in Solids, Liquids, Gases, Third Printing with Addendum, Academic Press, Inc., New York, 1960.

7. W. Seith and T. Hermann, Diffusion of Metals, Second Edition, Springer Press, Berlin, 1955.

8. G. V. Kidson, Journal of Nuclear Materials, Vol. 3, No. 1, January 1961, p. 21.

9. L. S. Darken, "Formal Basis of Diffusion Theory," Atom Movements, American Society for Metals, Cleveland, 1951.

10. J. E. Hilliard, Acta Metallurgica, Vol. 5, No. 1, January 1957, p. 38.

11. W. B. Pearson, A Handbook of Lattice Spacings and Structures of Metals and Alloys, Pergamon Press, New York, 1958.

12. J. J. English, "Binary and Ternary Phase Diagrams of Columbium, Molybdenum, Tantalum and Tungsten," DMIC Report 152, 1961.

13. J. Hansen, Constitution of Binary Alloys, McGraw-Hill Book Company, New York, 1958.

Approved for Public Release

Contrails

APPENDIX I

THE COMPUTER PROGRAM

C. S. Hartley and K. Hubbard (WADD)

In order to expedite the computation of diffusivities from experimental data, using the Boltzmann-Matano analysis, a computer program for the IBM 7090 was written.* The program performs the following operations:

(a) Converts concentration-distance coordinates to Gaussian coordinates. Such a coordinate system is linear in distance and in the argument of the error function or the cumulative normal distribution.

(b) Fits a least-squares, low order polynominal to the Gaussian plot. This is done separately in each single-phase region.

(c) Recalculates the concentration-distance curve using the functional relationship between the argument of the cumulative normal distribution and distance derived in (b). This data is tabulated at equal distance intervals for ease in subsequent numerical integration procedures.

(d) Finds the Matano interface by integrating the recalculated concentration-distance curve in the diffusion zone. The zero of the distance scale is then shifted to the Matano interface.

(e) Starting with the highest value of concentration of one of the components (100% in all cases here) less a selected computation interval (1% was used in this work) the interdiffusion coefficient is successively calculated in the single phase fields at points separated by the computation interval. The necessary areas are obtained by numerical integration, while the slopes of the concentration-distance curve are obtained by two essentially

- - - - - - - - - - -

* This program is available from ASTIA. The information in this appendix was taken from a personal communication to the authors of the present report.

Approved for Public Release

Contrails

independent techniques which are described below. The computation is continued to the lowest concentration of the reference component plus the computation interval, e.g. a typical computation on pure metal couples extends from 99 ^{a}/o to 1 ^{a}/o.

To prepare the raw concentration-distance data for input it is necessary to decide on the degree of the curve fit desired in various regions. First the data are plotted on Gaussian coordinates to determine whether they may be approximated by a single linear segment, a combination of linear segments, or a curve in a given single-phase region. The entire composition-distance curve is then divided into segments based on this examination. These are identified in the input, and the computer is told to fit either a first, second or third degree polynominal to a given segment. Phase interfaces are identified in the input by inserting a negative number instead of a concentration corresponding to the position coordinate of the interface. This serves merely as an indicator and is not used in subsequent calculations.

Slopes of the concentration-distance curve can be computed directly from the coefficients of the least-squares curve on Gaussian coordinates or by a graphical interpolation technique. The former utilizes the fact that the least squares fit is of the form:

$$z = \sum_{i=0}^{3} A_i X^i \qquad (1)$$

whence

$$\frac{dz}{dx} = \sum_{i=0}^{3} i\, A_i X^{i-1} \qquad (2)$$

The quantity z is given by

$$\frac{C-C_o}{C_m-C_o} = \frac{1}{\sqrt{2\pi}} \int_{-\infty}^{z} e^{-\frac{\alpha^2}{2}}\, d\alpha \qquad (3)$$

i.e. the argument of the cumulative normal distribution. Here C is the concentration at some point, X; and C_o and C_m are the maximum and minimum concentrations of the component in the diffusion zone. From equation 3

Approved for Public Release

Contrails

we obtain:

$$\frac{dc}{dz} = \frac{e^{-\frac{z^2}{2}}}{\sqrt{2\pi}} \tag{4}$$

so that:

$$\frac{dc}{dx} = \frac{dc}{dz}\quad\frac{dz}{dx} = \frac{e^{-\frac{z^2}{2}}}{\sqrt{2\pi}}\quad\sum_{i=0}^{3} iA_i X^{i-2} \tag{5}$$

The coefficients, A_i, apply to the segment of the total fitted curve on which the desired composition is located.

The interpolation technique approximates the true curve in cartesian coordinates in the neighborhood of the point of interest by a parabola drawn exactly through the nearest three tabular points (in the regenerated data). The slope of the parabola is then computed at the point of interest to give dc/dx directly without resort to the cumulative normal distribution. These two techniques usually agree to better than 5% depending on the form of the composition-distance curve.

It was found that the greatest discrepancy between hand calculated and computer calculated diffusion coefficients was due to the slope measurement. The variations were from two sources: (a) The computer will "draw" a curve through the experimental points different from that which one might draw from visual inspection. Depending on the particular data, the computer's curve may or may not be a better fit than the manually drawn one. (b) The inherent inaccuracies in measuring slopes experimentally leads to an error as high as 10%, depending on the curve being examined.

The fact that a "least squares" curve fit is used does not guarantee that the fitted curve will have the same shape as the experimental data. In some cases this discrepancy is quite noticeable, while in others the fitted curve is nearly exact. Where the fitted curve does not match the experimental curve an erroneous trend will be observed in a plot of $\widetilde{D}$ versus composition. However, the difference between the value of the computer calculated $\widetilde{D}$ and the best hand calculated value rarely exceeded 100%, even when the least squares curve was not exact.

Approved for Public Release

Contrails

The curve-fitting technique used here has a distinct advantage when applied to intermediate phases of narrow composition limits and terminal solid solutions for which the solubility of the minor component is extremely small. Both instances were observed in tungsten-platinum group systems. In these cases a straight line fit on probability coordinates was used to approximate the true curve. For this purpose it is sufficient to know the locations of the phase interfaces in the diffusion zone and to have two experimental composition-position points in the phase in question. In lieu of the latter, one experimental point and a phase boundary composition or two phase boundary compositions in an intermediate phase and the corresponding position coordinates will fix a straight line. While the diffusion coefficients calculated in these regions are certainly questionable, such a procedure allows the entire composition-distance curve to be constructed, and the errors introduced do not significantly affect computations in other regions of the zone where experimental data may be better. Phase boundaries determined in this way have been found to agree very well with those obtained by more accurate techniques.

Approved for Public Release

Contrails

APPENDIX II

CONSTITUTION DIAGRAMS OF SYSTEMS

TUNGSTEN-RUTHENIUM, TUNGSTEN-IRIDIUM, TUNGSTEN-RHODIUM,

TUNGSTEN-PLATINUM, COLUMBIUM-CHROMIUM AND MOLYBDENUM-SILICON

Approved for Public Release

Contrails

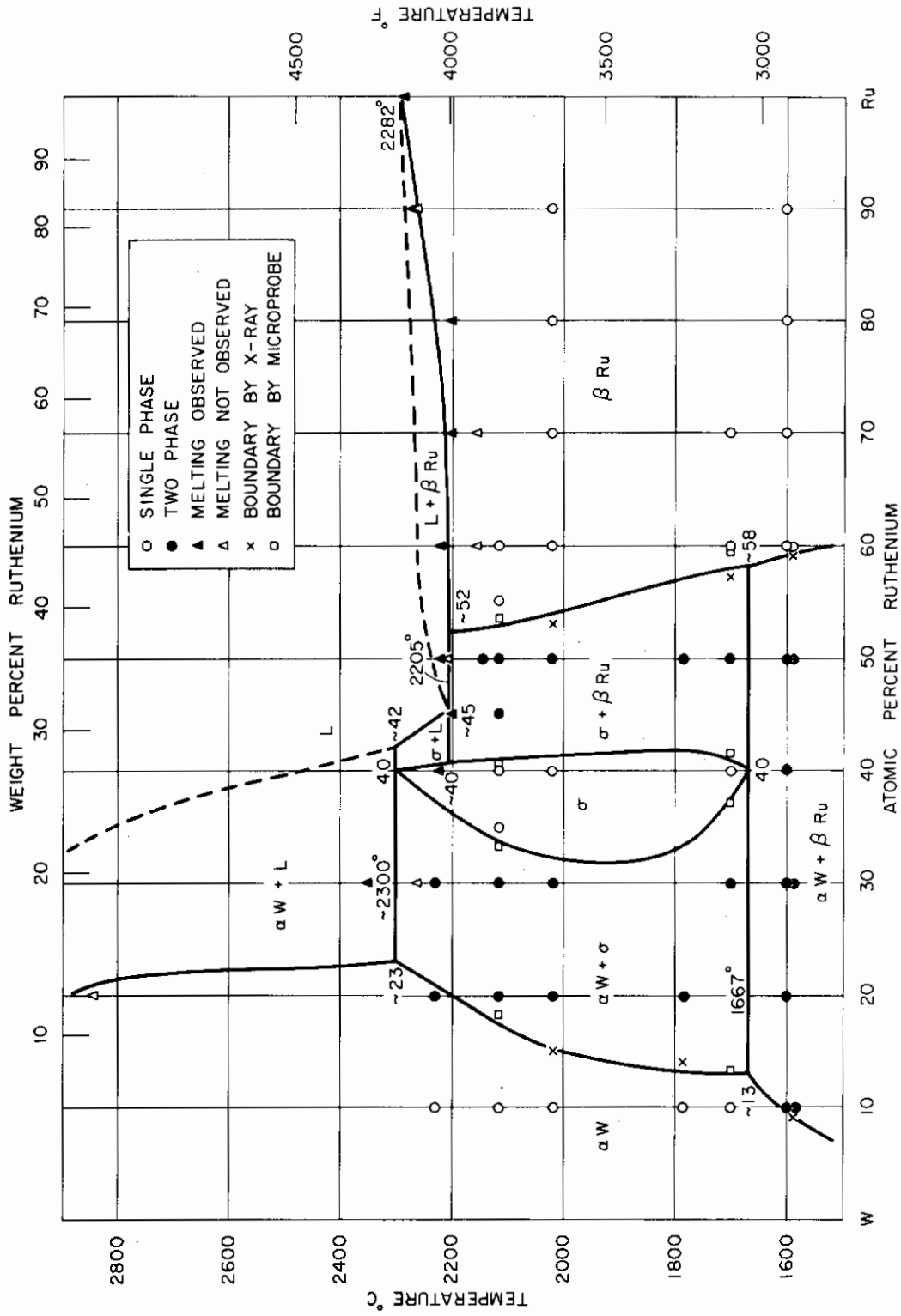

Figure 64. The Tungsten-Ruthenium Constitution Diagram.

Approved for Public Release

Contrails

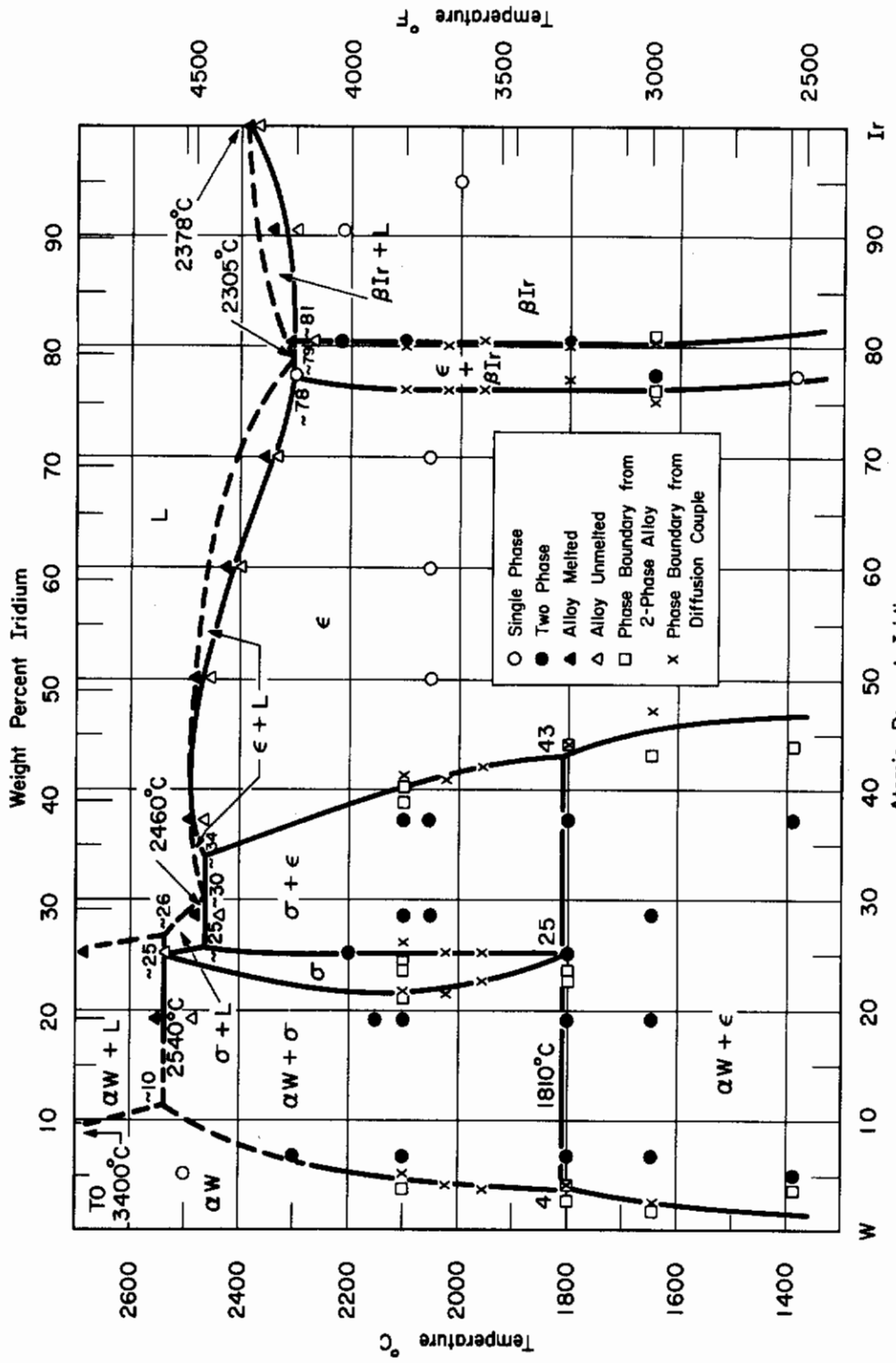

Figure 65. Tungsten-Iridium Constitution Diagram.

Approved for Public Release

Contrails

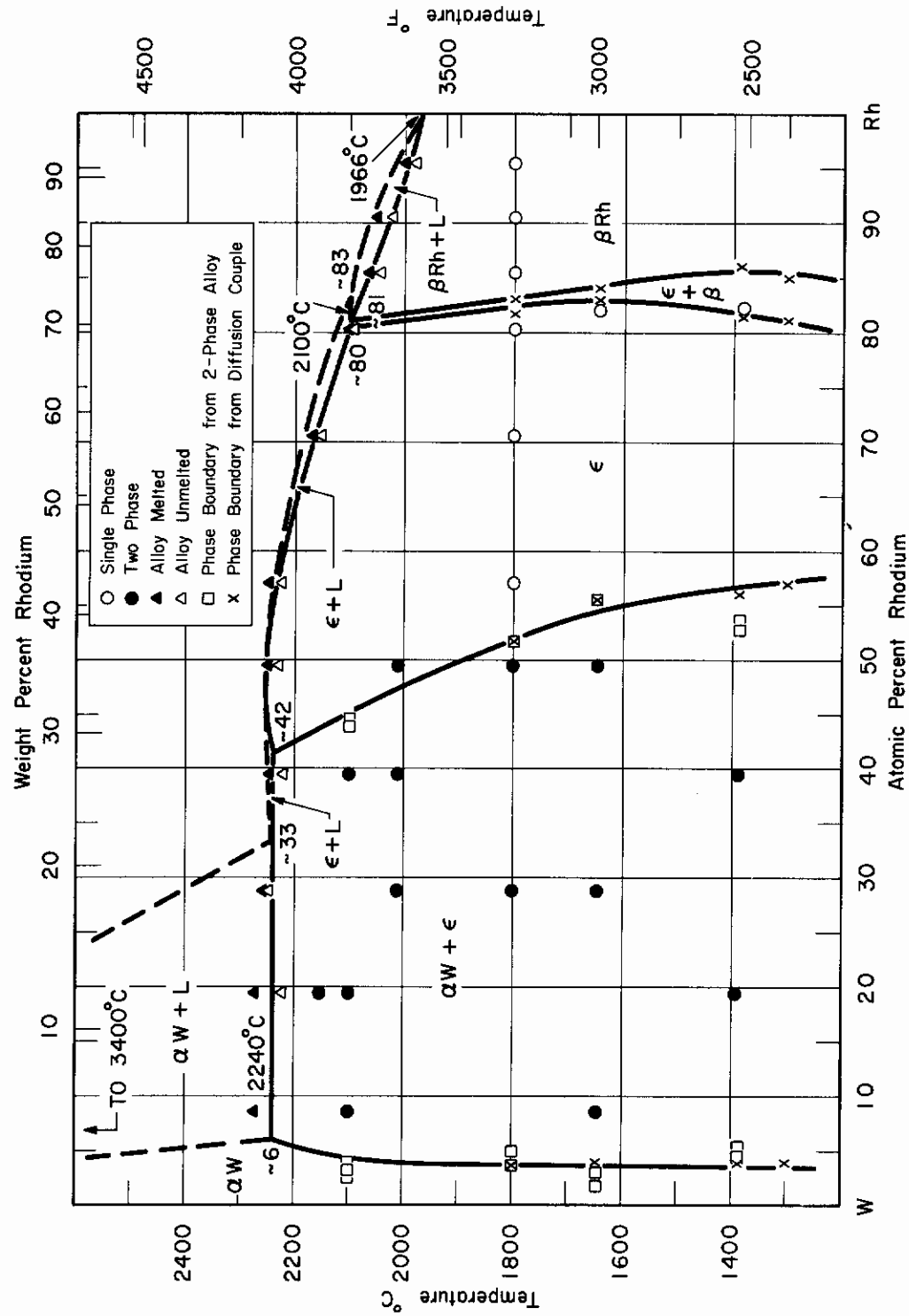

Figure 66. Tungsten-Rhodium Constitution Diagram.

Approved for Public Release

Contrails

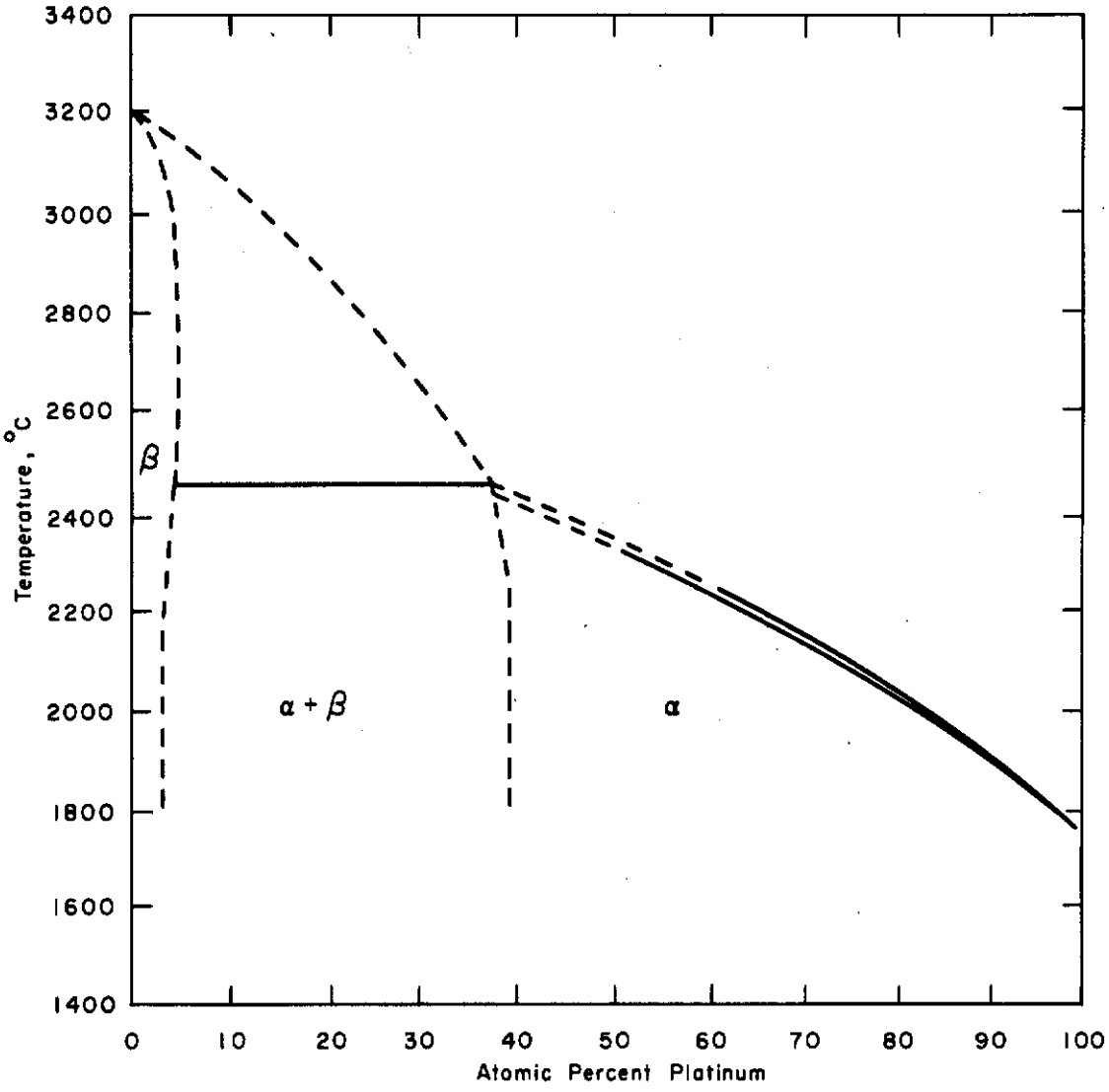

Figure 67. The Tungsten-Platinum Constitution Diagram (After English[12]).

Approved for Public Release

Contrails

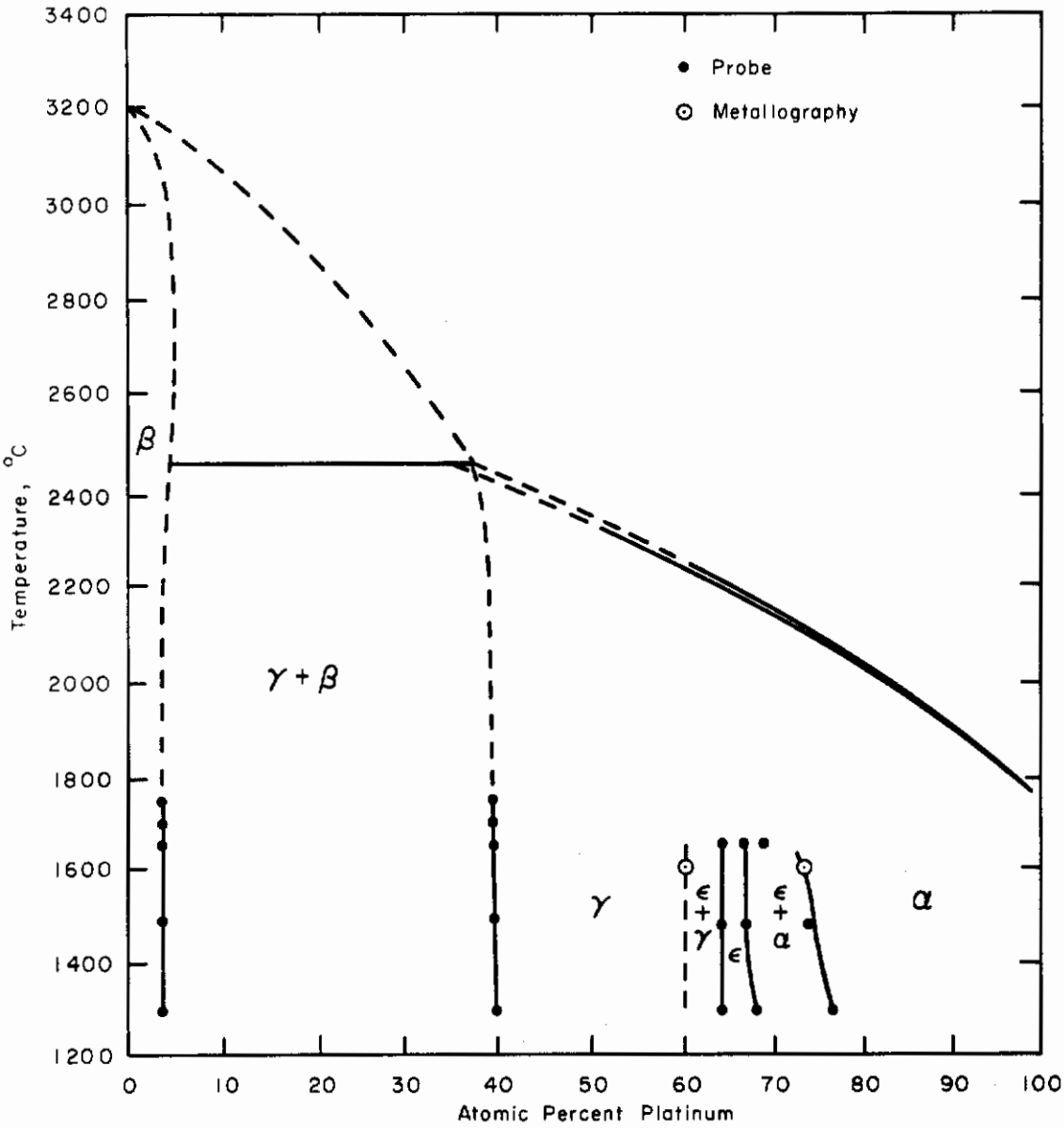

Figure 68. The Tungsten-Platinum Constitution Diagram Including Recent Data.

Approved for Public Release

Contrails

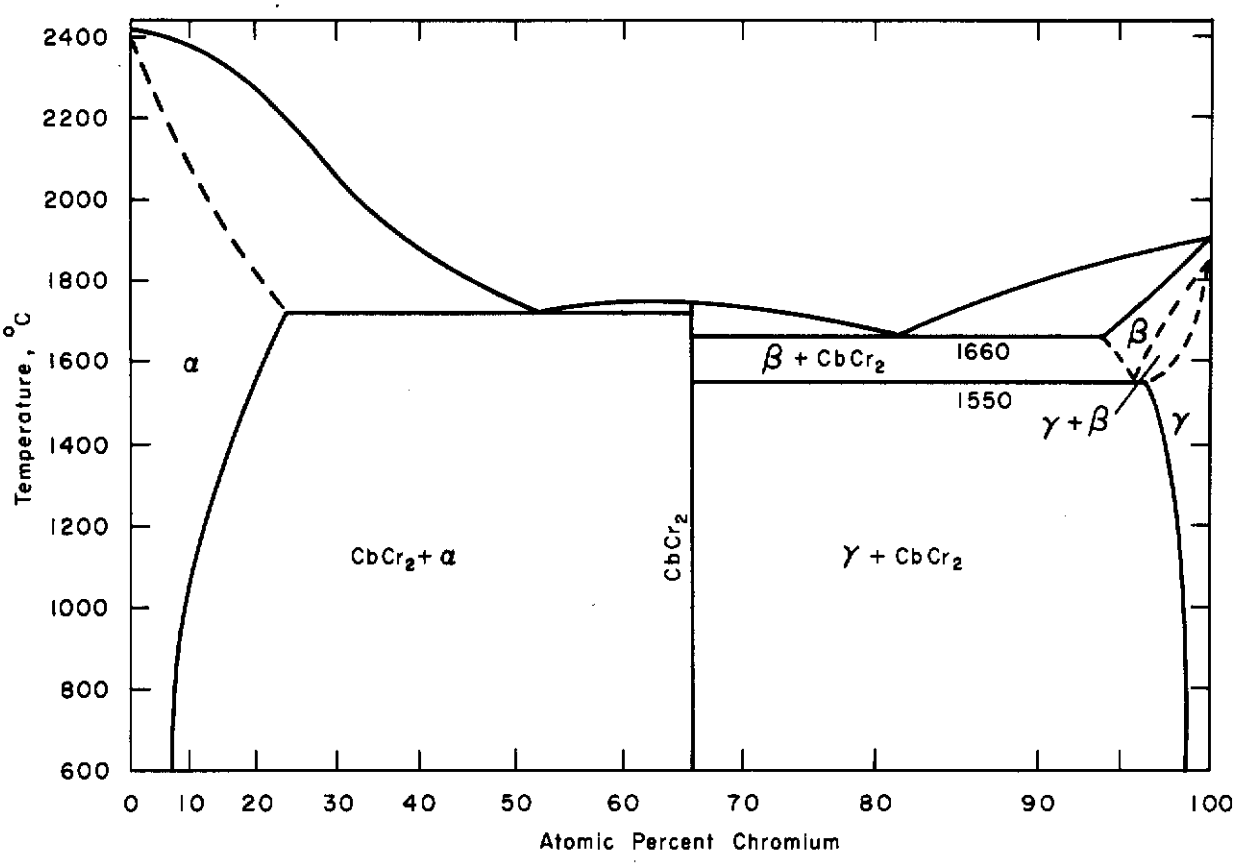

Figure 69. The Columbium-Chromium Constitution Diagram (After English[12]). This diagram does not contain the additional information obtained from the microprobe analysis of the diffusion couples (see text).

Approved for Public Release

Contrails

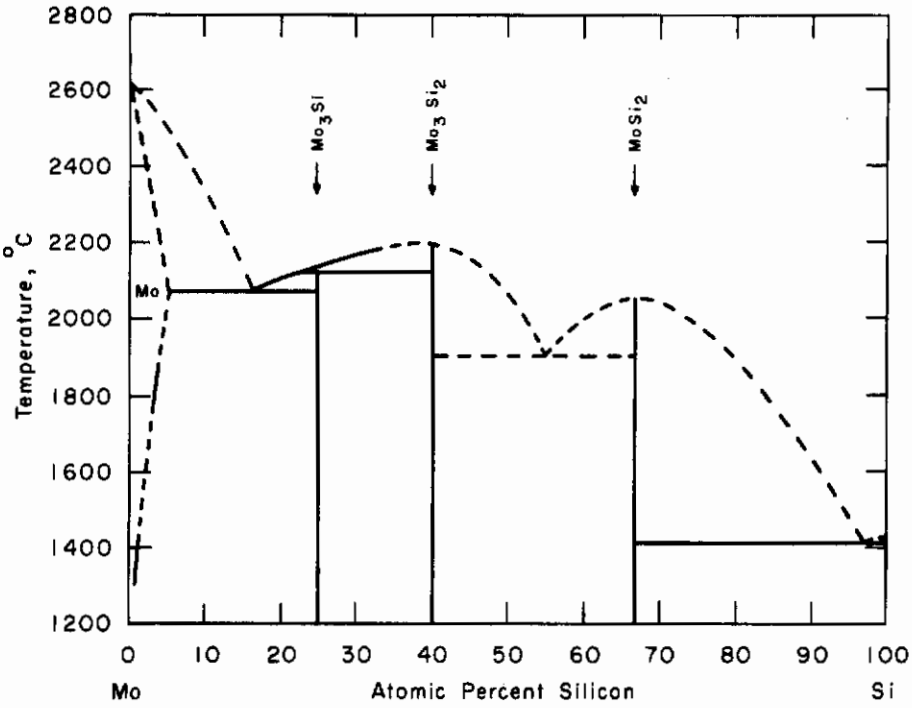

Figure 70. The Molybdenum-Silicon Constitution Diagram (After Hansen[13]). This diagram does not contain the additional information obtained from the microprobe analysis of the diffusion couples (see text).

Approved for Public Release